Title
The Effect of Resin Formulation and Processing on Stability of UV Cured Precision Replicated Composite Optics

Author
Ferrelli, Geena

Publication Date
2021

Peer reviewed|Thesis/dissertation

UNIVERSITY OF CALIFORNIA

Los Angeles

The Effect of Resin Formulation and Processing on Stability of UV Cured Precision Replicated Composite Optics

A thesis submitted in partial satisfaction

of the requirements for the degree Doctor of Philosophy

in Materials Science and Engineering

by

Geena Linn Ferrelli

2020

ABSTRACT OF THE DISSERTATION

The Effect of Resin Formulation and Processing on Stability of UV Cured Precision Replicated Composite Optics

by

Geena Linn Ferrelli

Doctor of Philosophy in Materials Science and Engineering

University of California, Los Angeles, 2020

Professor Jenn-Ming Yang, Chair

Replicated composite optics (RCO) are a promising technique to fabricate high-quality mirrors with reduced weight and processing time compared to conventional glass mirrors for space imagery technology, however, the optical layer is organic and susceptible to environmentally induced dimensional distortions that critically degrade performance. Therefore, environmental stability is the critical barrier to entry, and due to the lack of parametric material studies, little progress regarding critical controlling factors has been achieved. Conventional solutions, such as thermal curing to enhance polymeric cure state are not feasible due to the generation of CTE

mismatch stresses in the bonded RCO structure that degrade optical quality. In this study, optical quality and stability are balanced by the utilization of a UV-cured epoxy resin; furthermore, significant modifications to the cure state are attained at room temperature.

Replication surface quality was monitored as a function of processing conditions, cure temperatures, and exposure to different environments. Optical distortion in each was directly linked to a change in the residual stress state. It was found that replication optical quality degraded from that of the glass master due to the formation of residual curing stress, however, values were an order of magnitude smaller than those induced by a thermal cure. In response to hygrothermal environments, optical distortion was believed to be controlled by conventional material properties, specifically CTE and CME. However, stress relaxation was found to dominate optical stability by dictating dimensional drift and optical hysteresis in response to a hygrothermal environment. Even storage at RT can induce degradation over long periods of time, i.e. years. It was discovered that the relaxation rates are significantly accelerated by high stress, temperature, and humidity. As a result, maximized optical quality and stability are achieved in systems with a zero-stress state, high degree of crosslinking to resist relaxation, and enhanced properties.

By utilizing photopolymerization and manipulating its formulation and processing, a zero-stress replication with high thermal stability was fabricated at RT. This optimized processing protocol is very specific to this material system, and in general, all properties characteristic of maximized replication quality and stability are not simultaneously achieved. Several techniques were employed to minimize optical distortion; increasing CFRP laminate stiffness to reduce impact of stress on SFE change, performing gamma irradiation to induce additional crosslinking at RT and slow relaxation rates, and developing a novel processing technique to accelerate built-in residual stresses at room temperature with humidity cycling. The humidity cycling post-process

is specifically desirable to relieve large distortions from thermal curing in order to enhance optical quality, material properties, cryogenic performance, and long-term stability. Furthermore, this processing protocol is globally applicable to all resin systems and curing techniques.

The dissertation of Geena Linn Ferrelli is approved.

Pei-Yu Chiou

Aaswath Raman

Qibing Pei

Jenn-Ming Yang, Committee Chair

University of California, Los Angeles

2020

Table of Contents

List of Figures

List of Tables

Acknowledgements

I would like to acknowledge the contributions and support of the many people who made this work possible and their support throughout the journey.

Dr. Rafael Zaldivar, thank you for your immense leadership, mentoring, and support. I greatly appreciate how you always challenge me to be better than I was last week, lead by example to show me the scientist I strive to be, and "encouraged" me to work on other projects that only made my work in this dissertation and in general, stronger.

I also want to thank you Dr. Hyun Kim for his guidance and mentoring, but mostly his extreme patience. You have always made time to explain things in detail, especially how you approach technical problems and writing, for which I am infinitely grateful.

To my polymer and composites group, thank you to Robert Castaneda for his guidance in polymeric thermal characterization; Dhruv Patel and Dr. Joseph Severino for their expertise in composite manufacturing mechanical design, only sometimes laughing at how poorly I describe my ideas in 3D space; and Daniel Rivera-Bermeo for always being available to help when I need it, even if it was something extremely tedious.

I would also like to acknowledge several others at Aerospace who supported me; Dr. Jim Barrie for take an interest in me and for providing more than technical advice, Kelsey Folgner and Tait McLouth for spending the last few months inspiring me with tales of how much free time I'll have when I'm done, and our intern Daniela Marques.

Thank you to everyone who made this possible at Aerospace; my management Dr. Tim Graves, Dr. Jim Nokes, Dr. Rafael Zaldivar, and Dr. Alan Hopkins for allowing me to balance both work and school, the funding provided by the Aerospace Corporate Fellowship Program for the ability

to perform this work and simultaneously attend school, and the Aerospace Technical Investment Program (ATIP) for funding for this work.

I would like to thank everyone who made this possible at UCLA. My advisor, Dr. Jenn-Ming Yang for always being extremely helpful and available, even on short notice. Thank you to Dr. Aaswath Raman, Dr. Qibing Pei, and Dr. Pei-Yu Chiou for serving on my doctoral committee.

Finally, thank you to my family for your unending support. To my parents, thank you for always talking reason in me when I get distracted and for only sounding bored 50% of the time when I talk about my research. Thank you to my sister Sarah Ferrelli for always being there and providing necessary comic relief, but most importantly sending me chocolate to get me through the last few weeks. I would additionally like to thank my friends for their encouragement and patience when I take 3-5 business days to respond.

Portions of Chapters 4 and 6 are derived from the published work: G.L. Ferrelli, H.I. Kim, and R.J. Zaldivar. “The effect of photoinitiator concentration on hygroscopic stability of UV cured precision replicated composite optics,” *Applied Optics* 59 (16) 2020. A portion of Chapter 7 is derived from the published work: H.I. Kim, G.L. Ferrelli, and R.J. Zaldivar. “Effect of gamma radiation on the stability of UV replicated composite mirrors,” *Optical Engineering,* Volume 57(4), pp.047102 (2018).

Vita

2012-2013	*Laboratory Assistant* UCLA Nanoelectronics Research Facility, Los Angeles, California
2014	*Undergraduate Intern* NASA Glenn Research Center, Cleveland, Ohio
2015	*Bachelor of Science in Materials Science and Engineering* University of California, Los Angeles
2014 - 2017	*Undergraduate and Graduate Intern* The Aerospace Corporation, El Segundo, California
2017	*Master of Science in Materials Science and Engineering* University of California, Los Angeles
2017 - Present	*PhD Corporate Fellowship* The Aerospace Corporation, El Segundo, California

Relevant Publications, Presentations, and Patents:

1. H.I. Kim, G.L. Ferrelli, and R.J. Zaldivar. "Evaluating the use of self-assembled monolayer (SAM) release coatings for replicated optics," *Journal of Adhesion Science and Technology*, Volume 30, pp.2544-2556 (2016).

2. G.L. Ferrelli, H.I. Kim, and R.J. Zaldivar. "Lightweight replicated composite mirrors using UV cured resin," *The Composites and Advanced Materials Expo Conference Proceedings* (2016).

3. H.I. Kim, G.L. Ferrelli, and R.J. Zaldivar. "Hygroscopic and thermal stability of high precision replicated epoxy composite mirrors," *Optical Engineering,* Volume 56(11), pp.117103 (2017).

4. G.L. Ferrelli. "Effect of rein cure on the stability of high-quality replicated composite mirror surfaces," *M.S. Thesis, University of California, Los Angeles* (2017).

5. H.I. Kim, G.L. Ferrelli, and R.J. Zaldivar. "Effect of gamma radiation on the stability of UV replicated composite mirrors," *Optical Engineering,* Volume 57(4), pp.047102 (2018).

6. H.I. Kim, G.L. Ferrelli, and R.J. Zaldivar. "Fabrication Assembly and Methods for fabricating composite mirror objects," *Patent Granted No. US-9,956,587* (May 2018).

7. H.I. Kim, G.L. Ferrelli, and R.J. Zaldivar. "Fabrication Assembly and Methods for fabricating composite mirror objects," *Patent Granted No. US-10,022,747* (July 2018).

8. G.L. Ferrelli, H.I. Kim, and R.J. Zaldivar. “Underlying causes of hygroscopic stability in high-quality replicated composite optics,” *SPIE Defense and Commercial Sensing Conference Proceedings* (2019).

9. H.I. Kim, G.L. Ferrelli, and R.J. Zaldivar. “Deposition assembly and methods for depositing mold release layers on substrates,” *Patent Allowed #10562209* (2019).

10. G.L. Ferrelli, H.I. Kim, and R.J. Zaldivar. “Hygroscopic dimensional stability in high-quality replicated composite optics,” Presented at *Manufacturing Problem Prevention Program* (2019).

11. G.L. Ferrelli, H.I. Kim, and R.J. Zaldivar. “Method of Improving Dimensional Stability and Adhesive Strength of Bonded Structures,” *Patent Filed #16774971* (2020).

12. H.I. Kim, G.L. Ferrelli, and R.J. Zaldivar. “Systems and Methods for Gamma Radiation Based Stabilization of Replicated Mirror Structures at the Nanometer-Scale,” *Patent Publication No. US-2020-0025663-A1* (2020).

13. G.L. Ferrelli, H.I. Kim, and R.J. Zaldivar. “The effect of photoinitiator concentration on hygroscopic stability of UV cured precision replicated composite optics,” *Applied Optics* 59 (16) 2020.

Chapter 1. Introduction

1.1. Large-Aperture Precision Space-Based Optics

Large-aperture precision optics are a critical and enabling component of space telescopes because both the size and quality of the primary mirror determine the ultimate performance. Increased mirror diameter enhances the imaging resolution, collecting a higher luminous energy, and increasing the signal-to-noise ratio [1, 2, 3]. When imaging a distant point source such as a star, the mirror does not focus all light into a single point; instead, due to diffraction phenomena, reflected energy is spread into a spot [4]. Increased mirror diameter reduces diffraction-contributions, leading to higher imaging resolution. Specific satellite mission objectives must be identified to dictate the mirror size required to fulfill its needs [3, 4]. The National Aeronautics and Space Administration (NASA) and the European Space Agency (ESA) have explicitly called out future space mission goals; specifically in the UV/Optical/IR (UVOIR) regime, mirrors with a diameter greater than 8m have been specified based on angular resolution and light collection requirements [3]. Current UVOIR space-based telescope technologies do not contain mirrors large enough to provide adequate resolution or sensitivity necessary to observe the objects desired for these future scientific inquiries. The Hubble Space Telescope (HST) contains the largest primary mirror currently employed in all UVOIR space telescopes, however the mirror diameter is only 2.4m, substantially smaller than the >8m necessary for future missions [1, 2, 3].

While mirror diameter controls the theoretical resolution, in reality, that resolution is only achieved with a geometrically perfect (or nearly perfect) mirror [3, 4, 5, 6]. Imperfections formed during the manufacturing process introduce optical errors that cause light to focus improperly, scatter reflected energy, and degrade the image quality [2, 3, 4, 5, 6]. For optical applications, the

mirror surface error tolerated is measured in terms of the surface figure error (SFE), which is a root-mean-square (RMS) deviation of the optical surface from its ideal surface [3]. In UVOIR applications, for the system to operate at the theoretical limit, the SFE must be less than $\lambda/20$ where λ is the wavelength of interest (633nm) [1, 2, 3]. The SFE error is spread over a range of spatial frequencies that are attributed to common manufacturing errors. Low frequency ("figure") errors are global shape deviations that cause lower optical throughput forming conventional aberrations; mid frequency errors cause small-angle scatter degrading resolution; and high frequency ("finish") errors cause high-angle scatter degrading contrast [4, 5, 6]. While each region impacts different aspects of optical performance, the total error is critical because for a UVOIR mirror to perform at its theoretical design, deviations across all spatial frequencies must be less than 32nm ($\lambda/20$). In general though, the global shape errors are the largest in magnitude [3, 4, 5, 6, 1, 2].

Conventionally, UVOIR mirrors are fabricated via a time-consuming, multi-step subtractive process where a monolithic ultralow expansion (ULE) glass substrate is machined and ground to acquire the desired shape. This is followed by polishing to achieve the required optical quality and surface finish [7]. However, when scaling-up size for future applications, there are additional mechanical constraints since the structure must withstand gravity, load, and vibration distortions. Since glass has poor mechanical properties, the stiffness to resist these distortions is achieved in the structure by increasing the thickness, substantially increasing the mass of the optic. Even with state-of-the-art light-weighting techniques such as those used on the HST primary mirror where thin facesheets are bonded to a sandwich core structure, utilizing glass optics for these future space applications with >8m diameter is prohibitively heavy [1, 8, 2, 9, 3]. Due to these limitations in scaling, novel materials must be considered in the manufacture of future space based UVOIR mirrors.

1.2. Composite Optics

When considering new materials to fabricate large-aperture precision optics to meet future requirements, optics must be fabricated that are lighter-weight but achieve the required λ/20 surface quality [10, 8, 11]. The material type chosen can also impact fabrication method, cost, manufacturing time, health concerns, and risk of failure during manufacturing [1]. After the launch of HST in 1990, development began soon after for the next major space-telescope mission: the James Webb Space Telescope (JWST) [3, 2]. Beryllium was selected as the mirror material due to increased specific stiffness (elastic modulus/density) over ULE, producing a mirror with areal density ~43% of the HST [3]. While development began in 1996, the JWST is not set to launch until 2021, with significant delays marring manufacture. Utilizing 6 manufacturing facilities, polishing the toxic and anisotropic Beryllium mirror segments alone took approximately 9 years [12]. As we look past the JWST to the future, alternative fabrication methods in addition to new materials are desired to reduce manufacturing time, cost, and risk [12, 3]. While several other potential materials like Silicon Carbide exhibit excellent material properties, the optical surface is attained by polishing, a slow process that is the bottleneck in manufacture of large UVOIR telescopes [1, 9].

Carbon fiber reinforced polymer (CFRP) composites have the potential to be utilized in the next generation of UVOIR mirrors due to both the material property and processing advantages. CFRP composites have extremely high specific stiffnesses, some of the highest of all materials and allowing light-weighting by over an order of magnitude compared to glass [10, 8, 11]. The areal densities of glass mirrors for space telescopes ranging from 1-4m in size are typically on the order of 40 to 75 kg/m^2. In comparison, a CFRP mirror can achieve an areal density of approximately 1.5 kg/m^2 [3]. Additionally, the graphitic carbon fibers provide a high thermal

conductivity pathway through the structure and overall exhibit very low, potentially negative coefficients of thermal expansion (CTE) [13]. High conductivity and low expansion are crucial for thermal stability of mirrors because imaging can take hours and localized surface distortions due to thermal effects in that timeframe degrade resolution [3]. Most importantly though, fabrication of a CFRP structure utilizes a molding technique where it is cured against a mandrel with the inverse shape of the desired final structure. Manufacturing takes days compared to the months or years necessary to polish a conventional glass surface, produces a structure with over an order of magnitude in weight savings, and is substantially more damage tolerant [14, 7, 15].

Because of the advantageous material and processing characteristics of CFRP composites, these materials have been gaining increased attention in the optical community since the 1990's [14, 7, 15]. Following the launch of the HST, the demand for even larger mirrors focused on this material as a promising means to realize these goals. However, controlling the macroscopic dimensions of a composite structure is difficult on the micrometer-scale, let alone the nanometer-scale. This is because CFRP composites are cured to relatively high temperatures (350F) to achieve their excellent mechanical and thermal properties. As they are cooled, they can accumulate residual stresses due to cure shrinkage and CTE mismatch that cause spring-back, resulting in deviations from the intended dimensions of the mandrel [13, 16]. This effect can be minimized by mandrel material selection (Invar) or designing an undersized mandrel to account for spring-back; however, this is not possible for high precision parts where nanometer-level control is required [17, 16]. In addition to large global spring-back distortions, the individual carbon-fiber tows can print-through to the surface of the optical layer, causing a regular and sinusoidal perturbation [18]. Due to the diameter of the carbon fiber tows (~1mm), these perturbations occur in the mid spatial frequency

range, critically reducing the imaging resolution due to high intensity low-angle scatter [18, 6, 19, 20, 21].

Due to the complexities in high-fidelity composite manufacturing, the use of these optics have been limited to the IR imaging region where mirrors can tolerate higher SFE deviations [10, 11, 22]. Though dimensional requirements are less stringent in this regime, the maximum SFE allowed is still only 175nm, smaller than most as-fabricated composite structures [3]. Therefore, groups at Jet Propulsion Lab (JPL) [23, 24], Composite Optics Inc. [23], Composite Mirror Applications (CMA) [25, 26, 27, 28], US Air Force [18, 19, 20], US Navy [1, 27], NASA [25, 26, 18], ESA [28], and the Japanese Aerospace Exploration Agency (JAXA) [21, 29] have independently and jointly worked on manufacturing CFRP composite mirrors for IR imaging applications. Most of this research focused specifically on methods to reduce the roughness of the composite surfaces through polishing, tailoring prepreg resin contents, and co-curing neat resin layers on the surface to minimize print-through [19, 20]. While these studies were successful in reducing surface roughness to below 2 nm, less research has been directed at understanding global figure errors of CFRP mirrors.

Even with relaxed SFE criteria for IR imaging applications, few groups have manufactured more than one-off large, lightweight mirrors with high SFE errors. Generally, expensive ULE glass mandrels polished to high SFE quality are used during the composite cure and layups are carefully designed to minimize spring-back errors. The international leader in composite mirror technology is CMA, who produce composite mirrors with ~0.15λ (100nm) SFE values. However, this is accomplished with a time-intensive, post-polishing technique [25, 26, 30]. For future applications where improvements to both mirror mass and manufacturing time are required, a higher fidelity replication process is necessary [3].

1.3. Epoxy Thin-Film Replicated Composite Optics

The benefits of CFRP composites can be realized for precision UVOIR mirror applications without the need for post-polishing through a process called epoxy thin-film replication. Replication is the general process of transferring an optical surface to one or more copies and can be used to describe the composite manufacturing processing, but in this case refers to a thin layer of epoxy resin as demonstrated in Figure 1. In this process, uncured resin is sandwiched between the CFRP substrate and a glass master coated in mold release (shown in Figure 1a), cured, and separated at the glass-resin interface (Figure 1b). Not only are the thermomechanical properties controlled by the CFRP substrate, but the resulting mirror ideally attains the same quality as the glass master (Figure 1c) because the replicating resin fills in the micron-sized perturbations on the composite surface. Additional benefits of this process are that multiple exact copies can be made from a single master for drop-in replacements or segmented mirrors, and each of these copies can be fabricated extremely quickly, in a matter of days or weeks [14, 7, 15, 31, 32, 33].

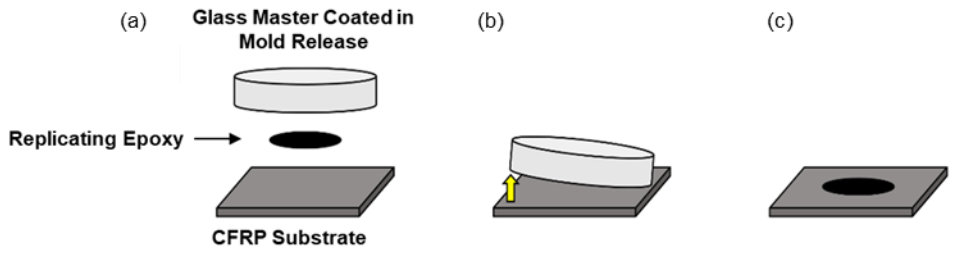

Figure 1. Schematic of epoxy thin-film replication with (a) assembly components (b) separation in peel mode and (c) final replicated mirror.

1.3.1. Optical Quality Considerations

Epoxy thin-film replication as a technique to fabricate optics is not a new development, and in theory, the replication should be an exact inverse copy of the glass master. In reality, though,

replication surfaces deviate from the master, so the materials and processing of replicated mirrors have changed over the years in an effort to produce λ/20 SFE mirrors [34, 7, 15]. In the 1960's, the optical community first became interested in utilizing a replication technique to manufacture precision optics. However, bulk polymer optics were not promising because optical instability in different environments is a known issue. Polymers are organic materials and undergo dimensional changes in response to varying thermal and hygroscopic environments. Therefore, epoxy thin-film replication technique was developed, reducing the thickness of the polymer layer, and consequently, its dimensional distortion in environment. These replications were manufactured by sputtering a metal release layer onto the precision glass mandrel, thermally curing the resin between the mandrel and a metal substrate, then separating the structure through thermal shock and CTE mismatch. This process induced large strains and reduced optical quality, only producing small parts (6") with "good" optical quality (λ/4) [34, 7, 8, 35, 15]. The replicated epoxy mirror technology has largely existed in this size and quality regime since then, commercially used in the production of diffraction gratings.

A group at JAXA working on CFRP mirrors pivoted from solely composite mirrors to an epoxy thin-film replication technique in anticipation of manufacturing the Small-JASMINE infrared telescope in the early 2000's. Processing details are sparse, but a λ/20 SFE metal mandrel was first used to manufacture a curved cyanate ester composite honeycomb shell. Then, a two-part epoxy replicating resin was cured between the CFRP substrate and the same mandrel to match global shape and ensure a uniform bondline. The incorporation of the epoxy resin layer significantly reduced the microroughness to 6 nm; linear striations were visible but not consistent with the fiber direction. These features were attributed to the texture of brushing on the mold release [36]. Even so, only "good" optical quality (λ/10) were achieved by utilizing an epoxy thin-

film replication technique at small scales. When larger replicated mirrors were fabricated, the SFE accuracy linearly increased with mirror diameter [37, 38, 36]. Additionally, no parametric studies were performed from a materials science point of view to enhance the as-replicated optical quality, and instead utilized a singular material and cure profile. However, recent breakthroughs (US Patent 10,562,209, US Patent 9,956,587, US Patent 10,022,747, US Patent 2020/0025663, and US Patent Pending 16/774,971) were made at The Aerospace Corporation where $<\lambda/20$ SFE replicated composite optics are routinely manufactured. This was achieved by optimizing material selection and processing of each individual component [39, 40, 31, 32, 33].

The first and most-critical component I investigated was the mold release layer. In current composite and epoxy thin-film replicated optics described in literature, the mirrors are not a perfect copy of the glass master [37, 38, 36]. Conventional mold release layers used in these applications are siloxane-based materials that provide a good physical barrier between the mandrel and low release forces, however, controlling the coating thickness on the micrometer-scale is difficult and, on the nanometer-scale, impossible. This is reflected in the work at JAXA where striation-induced microroughness was attributed to brushing the mold release layer on in a non-uniform manner [36]. For that reason, a self-assembled monolayer (SAM) was selected as the precision mold release layer. A SAM is an organic molecule consisting of a reactive head-group and a passive tail group that spontaneously forms large-ordered domains [39, 41]. These molecules are ideal for a manufacturing a hydrophobic mold release layer because, in theory, they are characterized by a self-terminating chemistry that forms a single molecule thick coating (2-3nm) and does not degrade the quality of the glass master. Additionally, the chemistry of the tail group can be modified to change adhesion strength with different materials; in the case of replication, a fluorocarbon to minimize interaction with resin.

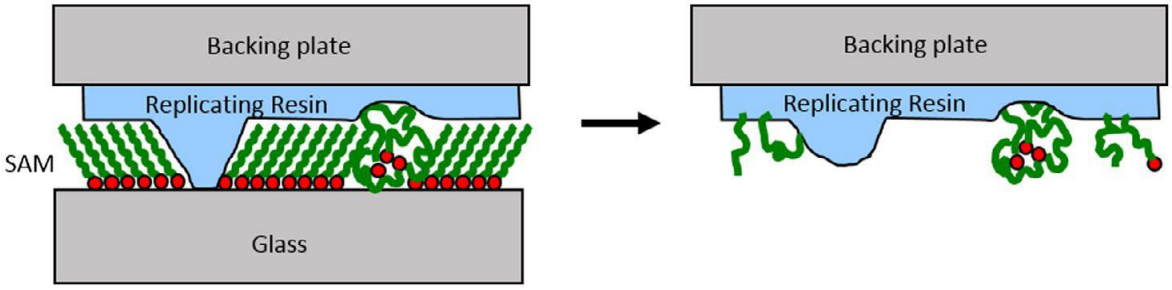

Figure 2. Illustration of (a) SAM defects and (b) how they can degrade replication quality.

While investigating SAM material and processing for replication, it was discovered that the SAM films exhibit nanoscale defects that degrade the replication quality. Two common defects (pinholes and agglomerations) are shown in Figure 2a, and their impact on replication quality are shown in Figure 2b [39, 41]. Pinholes specifically are unacceptable because they allow the replicating resin to penetrate the mold release layer and bond to the master mandrel, causing excessively high separation loads and localized deformations. Significant processing studies were performed to develop a defect-free coating that minimized release force and produced a near-net replication. This was achieved by incorporating a dual step process that allowed re-infiltration of a secondary, lower molecular weight SAM molecule to eliminate a vast majority of the imperfections. Atomic force microscopy (AFM), X-ray photoelectron spectroscopy (XPS), adhesion strength, and optical quality measurements were used to verify the efficacy of the process [39]. Material selection and processing of the mold release layer were crucial to enabling the manufacture of λ/20 quality replications.

Once the mold release was optimized, focus turned to the composite substrate fiber and matrix material selection due to the critical impact on light-weighting and structural performance of the replicated structure. The selection of carbon fiber constituent is primarily driven by CTE and stiffness contributions. Higher stiffness pitch-based carbon fibers allow maximum mass

reduction due to a thinner laminate required to achieve equivalent stiffness. In addition, higher stiffness carbon fibers are usually consistent with lower or negative longitudinal CTE values. Pitch-based derived carbon fibers such as the Mitsubishi K13C2U fiber have an exceedingly high longitudinal stiffness of 895GPa, close to double the value of an ultra-high modulus PAN-based derived carbon fiber [13]. Selection of the matrix constituent material selection is driven by environmental stability concerns due to its organic nature. Cyanate ester formulations (such as Toray RS3C) are characterized by a higher glass transition temperatures (Tg) and lower moisture absorption than their epoxy counterparts, demonstrating enhanced environmental stability [42]. These types of fiber-matrix systems are often utilized with a symmetric, quasi-isotropic layup in composite optical benches, where, similarly to replication, stiff and stable structures are required.

In addition to controlling the thermomechanical performance, the composite must exhibit high adhesion to the replicating resin layer. Proper surface preparation at the composite interface is necessary to remove contaminates and enhance wetting to maximize bond strength of the replicating resin and composite. However, the graphitic nature of pitch-based fibers that enhance the stiffness also cause them to exhibit poor bonding characteristics [43]. Traditional surface preparation methods such as surface roughening through abrasion can cause subsurface damage and debonding due to the very weak fiber-matrix bond strengths of the composite [43, 44]. It is highly desirable to utilize a non-contact method, such as atmospheric plasma, that can clean and activate the composite surface without causing potential damage. However, overtreating cyanate ester materials with plasma can reduce adhesion strength due to the formation of oxidized and unanchored ash on the composite surface. Plasma treatment was monitored via contact angle, XPS, and lap shear strength (LSS) to identify an optimized surface treatment method to maximize

adhesion of the K13C2U-RS3C composite system while limiting matrix damage due to oxidation [43].

The final critical component of the replication process I investigated was the replicating resin. For general processability concerns, the resin must exhibit a low viscosity, long pot life, and high adhesion characteristics, leading to the selection of an epoxy resin. Epoxy resins display all the characteristics critical to the replication process, however, there are many classes, hardening agents, and polymerization mechanisms of epoxy resins [14, 34]. To down select a specific resin and processing, the relationship between optical quality and optical stability are considered. For optical quality concerns, the resin must be unfilled and cured at room temperature. Since replications are bonded structures, elevated thermal profiles can lead to residual stress formation that degrades optical quality [14, 34]. While a RT cured epoxy is preferred for optical quality concerns, the replicating resin material selection and processing cannot be discussed without considering optical stability. Polymer mirrors have always been known to exhibit environmental instability because the optical layer is an organic material that experiences dimensional distortion in thermal, hygroscopic, and radiation environments. In general, the higher the cure state, the greater the stability of a resin, however, this is conventionally achieved with an elevated temperature exposure.

This tradeoff in quality and stability with a thermal cure is shown in Figure 3. The degradation in optical quality is shown in Figure 3a and Figure 3b where interferometer images are compared for one resin cured at RT and 120°C. The replication cured at RT (Figure 3a) has an ultra-high optical quality ($\lambda/40$) suitable for precision space UVOIR applications. By post-curing the resin to 120°C, a CTE mismatch between the replicating resin and the CFRP substrate leads to large thermally induced residual stresses that degrade the optical quality. With this elevated

temperature post-cure, the SFE degrades to λ/6, which is still "good" but unsuitable for space telescope applications. While excellent optical quality is achieved with a RT cure, the optical stability is compromised, demonstrated by the neat resin moisture absorption behavior in Figure 3c for the two cure states. The resin cured at RT absorbs substantially more water than the post-cured resin, which translates to a hygroscopic instability. On the other hand, the resin cured to 120°C absorbs significantly less moisture (higher hygroscopic stability), but the optical quality is degraded past λ/20 SFE. Due to the tradeoff in quality and stability with a conventional thermally cured epoxy, a UV cured polymerization method was selected for my studies because it can achieve a relatively high cure state with RT processing. These systems exhibit numerous other advantages, such as a long pot life and quasi-instantaneous conversion from liquid to solid.

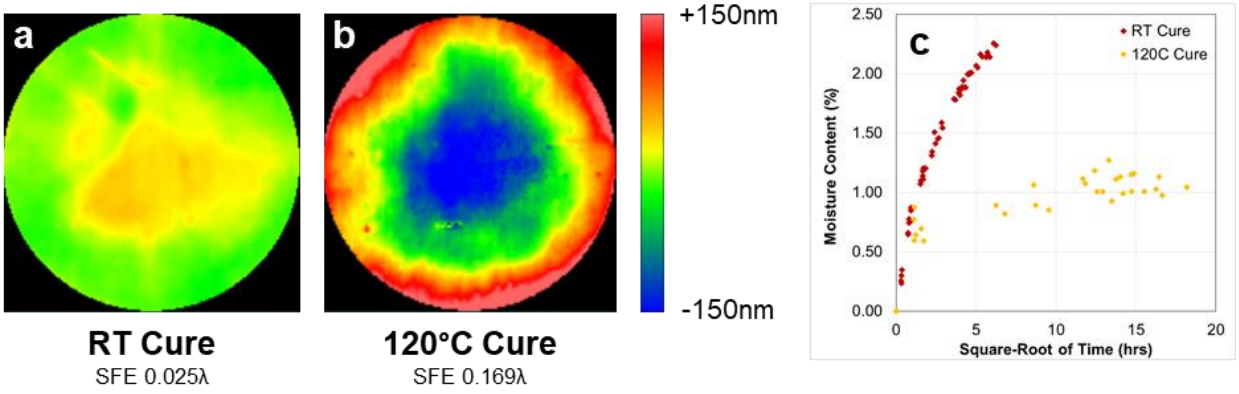

Figure 3. Optical quality-stability tradeoff with thermal processing. (a) Interferometer image of RT cure and (b) 120°C cure. (c) The neat resin moisture absorption of both cures.

Replications manufactured at The Aerospace Corporation resulted in the repeatable manufacture of optics with SFE quality <λ/20 due to the combination of optimized material selection and processing for each component of the replication process [33, 31, 32, 40]. Specifically, breakthroughs in a defect-free molecular mold release layer, ultrahigh-stiffness CFRP composite, and a UV cured resin at RT allow high-fidelity replications of the glass mandrel

structure. These studies and innovations have the potential to revolutionize the replicated composite optics technology and enable the application of this technology to precision UVOIR space applications once dimensional stability concerns and their impact on the ultimate performance of the mirror is fully understood.

1.3.2. Optical Stability Considerations

Manufacturing the required optical precision for space-based UVOIR telescope mirrors is the first step in employing epoxy thin-film replicated composite optics for these applications. However, once an appropriate surface quality has been fabricated, it must retain its shape in 1. varying hygrothermal environments prior to launch 2. space environment and 3. long term orbit [29]. Replication stability is a critical barrier to entry for this technology because polymeric materials are known to change dimension under these environmental conditions, and any change to the mirror surface can degrade optical performance. Even if these changes are well-behaved, spherically uniform distortions, they can cause optical errors and result in blurry images. For example, the HST was initially polished to the wrong power, preventing energy from focusing on the system's focal plane, and required corrective optics to be manually installed by astronauts [45]. Therefore, even small distortions in polymer optics occurring due to time or environmental effects can critically and irreversibly damage the imaging performance.

While CFRP composite substrates are comprised of an organic matrix material, compared to the epoxy resin optical layer, environmental dimensional distortions are negligible due to the large volume fraction of stiff, inorganic carbon fibers [23, 38, 24]. The CTE and coefficient of moisture expansion (CME) values of composite structures are only fractional when compared to neat resin values. For example, the CTE of a neat epoxy resin is on the order of 60μm/m/°C and the

corresponding value for a K13C2U-RS3C (60% V_f) composite laminate is approximately -0.5µm/m/°C; nearly two orders of magnitude smaller than the neat resin. Stability issues in the replicating resin layer are critical because its properties ultimately dominate the optical performance of the resulting mirror. Polymeric bulk properties relating to dimensional stability have been well characterized on the macro- and microscopic level because conventional polymeric characterization tools operate on the micrometer-scale, however very limited data exists on the nanometer-scale stability of polymers, let alone a bonded replicated structure [46, 47].

Additionally, there appears to be a lack of practical understanding or literature regarding the stability of the replicated resin layers in various environments. Epoxy-thin film replicated mirrors on metal substrates have long been used in industrial applications, however little information regarding the stability of these structures has been published. Some studies from the 1980's have focused on the impact of different metal substrates in thermal stability considerations due to CTE mismatch. Since the resin layer was constant and substrate material changed, this work is mostly irrelevant to the stability concerns at hand [35]. However, the JAXA group working on the Small-JASMINE replicated infrared telescope have performed stability tests of replicated composite optics [37, 29, 38, 48]. Samples underwent thermal cycling, however cryogenic temperatures induced cracking in the composite structure and the SFE experienced hysteresis during a second thermal cycle due to permanently induced-damage [38, 29]. Additionally, samples were exposed to 60°C/90% relative humidity (%RH) conditions and distortion monitored. Deformations were spherically uniform, and the moisture-induced distortions reported were on the order of 100x those induced by thermal [37, 48]. CME values are already known to be ~100x CTE values for epoxy resins and these studies were performed on a single, unnamed resin material and cure. Previous

studies do not focus on the replicating resin layer as the controlling factor in stability concerns or approach the problem from a materials science point of view.

Preliminary investigations at The Aerospace Corporation examined the impact of replicating resin material properties and cure state on environmental stability. In this work, the cure state of a single UV cured epoxy resin formulation was modified with different post-thermal exposures. The replication dimensional changes were monitored in response to time, temperature, and humidity environments and the optical changes correlated with several material properties [33, 31, 32, 40, 43]. With increasing thermal cure, the Tg and elastic modulus of the resin increased while the CTE and moisture absorption decreased, leading to observed increases in thermal, thermal cycling and humidity cycling stability. While these studies are the first to explore replication stability from a materials science point-of-view by focusing on the resin material properties, future investigations can further improve. The material properties increasing with thermal cure are all conventionally related to dimensional distortions, therefore, the relative importance of each is unknown. Additionally, due to the thermal exposures, the enhanced stability was achieved at the expense of optical quality. Finally, due to intermittent data acquisition, the nuances in behavior between samples as a function of material properties were overlooked. Parametric studies in real-time, on room-temperature cured systems, and as a function of individual resin properties is crucial to understanding long-term and environmental replication stability.

This preliminary work, along with those performed by others, highlights the need for more comprehensive investigations into replication stability to understand critical controlling parameters, as well as potential tradeoffs between replication quality and stability. Since the thermal tradeoff relationship is already known, a high cure state and material properties are desired without an elevated temperature exposure. One of the benefits of photopolymerization, which was

originally selected for its processing advantages, is that the cure state of a polymer can be modified without thermal exposures. By modifying the formulation or processing parameters of a UV cured epoxy resin, high-quality replications can be manufactured at room temperature with a large range of material properties. Followed by parametric environmental studies as a function of different properties, a more fundamental understanding of replication environmental stability concerns and quality-stability relationships can be achieved. These studies are crucial to developing a mirror capable of fulfilling the stringent requirements for utilization in space based UVOIR telescopes.

Chapter 2. Motivation and Objectives

Epoxy thin-film replicated composite optics offer a promising means to rapidly-manufacture ultralightweight precision mirrors for large-aperture space-based imaging applications. Despite numerous material and processing advantages, it has been difficult to manufacture replicated composite mirrors that satisfy both the accuracy and the stability required of UVOIR telescope mirrors. Recent research has focused on replication optical quality; with intelligent material selection and processing of each component, the consistent manufacture of $< \lambda/20$ SFE surfaces was achieved without the need for post-polishing. Substantially less progress regarding replication stability has been accomplished even though polymeric dimensional distortion under time, temperature, humidity, and radiation environments is the critical barrier to entry for this technology. There exists a need to understand replication stability in different environments and the critical material properties that control it.

It is the purpose of this dissertation to understand fundamental material properties that govern the hygrothermal and radiation stability in RCO in order to develop replicating resin processing protocols that minimize environmentally induced distortions without impacting replication quality as occurs with thermal post-curing. My approach is to modify the formulation and processing of a UV cured replicating epoxy at room temperature in order to manufacture polymers with a wide range of material properties, fabricate replications as a function of properties, and then monitor the dimensional changes in different environments to investigate critical parameters relating to minimal distortion. The specific objectives of this research are as follows:

1. Gain a deeper understanding of factors controlling replication stability by developing an analytical technique to quantitatively relate optical distortions in different environments to a specific resin material property or parameter

2. Relate differences in the replicating resin material properties to formulation and processing modifications to develop processing-structure-property relationships, specifically to control ultimate properties of the cured resin

3. Utilize knowledge we gain from these comprehensive studies to modify formulation and processing, or design a post-processing protocol, in order to maximize replication global stability without degrading optical quality

Chapter 3. Experimental Procedures

3.1. Replication Materials and Processing

3.1.1. Glass Master and SAM Mold Release Coating

High-quality fused silica glass mandrels (SFE < λ/20) were purchased from Russell Optics and were coated in mold release to fabricate replications. Two self-assembled monolayer molecules were used as the mold release layer that coat the glass mandrel. A primary perfluoropolyether monomer (PFPE) with a trimethoxysilane functional group on one end of the polymer chain was purchased from Daikin and a secondary PFPE monomer molecule, 1H,1H,2H,2H-Perfluorooctyltriethyoxysilane (POTS) was purchased from McMaster Carr. Monolayer solutions prepared were 0.1 volume percent in a fluorocarbon solvent (3M Novec 7200). Details of the process can be found elsewhere [39].

3.1.2. CFRP Composite Manufacture

All CFRP composite substrates (2" square) unless otherwise stated were fabricated from a pitch-based ultrahigh modulus Mitsubishi K13C2U carbon fiber and a low moisture absorbing Toray RS3C cyanate ester matrix. The laminates were prepared with a quasi-isotropic $(0, +45, -45, 90)_{8s}$ layup and cured in an ASC Process Systems 2x4 Econoclave Autoclave. Under vacuum (-14.7psig), the laminate was ramped to 250°F at 2°F/min. A pressure of 50psig was applied, the sample held at 250°F for 1 hour and then ramped to 350°F at 3°F/min. After holding at 350°F for 2 hours, the sample was cooled. Variations in the composite substrate via fiber identity and laminate thickness are used to vary flexural stiffness in Section 5.4.2. The other fibers used were Toray T300 and Toray M55J pan-based carbon fibers. The variations in laminates manufactured

for Section 5.4.2 are summarized in Table 1. The autoclave cure profile remains the same. Plasma surface preparation of the composites prior to replication was performed and details can be found elsewhere [43].

Table 1. Summary of CFRP composite substrates used in Section 4.1.

Composite System/Layup	Fiber Stiffness (GPa)	Substrate Thickness (mm)
32 Ply – T300/RS3C	230	3.46
48 Ply – M55J/RS3C	540	3.49
32 Ply – K13C2U/RS3C	895	3.59
16 Ply - M55J/RS3C	540	1.38
32 Ply - M55J/RS3C	540	2.55
64 Ply - M55J/RS3C	540	5.55

3.1.3. Replicating Resin Formulation and Curing

All photoinitiators and epoxy monomers were purchased from Sigma Aldrich. When fabricating replications, a series of replicating resin formulations are prepared by combining a diglycidyl ether-based epoxy monomer with varying concentrations (0.25, 0.50, 0.75, 1.00, 1.50, 2.50, and 5.00 weight %) of a sulfonium salt photoinitiator with antimony hexafluoride anion. The mass of components was measured on a Sartorius CPA225D microbalance with 0.01mg accuracy and mixed in a Flacktek DAC150.1 FVZ-K speed mixer for 2min at 2000rpm before storage under a nitrogen purge in UV opaque amber containers. The epoxy monomer formulations are all cured with a Dymax Bluewave LED Flood Curing System with a 365nm source for 7 minutes with varying intensity from 25mW/cm^2 to 300mW/cm^2 (unless otherwise stated, the cure intensity was 50mW/cm^2). The intensity was measured with an OAI Instruments Model 306 UV Powermeter with ±3% accuracy.

3.1.4. Replication Processing Scheme

Replications are fabricated according to the general schematic shown in Figure 1. A small amount of resin is placed between the CFRP composite substrate and the glass mandrel coated in

release agent. The bondline is controlled at a uniform 75µm with steel shims and the resin layer is cured with UV radiation through the glass master. The replication is separated at the resin-glass interface using a fixture in peel mode. The final replication diameter is ~1".

3.2. Neat Photoinitiator Characterization Techniques (Molar Absorptivity)

An Agilent Cary 7000 Spectrophotometer was used to measure the molar absorptivity of the photoinitiator. The absorptivity was measured from 350-400nm with a 1nm interval across a 1cm path length. The photoinitiator is suspended in a polypropylene solvent, so a polypropylene sample was used as the reference material in a sample holder. Three solutions with varying photoinitiator concentrations were used to measure molar absorptivity and the data averaged.

3.3. Replicating Resin Curing Characterization Techniques

3.3.1. Conversion and Kinetic Characterization with RT-FTIR

A ThermoScientific Nicolet 6700 Fourier Transform Infrared Spectrophotometer (FT-IR) with a diamond ATR crystal is used to monitor the degree of conversion and polymerization rate as a function of time. The disappearance of the oxirane group at 914 $cm^{-1}$was monitored with time. An internal normalization peak not involved in polymerization is the phenol (C=C) group that has a peak at 1606 cm^{-1}. The degree of conversion and rate of polymerization (R_p) were calculated using Equations 1 and 2, respectively, where I is peak intensity, M_0 is the initial monomer concentration, and dC/dt is the conversion rate as a function of time [49].

$$\% \text{ Conversion} = \frac{(I_{\text{Consumed}}/I_{\text{Standard}})_t}{(I_{\text{Consumed}}/I_{\text{Standard}})_{t0}} \text{ x } 100 \quad (1)$$

$$R_p = [M_0]\frac{dC}{dt} \quad (2)$$

3.3.2. In-Situ Cure Shrinkage Characterization

A TA Instruments Ares G2 Rheometer with a UV curing attachment was used to measure cure shrinkage of the replicating resin. Different uncured resin formulations were placed between two parallel plates, the top made of transparent acrylic, and a controlled 1mm gap was set. A shear strain of 2% was applied with zero axial force. The gap was monitored for 10 minutes before, throughout, and following irradiation until gap stabilization (~60min). The change in gap was converted to a cure shrinkage.

3.3.3. Gas Chromatography–Mass Spectroscopy

An Agilent 7890B and an Agilent 7200A quadrupole time of flight MS were used for the GC–MS analysis of resin before and after gamma radiation to evaluate the presence of photoinitiator and certain polymer fragments. The GC column was Phenomenex, Zebron ZB-1 HT, 60-m long, 0.25 mm i.d., and 0.25-μm film thickness, and a helium carrier gas rate of 1.2 mL/min. The MS detector was set for electron impact ionization and programmed to scan the mass range from 15 to 400 m⁄z. The resulting mass spectral data for the compounds identified were cross referenced to the NIST14 and Wiley 10th edition MS libraries.

3.4. Cured Replicating Resin Characterization Techniques

3.4.1. Tensile Testing

Resin was cast in Type V silicone dogbone molds, cured, and machined flat following cure. The tensile coupons were strained at 0.1% strain/min to failure in an Instron E10000 Electroplus frame with a 10kN load cell. Five samples per group were tested and the elastic modulus was measured between 0 and 0.025in/in strain.

3.4.2. Thermal Characterization

Both a TA Instruments Q850 Dynamic Mechanical Analyzer (DMA) and a TA Instruments Q800 DMA are used to characterize the glass transition temperature, elastic modulus, and time-temperature superposition (TTS) behavior of the cured polymers. A TA Instruments Q400 Thermomechanical Analyzer (TMA) is used to measure the CTE of the cured polymer.

To measure the glass transition temperature, the DMA is used in single cantilever mode from 0-200ºC with a 5ºC/min heating rate, 20μm deflection, and 1Hz frequency. Sample dimensions are 10mm x 5mm x 1mm. The glass transition temperature reported is the peak of the loss modulus curve.

Due to faster testing with reduced number of samples and material, for instances where tensile failure is not needed, the DMA is used with a three-point bending fixture to measure the elastic modulus. To equate the elastic modulus (desired) with the flexural modulus (measured), samples are run with a span-to-depth ratio of >10 to decouple the shear component from the elastic component of flexural modulus. Neat resin samples (25mm x 6mm x 2mm) were tested with a 0.1% strain/minute linear ramp rate to 0.5% strain to generate stress-strain curves and elastic modulus values.

TTS plots are a method to perform accelerated in a manner to predict long-term stress relaxation behavior of neat resin in a matter of several hours. The testing methodology operates under the assumption that polymer chain relaxation of viscoelastic materials occurs by the same mode at higher temperatures and longer times. Therefore, the relaxation modulus can be measured at increasing temperatures and shifted to predict relaxation behavior data far into the time-domain [50]. TTS master curves were generated by frequency sweep method on a DMA with a three-point

bend fixture. A 0.1% strain was applied from 2.5 to 25Hz frequencies (20 points per decade) with 5°C increments. The curves were superimposed via the Arrhenius method in the TA Instruments TRIOS software to generate a master curve in the frequency regime that was translated into the time regime. The DMA was coupled with a TA Instruments Relative Humidity accessory to generate TTS master curves as a function of %RH. The accessory has an accuracy of ±3%RH from 5-90%RH and a ±5%RH over 90%RH. Samples were pre-saturated in 0, 50, and 100%RH environments at room temperature prior to testing.

A TMA was used to measure the thermal expansion of cured polymers with a macro expansion probe from -100-200ºC with a 5ºC/min heating rate and 0.001N probe force. Coupons were ~20mm in height and CTE values were reported between -50 and +50°C.

3.4.3. Hygroscopic Characterization

Free standing replicating resin layers ~25mm in diameter and ~75µm thickness were fabricated for moisture absorption testing. The samples were initially dried under nitrogen until the weight stabilized, measured with a Sartorius CPA225D scale accurate to 0.01mg. Samples were then placed in a sealed 100%RH humid container (measured with Omega OM-24 humidity logger with ±5%RH accuracy) and periodically weighed as they absorbed moisture. The moisture content was measured gravimetrically with time (m_t) and converted to moisture content percentage (M(t)) using Equation 3, where m_{dry} is the mass of the fully dried sample [51].

$$M(t) = \frac{(m_t - m_{dry})}{m_{dry}} \, x \, 100\% \qquad 3$$

$$D = \frac{\pi L^2}{16 M_\infty} \left(\frac{M(t)}{\sqrt{t}} \right)_i^2 \qquad 4$$

When the moisture content is plotted as a function of the square-root of time, according to the Fickian moisture model, the absorption is initially linear before slowly turning over and reaching a plateau at the saturated moisture content, as shown. The diffusion coefficient is calculated using Equation 4, where L is the film thickness, and M(t)/$\sqrt{t}$ is the slope of the linear portion of the absorption curves [51].

3.4.4. Microstructural Characterization

A Park Systems NX20 AFM was used in tapping mode to characterize the replicating film microstructure. A cantilever tip characterized by a 42N/m spring constant and 330kHz resonance frequency were used to obtain phase images with a 500nm x 500nm field of view. Replications were fabricated as a function of PI concentration onto glass substrates with 75μm film thicknesses for AFM characterization.

3.4.5. Thermal Post-Cure Cure Shrinkage Characterization

A TA Instruments Q400 TMA was used to measure the thermally induced cure shrinkage of polymers after UV exposure. Coupons ~20mm in length were equilibrated at the desired temperature and held for 16hrs then cooled to RT again. The cure shrinkage was measured as the change in dimension between the initial and final lengths at RT.

3.5. Replication Optical Quality Measurements

3.5.1. Laser Interferometry

Replication optical quality was measured via laser interferometry. Both a Zygo brand (Verifire AT) and a 4D brand (AccuFiz) interferometer were used that have a 633nm wavelength

laser. Since the Zygo brand interferometer does not have an automatic lateral calibration, calibration coupons were measured in the 4D and used to calibrate the Zygo. Regardless of interferometer used, the samples were evaluated in the MetroPro software. The field of view for both instruments is 100mm, large enough to capture the entire replication surface. The surface quality is represented as the SFE in terms of λ (633nm), for the center 90% with the outer 10% masked due to roll-off errors.

3.5.2. Ultrasonic Inspection

Ultrasonic testing (UT) was performed with a 100MHx water-coupled transducer used in pulse-echo mode to inspect for internal flaws. A-scans were generated with ~1.5mm pixel size and processed to generated C-scans images as a function of depth with ~1μm resolution.

3.6. Replication Environmental Stability Facilities and Testing

3.6.1. Temporal Stability

The change in optical quality of replications over time was measured by manually taking interferometer measurements as a function of time. Samples were stored in a nitrogen backfilled chamber immediately after fabrication and removed for less than 5min at a time to make measurements before returning to the dry chamber.

3.6.2. Thermal Stability

Thermal stability of replications was desired after different thermal exposures. Samples were heated in Memmert UN55 convection oven backfilled with nitrogen to keep a dry environment throughout the exposure. Thermal exposures ranged from 50-100°C for times ranging

from 1 to 24hrs. Optical measurements were made manually before and after the thermal exposures while samples equilibrated at RT and dry (prevent moisture distortions).

3.6.3. Hygroscopic Stability

Hygroscopic optical stability was desired to be measured *in-situ* so an environmental chamber was designed with external humidity control that could be placed in the path of the interferometer. The humidity was controlled at 100%RH with water, 0%RH with W.A. Hammond Drierite^{TM}, and monitored with an Omega OM-24 humidity logger. The chamber is equipped with an antireflective coated lens and external tip/tilt control for non-interfering imaging and alignment. Replications were placed in the chamber and monitored as a function of time in different environments with the interferometer by taking automatic measurements every 15 minutes.

3.6.4. Thermal Cycling and Interfacial Adhesion Stability

Replication stability with thermal cycling was evaluated by manually measuring the optical surface before and after the exposures. Samples were cycled in a Cincinnati Sub-Zero Z16 Plus Environmental Test Chamber backfilled with nitrogen.

Interfacial adhesion was compared between samples by cooling them from RT to 0, -25, -50, and -70°C at ~5°C/min in a Cincinnati Sub-Zero Z16 Plus Environmental Test Chamber backfilled with nitrogen. Samples were then equilibrated for 1hr before returning to 25°C at 5°C/min. Replications were manually imaged before and after each thermal excursion. The minimum temperature achievable by the chamber is -70°C.

3.6.5. Gamma Radiation Stability

A J.L. Shepard high dose rate irradiator was used to expose polymer samples and replications to gamma radiation. The chamber consists of three 60^{Co} rods to achieve up to 50 rads⁄s. A fully enclosed, positive pressure, nitrogen filled box was used to keep samples in an inert environment during exposure to eliminate oxidative degradation. The area of simultaneous exposure, i.e., the size of the enclosure, was ~1 ft × 1 ft. Prior to the sample exposure, dosimetry was used to map a grid of varying dose rates at different locations. Each sample was treated to a different exposure time to match the total final dosage within 5%. Replication optical quality was measured at 0, 10, 30, and 50Mrad total dose.

Chapter 4. Effect of Resin Formulation and Processing on Material Properties

4.1. Introduction

The replicating resin layer is crucial to controlling replication stability because its material properties dictate the dimensional response to varying environmental conditions. In general, the higher the cure state, the greater the stability of a resin. However, conventional thermal curing to enhance the polymeric cure state can induce CTE mismatch stresses; the optical quality-stability tradeoff was previously demonstrated in Figure 3 [14, 34]. Therefore, a UV cured epoxy resin was selected as the polymerization mechanism because of its ability to achieve a high cure state with room temperature processing. A general schematic of the curing process is shown in Figure 4; formulations consist of a photoinitiator (PI) and a reactive epoxy monomer. When exposed to UV radiation, the photoinitiator dissociates to form reactive ions that crosslink the epoxy monomer [52, 53]. Once the photoinitiator dissociates, polymerization occurs by chain growth until diffusion limitations prevent further crosslinking, even after UV radiation is removed [52, 54]. While both material selection and processing have been shown to impact the polymerization kinetics and material properties [55, 56], in this study, the material selection is fixed and processing varied in order to parametrically modify the cure state without changing the chemistry.

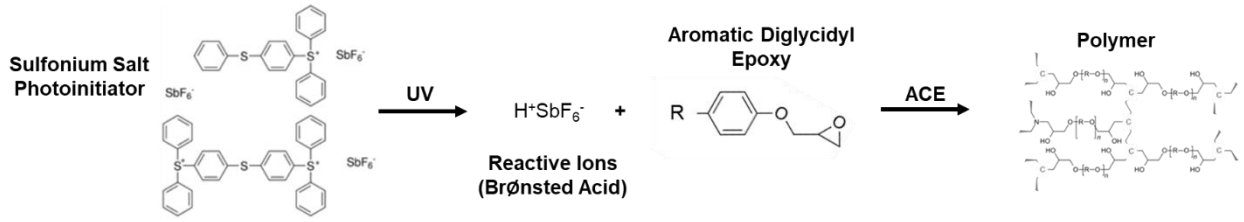

Figure 4. UV cured epoxy polymerization components and reaction schematic.

In literature, the photoinitiator concentration, *in-situ* curing temperature, and UV curing intensity are methods commonly employed to modify the cure state in photopolymerized epoxies [54, 56, 57, 58]. In this work, elevated thermal exposures during the photocuring process are not investigated in order to minimize CTE mismatch stress during cure. Additionally, while the UV curing time plays a large role in the cure state of radiation-cured acrylic systems, UV curing time is insignificant in epoxy resin photopolymerization because of the oxygen insensitivity, complete photolysis in seconds, and few termination reactions [59]. The cure state of UV cured resins can be modified without temperature by varying the photoinitiator concentration and UV curing intensity. These parameters impact the number of reactive ions generated, which in turn, impacts polymerization rate, conversion, and ultimate polymeric properties [54, 56, 52, 57, 58, 60]. While it might be assumed increased intensity and photoinitiator concentration result in a higher cure state, that is not always the case. In the literature, optimal-type trends as a function of several different properties have been documented; for example, cure depth as a function of UV curing intensity [61]. The behaviors and trends are extremely material and processing dependent, therefore, the system used in the replication process must be fully characterized.

In this chapter, we investigate how processing modifications impact material properties in order to perform parametric replication stability studies later in this dissertation. We first vary photoinitiator concentration to characterize the impact of changing catalyst concentration and polymerization kinetics on microstructure development, overall conversion, and final material properties. Then UV curing intensity is varied to generate comprehensive processing-structure-property relationships that govern the specific monomer and photointiator system, as well as any limitations in processing that degrade the material properties. Finally, several thermal post-cures are performed to characterize the shift in properties as a function of temperature and photoinitiator

concentration in order to ultimately compare replication stability to conventional, thermally cured systems. These studies are performed with a single epoxy monomer and photoinitiator identity to prevent chemistry changes from complicating the impact of properties on parametric stability tests.

4.2. Material Selection

Since material selection is fixed, it is carefully performed to produce polymers with material properties most likely to benefit to environmental stability tests. Dozens of photosensitive onium salt initiators can be purchased off-the-shelf, and hundreds can be synthesized, therefore intelligent selection to maximize material properties is critical. The PI chosen for this work is shown in Figure 4 and selected due to its ionic constituents. The cation is the light-absorbing component that controls the dissociation characteristics, in this case selected due to its dissociation wavelength and high-photolysis efficiency. After dissociation, the anion component forms reactive BrØnsted acids which controls the rate of oxirane ring opening kinetics [53, 62, 59]. Studies performed by Crivello demonstrated maximized initiation efficiency, propagation rate, and minimized termination reactions with lower nucleophilicity anions (SbF_6^- > AsF_6^- > PF_6^- > BF_4^-) because they form stronger acids [53]. The impact of anion chemistry on cured properties is showed in Table 2, where the Tg of a polymer cured with same cation, PI concentration, and epoxy monomer are compared. Due to higher efficiency of oxirane ring-opening with the SbF_6^-, a polymer with a higher cure state is produced, which is necessary to maximize replication stability.

Table 2. Tg of epoxy monomer cured with 1.00% PI concentration and different anion identity.

Anion Identity	Tg (°C)
PF_6^-	44
SbF_6^-	104

The epoxy monomer selection is crucial to the physical characteristics of the cured polymer system because the functionality, epoxy class, and backbone chemistry all impact the

processability, kinetics, and ultimate material properties [55, 56]. While an exceedingly high number of epoxy monomers are commercially available, they are not all conducive to UV curing due to processing concerns. Most monomers with a functionality greater than two are a solid at room temperature. Additionally, even if epoxy monomers are highly processable, they may not produce cured polymers with material properties conventionally related to dimensional stability; specifically, mechanical, thermal, and hygroscopic properties. For example, epoxy monomers with linear backbones produce rubbery structures when cured, impractical for replication applications where a high resistance to distortions is required. That leaves two common classes of photopolymerizable epoxy monomers: cycloaliphatic diepoxides and alkyl diglycidyl ethers. To explore the impact of epoxy chemical class on polymerization kinetics and ultimate cured material properties, an off-the-shelf monomer from each class were chosen to study. First, the polymerization kinetics for both systems are monitored in Figure 5 using Real-Time (RT) FTIR methodology to monitor degree of conversion and polymerization rate as a function of time (details in Section 3.3.1). A fast and high overall degree of conversion are desired because they generally trend with cure state of the cured polymer.

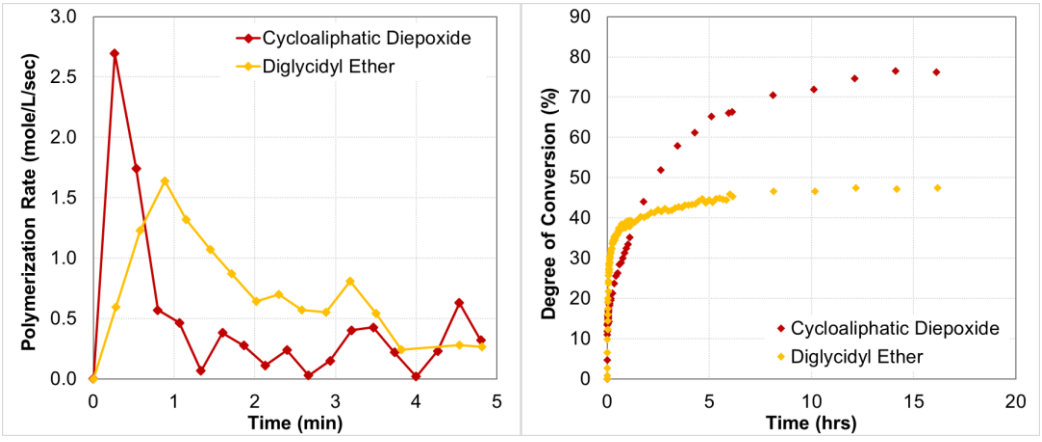

Figure 5. Cure kinetics for two classes of epoxy monomer with 1.00%PI in terms of (a) polymerization rate and (b) conversion.

Most information on polymeric UV curing utilizes RT-FTIR because photopolymerized epoxies are generally employed in industries where ultrafast reactions producing tack-free, highly converted layers are desired. In Figure 5a, the polymerization rate is plotted as a function of time and initially accelerates due to a reduction in termination reactions as the viscosity increases, then plateaus, before decreasing again as monomer mobility and any subsequent and additional crosslinking becomes diffusion limited [59]. While UV curing intensity, PI identity, and PI concentration impact polymerization rate [54, 56, 59, 52], it is apparent in Figure 5a that the maximum polymerization rate is higher for the cycloaliphatic monomer even though the only difference between these systems is the monomer. According to studies performed by Decker, the process of PI dissociation is completed within seconds of UV exposure for sulfonium salt photointiators, and the polymerization rates are due to slow monomer propagation, not limited by initiation [56, 59]. Compared to diglycidyl ether monomer, the cycloaliphatic monomer exhibits higher reactivity due to the extra ring strain associated with the oxirane group bonding directly to the aliphatic ring, and consequently, a faster polymerization rate [63, 64, 65]. Additionally, the overall conversion of the cycloaliphatic monomer in Figure 5b is substantially increased (30%). Higher polymerization rates have been correlated with higher conversion values due to a temporary excess of free volume; cure shrinkage due to crosslinking cannot occur at the same rate as the chemical crosslinking reaction occurs. The increased free volume enhances monomer mobility to reaction sites [59, 52]. With a higher final conversion value, the cycloaliphatic monomer is expected to produce polymers with enhanced elastic modulus, saturated moisture content, and glass transition temperature values.

The physical properties are compared for the two cured epoxy systems in Table 3. Both the elastic modulus and the Tg are significantly higher for the cycloaliphatic polymer than diglycidyl

ether polymer. Due to the lack of stiff aromatic groups in the backbone of cycloaliphatic system, the high elastic modulus value is surprising. However, it is characterized by a significantly higher conversion, which must overcome the lack of the aromatic groups. The cycloaliphatic polymer is also characterized by a Tg of 160°C, which is extremely high for any epoxy, let alone a system cured at room temperature. For comparison, an ultrahigh-performance epoxy resin (Toray 3900) used in composite manufacturing is characterized by a 200°C Tg, though only after a 177°C thermal cure. While the thermomechanical properties of the cycloaliphatic system are extremely high, unfortunately the cured polymer absorbs exorbitant amounts of moisture due to the high concentration of polar hydroxyl groups that attract water molecules. The polymer absorbs nearly 14% water by weight, which is 5x more than the diglycidyl ether. Absorbed moisture is a critical stability concern in replicated composite optics because it can cause large swelling strains (CME ~ 100x CTE values) and degrade the interface between the replicating resin and the composite, causing significant optical distortion or even delamination. Hygroscopic stability of thin epoxy films (similar to the replication configuration) has been widely characterized in the microelectronics industry and touted as the biggest contributor to failure [66, 67]. Though there are several other commercial cycloaliphatic monomers available commercially, due to the relatively high hydroxyl concentration compared to diglycidyl ether monomers, these systems exhibit the same high moisture instability.

Table 3. Summary of physical properties for two classes of epoxy monomer with 1.00%PI.

Modulus (ksi)	Elastic Modulus (ksi)	Saturated Moisture Content (%)	Glass Transition Temperature (°C)
Cycloaliphatic Diepoxide	530	13.8	160
Diglycidyl Ether	415	2.8	104

While the diglycidyl ether monomer appears to be selected by default with inferior thermal and mechanical performance compared to cycloaliphatic, its stiffness and Tg are both still very

high, especially for a material cured at room temperature. However, to see if these properties can be improved upon with a different epoxy monomer in the same class, the material properties of several diglycidyl ether monomers with different backbone structures are summarized in Figure 6. Due to the high stiffness and Tg and low moisture absorption, diglycidyl ether #1 is the clear choice between these monomers to be utilized in replicated composite optics. While the strain-to-failure is reduced compared to the more other, more compliant monomers, this application will never go to those extremes. Of course, in addition to selecting a single photointiator and epoxy monomer, the resin formulation can be tailored in a number of other manners: adding monofunctional diluents to higher functionality monomers to lower viscosity [56], vinyl ethers to increase toughness [63], chain transfer agents to modify polymerization kinetics and network formation on the molecular scale [64], epoxy-siloxane or epoxy-acrylate hybrid systems to enhance thermomechanical and hygroscopic performance [68, 59], etc. However, the goal of this dissertation is a material science approach and parametric study of replication environmental stability, chemistry details can always be later modified once the overarching governing properties are understood.

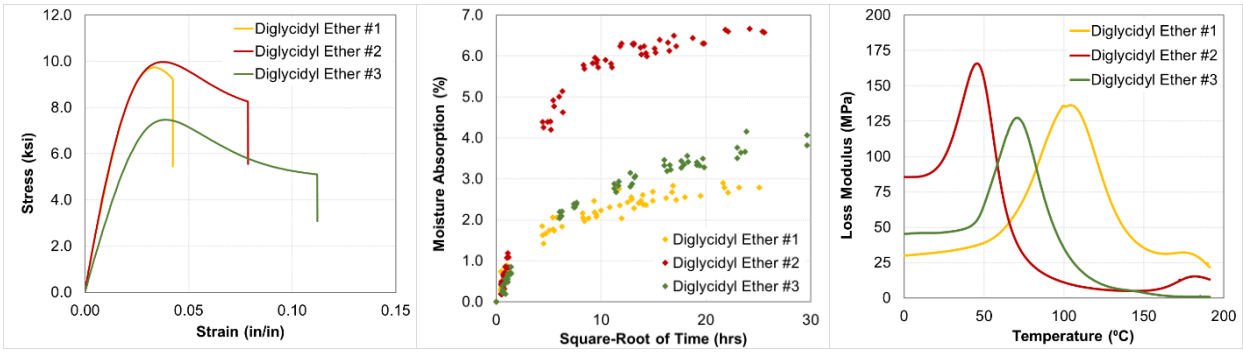

Figure 6. (a) Tensile stress-strain curves and (b) moisture absorption and (c) DMA loss modulus Tg curves for several diglycidyl ether epoxy monomers cured with 1.00%PI.

4.3. Effect of Photoinitiator Concentration

The first modification to the epoxy formulation investigated is the photointiator concentration. Most studies regarding the impact of photointiator concentration are evaluated in terms of the polymerization rate and overall conversion due to use in coating industry. In general, the polymerization rate (as well as conversion due to excess free volume) is expected to increase with PI concentration due to a higher number of reactive ions generated [69, 70, 60, 71]. While most groups [70] indicate polymerization rate and conversion increase as a function of photoinitiator concentration, some groups experience decreasing values above some specific concentration [71, 60]. The latter observation is sometimes attributed to the inefficiency of higher populations of reactive sites competing, causing the reaction rate to be controlled by monomer diffusion to the reactive species instead of proportional to ion concentration. Additionally, if PI concentration is too large, it or its photolysis products can block UV radiation from penetrating deeper into the film, reducing conversion. To better understand whether there are limits in our specific system, characterization is performed for PI concentrations between 0.25% and 5.00%.

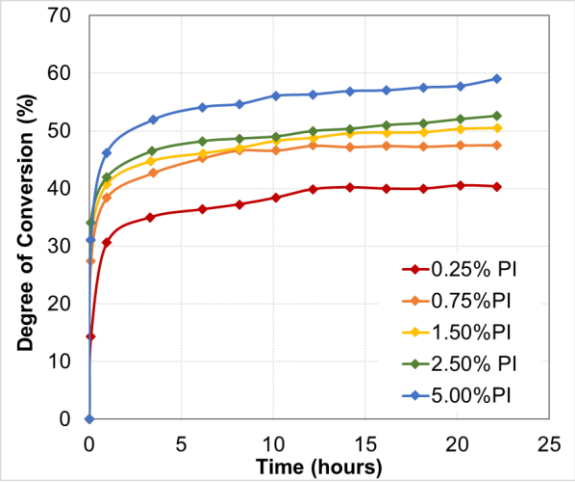

Figure 7. (a) Degree of conversion and (b) polymerization rate versus time as a function of PI concentration.

As shown in Figure 7, the degree of conversion continuously increases with PI concentration between 0.25% and 5.00%. Something to note is the maximum degree of conversion for the 5.00% PI specimen. While 60% conversion is considered low for a thermally cured thermosetting resin, it is a typical conversion value for UV cured epoxy systems [60]. Table 3 and Figure 6a-c demonstrated that even with these low conversion values, the material properties of the cured polymer are high. These low conversions characteristic of photocuring are a result of the ultrafast polymerization reaction because vitrification occurs almost instantaneously, and after several seconds, all conversion is diffusion limited [59, 64, 56]. Since additional crosslinking is diffusion-controlled, conversion is expected to increase with thermal exposures due to enhanced monomer mobility. While the degree of conversion is low compared to a thermally cured system, they increase with higher levels of photoinitiator concentration, which suggests that material properties supporting stability would improve, however, anomalous behavior is detected in the polymerization rate with increasing PI.

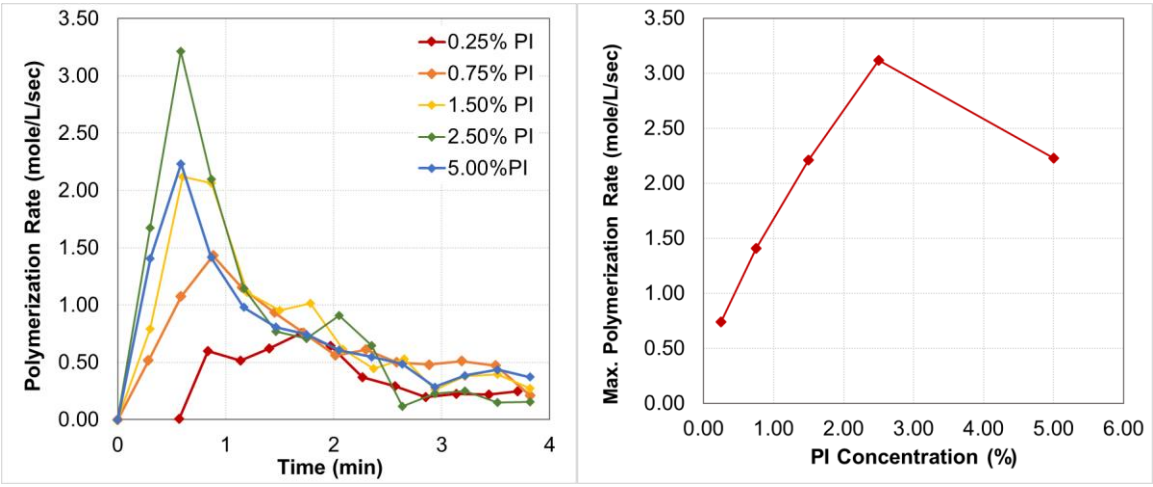

Figure 8. (a) Polymerization rate versus time and (b) maximum polymerization rate versus PI concentration for 0.25, 0.75, 1.50, 2.50, and 5.00% PI.

The polymerization rate is plotted as a function of time in Figure 8a for the different PI concentrations. As the PI concentration increases, there are several changes in the kinetic behavior: the induction time and the time at which the maximum rate occurs are reduced, both due to a higher number of reactive ions instantaneously generated upon irradiation. However, if we focus specifically on the maximum polymerization rate and plot it against the PI concentration, as in Figure 8a, the behavior deviates from the expected. Initially, the maximum polymerization rate increases in a linear manner between 0.25% and 2.50%PI. This behavior is anticipated as polymerization rates have been shown by Decker to be proportional to the number of reaction species generated [56, 59]. At PI concentrations above 2.50% PI, however, that relationship does not hold true and the polymerization rate decreases for the 5.00% PI. In literature, high concentrations of PI/photolysis species have been related to the prevention of UV penetration to deeper regions of the film [72]. Since RT-FTIR monitors conversion on the side of the film not exposed to radiation, and the degree of conversion increases continuously with PI concentration, the reduction in polymerization rate is likely not due to the prevention of UV penetration. Instead, this deviation from theoretical behavior is likely due to the formation of too many reactive sites. The polymerization rate is no longer limited by the rate of reactive ion generation, but by the diffusion of monomer to the reactive sites. While degree of conversion is conventionally associated with high material properties, the deviation from ideal polymerization behavior at higher PI concentrations may impact the material properties.

Material properties commonly attributed to polymeric stability are the elastic modulus, glass transition temperature, and saturated moisture absorption of the resin [73, 74, 35]. The glass transition temperature of a polymer is often related to the chemical structure and degree of polymerization of the resin, and correlates to thermal stability. The elastic modulus is more

correlated to the physical property of stiffness and relates to polymeric resistance to dimensional changes. The saturated moisture content is related to stability through the CME, ratio of hygro-swelling strain to moisture absorption. Therefore, both a high elastic modulus (resistance to dimensional changes) and low moisture absorption (concentration of medium that causes swelling) are required for hygroscopic stability [75]. The saturated moisture content is related to the chemistry and cure state of the polymer. Since the same monomer was used for all PI concentrations, the polarity is similar, and the differences in saturation are likely due to crosslink density and would be expected to track with degree of conversion.

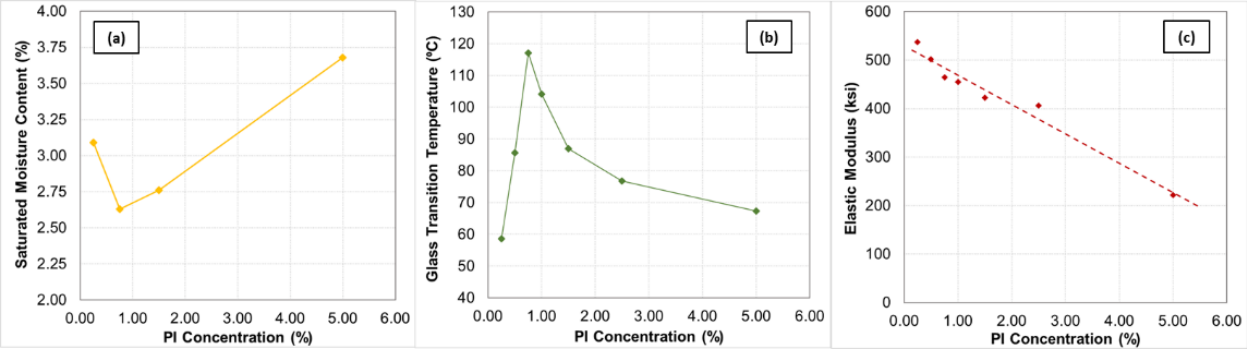

Figure 9. Material properties (a) saturated moisture content (b) glass transition temperature and (c) elastic modulus as a function of PI.

The saturated moisture content, glass transition temperature, and elastic modulus are plotted as a function of photoinitiator concentration and shown in Figure 9. These properties were all expected to increase with PI concentration. However, not only do they exhibit different trends as a function of concentration, none of them are correlated with an increased degree of conversion. The moisture absorption (Figure 9a) and glass transition temperature (Figure 9b) behaviors appear to coupled. There is a minimum saturated moisture content at 0.75%PI, which coincides with the PI concentration with the maximum glass transition temperature. Where the Tg is reduced on either side of the optimal 0.75% PI concentration, the moisture absorption increases. At first glance, one

might think this is related to the kinetic behavior in Figure 8a where a maximum polymerization rate was observed at an optimal PI concentration. However, neither the polymerization rate nor the degree of conversion is maximized for the 0.75%PI concentration. Additionally, the trend in elastic modulus with PI in Figure 9c is entirely different. The modulus linearly decreases with increasing photoinitiator concentration, which is not consistent with the other material or kinetic properties. The 0.25%PI has the highest elastic modulus but exhibits the lowest degree of conversion. The material properties do not behave as anticipated with PI concentration and focusing on the trends or polymerization kinetics does not provide insight into the behavior. In order to control material property formation in future stability studies, we must understand it, therefore a closer look at the raw data is performed.

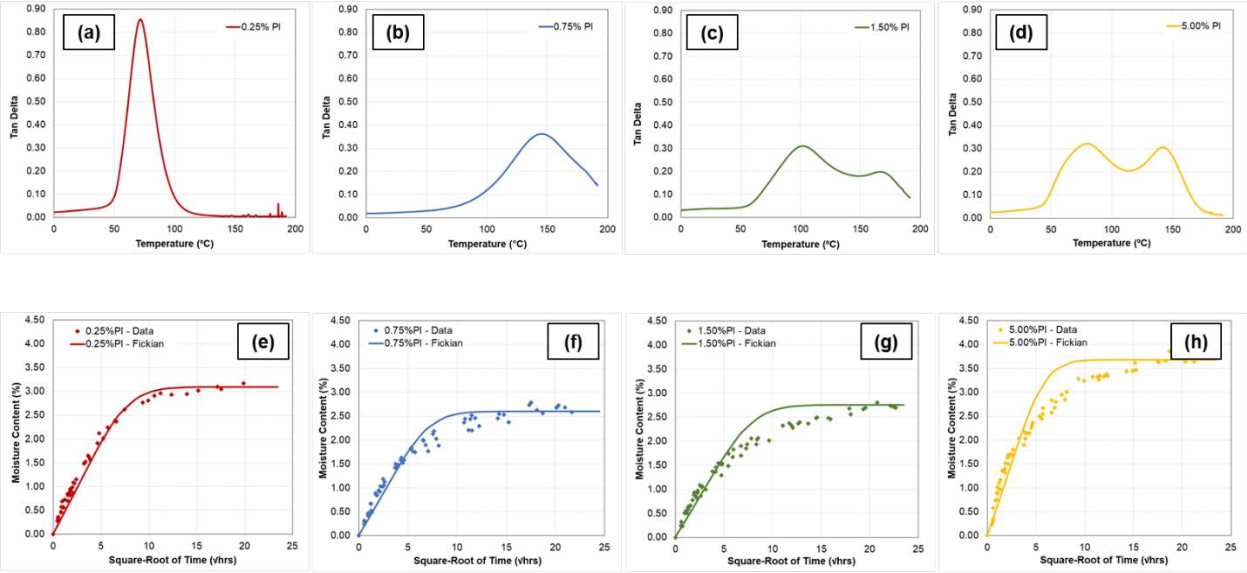

Figure 10. Tan delta curves for (a) 0.25%PI (b) 0.75%PI (c) 1.50%PI and (d) 5.00%PI. Moisture absorption versus square root of time with real data plotted against a Fickian model for (e) 0.25%PI (f) 0.75%PI (g) 1.50%PI and (h) 5.00%PI.

First, a closer examination of the tan delta curves is performed because the heterogeneity of the network can be qualitatively observed by examining the width of the tan delta peak [76]. The tan delta curve can be used to identify the glass transition temperature of a polymer and

represents the thermal transition from a glassy to rubbery state of the polymer. The tan delta curves from our DMA scans are displayed in Figure 10a-d as a function of photoinitiator concentration. For 0.25% PI concentration (Figure 10a), the curve is sharp and narrow, indicating a highly homogenous structure with a low temperature transition at approximately 60°C. The glass transition temperature increases for the 0.75% PI concentration to approximately 115°C as shown in Figure 10b. However, the shape of the peak is broader and appears to be developing a shoulder to the right of the thermal profile. The full width half maximum (FWHM) of the tan delta curve nearly triples, increasing from 24.6°C to 72.5°C, relating to a reduction in the homogeneity of the network as PI is increased from 0.25% to 0.75%. Above 0.75%, the tan delta curves split into two distinct peaks that change in relative height compared to each other. The shape of the tan delta curves indicates further heterogeneity of the polymer network as a function of photoinitiator concentration. Physically, the change in tan delta curve shape and width provides a measured of mobilities that exist within the polymer. Kannurpatti et. al. has described similar networks as highly localized crosslinked regions (microgels) of extremely restricted segmental mobility among areas with loosely crosslinked regions [71]. These features lead to a very broad distribution of mobilities or relaxation times as described by Cook et. al [76]. This description is consistent with the tan delta data collected in Figure 10a-d. Since the UV cured formulation consists of a single monomer, the differences cannot be attributed to phase separation or chemistry differences alone.

In addition to presenting in the shape of the tan delta curves, heterogenous polymeric microstructures often appear as anomalous moisture absorption behavior [75, 77, 74]. The neat resin moisture absorption profiles as a function of photoinitiator concentration are shown in Figure 10e-h plotted against a Fickian model generated from each dataset. The Fickian model describes ideal transport of moisture through a polymer and is described by a diffusion coefficient and a

saturated moisture content [75, 78, 77, 74, 51]. Both the diffusion coefficient (speed) and saturation content are related to the chemistry and cure state of the polymer, for which the trend is summarized in Figure 9a with a minimum at 0.75% PI. However, what is important to note in Figure 10e-h, are the deviations between the data and model as a function of PI concentration. The moisture absorption data for 0.25% PI strongly agrees with the model, indicating the moisture absorption behavior is ideal and can be characterized by a single diffusion coefficient and saturation. With increasing PI concentration, though, there are increasing deviations between the data and the ideal model. Jacobs, et al. demonstrate anomalous moisture absorption behavior with an increasingly heterogenous microstructure and calculate separate diffusion parameters relating to microstructural phase differences [74]. This description is consistent with the data in Figure 10e-h where more than one diffusion coefficient and saturation value are needed to fully characterize the system's moisture absorption behavior due to an increasingly heterogenous microstructure forming with increasing PI concentration.

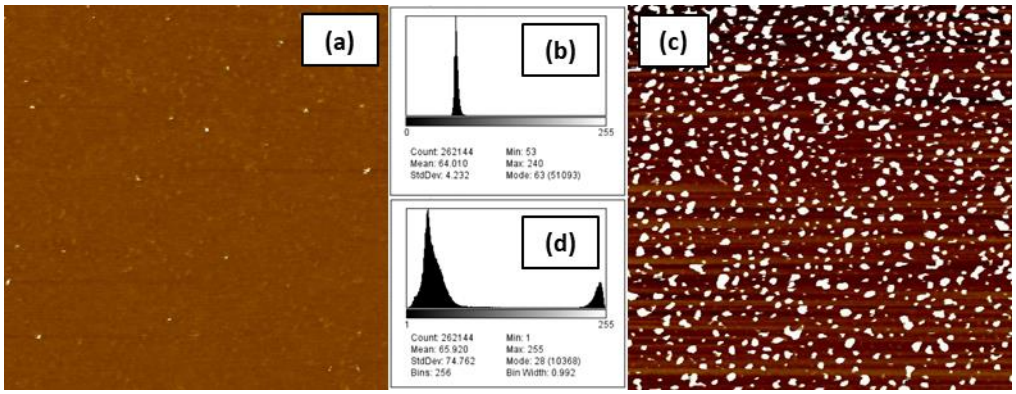

Figure 11. 0.25%PI (a) AFM phase image (1μm x 1μm) and (b) histogram of phases. 5.00%PI (c) AFM phase image (1μm x 1μm) and (d) histogram of phases.

To better corroborate the physical structure of this heterogenous network with the DMA tan delta and moisture absorption results, AFM phase imaging was performed for two extreme PI concentrations. AFM allows for the detection of nanoscale resolution variations in stiffness via

phase lag between the probe oscillation and the material response in tapping mode. In Figure 11a, the phase image of a polymer cured with 0.25% photoinitiator concentration is shown. The image is highly uniform, which is reflected by the sharp and narrow histogram of the image in Figure 11b. However, the 5.00% concentration shown in Figure 11c has two separate, distinct phases visible. The white nodules correspond to the stiffer material suspended within the matrix. The histogram for 5.00% specimen (Figure 11d) indicates these white nodules are on the order ~20nm and are suspended in a loosely crosslinked matrix. These regions correspond to the two peaks on the tan delta curve where the lower temperature peak corresponds to the matrix material and the higher temperature corresponds to the highly crosslinked nodules.

This analysis is consistent with commonly observed microstructures in free radical curing of acrylate systems [79, 59, 80]. Additionally, studies by Kowandi, et al. [81] observing variations in crosslink density for cationic photoinitiation of epoxies provides further evidence for the development of a heterogenous network in our system. Kinetic-gelation models have been utilized to describe network formation as microgels of local cyclization reactions as opposed to crosslinking reactions that are prevalent at low conversions and later joined together [80]. Increasing photoinitiator concentrations result in a more heterogenous microstructure due to a higher number of microgel initiation sites. Since these nodules are highly crosslinked but not strongly anchored to the network, they increase conversion values which erroneously indicate enhanced material properties. While the Tg and moisture absorption initially benefitted from additional crosslinking with PI concentration up to 0.75% PI, material properties ultimately degraded with additional PI due to low conversion values in the matrix regions. A study by Krzeminski, et al. indicated that while the crosslinking spatial variations are low with reduced PI concentrations, the heterogenous nature still exists [79], as is apparent in the linear degradation

behavior of the elastic modulus with PI concentration and increasing FWHM in the tan delta curves prior to the formation of two distinct peaks.

Conventional studies of the photopolymerization process are performed by monitoring the polymerization rate and overall conversion since fast and highly converted systems are desired in the coating industry. However, this technique was not able to accurately predict the trends in material properties due to the formation of an increasingly heterogenous microstructure. Higher PI concentrations exhibited higher polymerization rates and conversions due to the highly crosslinked nodules, however, the material properties were controlled (and degraded) by the lightly crosslinked matrix. Additionally, no single concentration exhibits maximized properties in all environments. Therefore, additional modifications to the formulation and processing are required in order to understand how to tailor individual properties without impacting others.

4.4. Effect of UV Curing Intensity

Now that we have characterized each formulation at a nominal curing intensity and understand how microstructure impacts properties, we are interested in studying the impact of UV curing intensity. Literature studies show that the PI photolysis rate is linearly related to the curing intensity, activating a higher number of photoinitiator molecules, and causing a faster and more complete polymerization reaction [59, 56]. However, as was observed in the study of photoinitiator concentration on properties, a higher polymerization rate and final conversion do not necessarily result in enhanced material properties. In fact, the opposite was shown. By modifying the number of reactive ions generated at a time with UV curing intensity, some high PI concentration formulations may benefit from decreased polymerization rates in forming a more homogenous

microstructure. On the other hand, some low PI concentration formulations may undergo additional crosslinking with a higher curing intensity that enhance the material properties.

To characterize the impact of UV curing intensity on different formulations, the Tg of cured polymers for several PI concentrations is measured between 25-300mW/cm^2 in Figure 12a. The behavior of each PI concentration is entirely different. Starting with the low 0.25% PI concentration, the Tg is not impacted by increasing UV curing intensity. At intermediate PI concentrations (0.75% and 1.50%), the Tg initially increases as a function of UV curing intensity before ultimately decreasing again. It appears that initially, increasing the cure intensity is beneficial, however, at some point, the material properties start to degrade. At the extremely high 5.00% PI concentration, the Tg only decreases with a maximum Tg at the lowest curing intensity. The relationship between PI concentration and UV curing intensity on glass transition temperature is apparent when the UV curing intensity corresponding with the highest Tg is plotted as a function of PI concentration in Figure 12b. The processing parameters appear to be inversely related to each other, likely through reactive ion generation and polymerization rate.

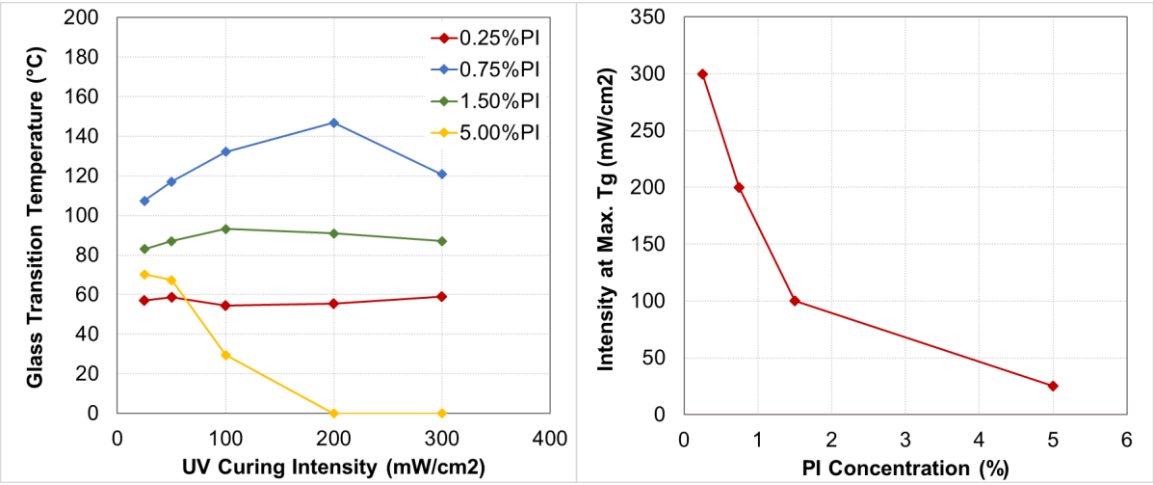

Figure 12. (a) Impact of increasing UV curing intensity on Tg and (b) intensity at maximum Tg as a function of PI concentration for 0.25, 0.75, 1.50, and 5.00%PI.

With high concentrations of PI in conjunction with a high UV curing intensity, the cured polymer exhibits a degradation. A decrease in polymerization rate was previously described for the 5.00%PI sample cured at 50mW/cm^2 due to an extremely high number of reactive species forming and competing. It appears that higher curing intensities of that formulation only exacerbate the problem and a polymer solidified through the entire thickness was not achieved above 100mW/cm^2. On the other hand, slowing reactive ion generation with a lower UV curing intensity appears to benefit that formulation. At extremely low PI concentrations (0.25%), on the other hand, the Tg is relatively insensitive to the UV curing intensity. By modifying the UV curing intensity by over an order of magnitude, the Tg fluctuations are due to testing noise. However, the behavior most interesting to replication stability concerns is the 0.75% PI concentration. This formulation exhibited the highest Tg of all PI concentrations at a nominal curing intensity and can be shifted even higher with UV curing intensity. It is necessary to understand how this impacts other conventional material properties, so the saturated moisture content and elastic modulus are plotted in Figure 13.

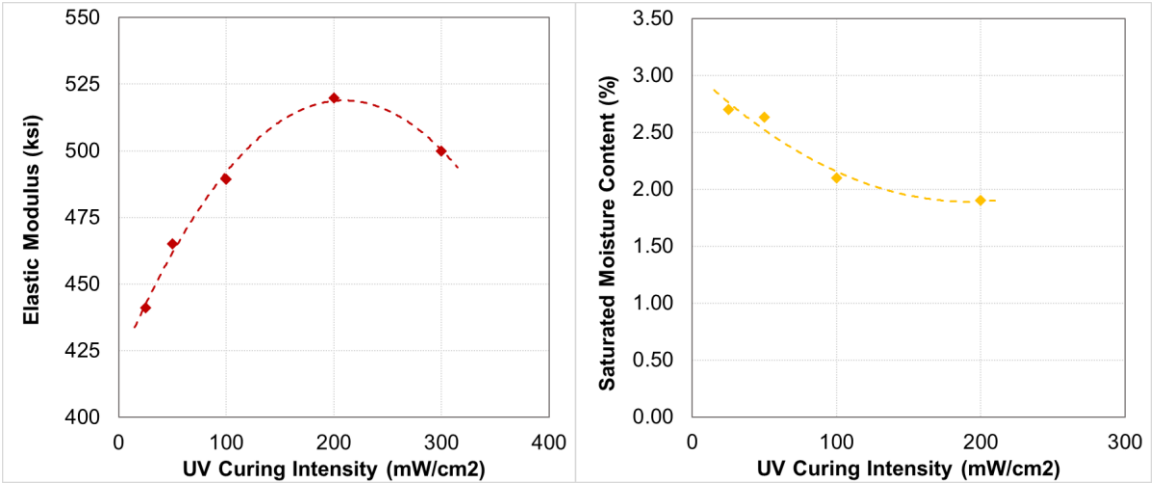

Figure 13. Material properties of 0.75%PI as function of UV curing intensity (a) elastic modulus and (b) saturated moisture content.

The elastic modulus in Figure 13a, behaves similarly to the Tg; the value increases between 25 and 200mW/cm^2 followed by a decrease at 300mW/cm^2. At the maximum, 200mW/cm^2, both Tg and modulus values are similar in magnitude to the cycloaliphatic epoxy monomer properties in Table 3. While the saturated moisture content reduction in Figure 13b with increasing UV curing intensity is not particularly dramatic, the polymer only absorbs 15% of the moisture compared to the cycloaliphatic monomer. By optimizing the material selection, formulation, and processing of a UV cured epoxy resin, the physical properties can be highly modified to produce a replicating resin with properties likely to benefit stability applications. While the properties of the 0.75%PI formulation with 200mW/cm^2 curing intensity are maximized, we still need to understand why the properties are decreasing above that intensity. An interesting point about the Tg and modulus decreasing from 200 to 300mW/cm^2 is that a similar trend was observed as a function of increasing PI concentration due to the heterogenous microstructure.

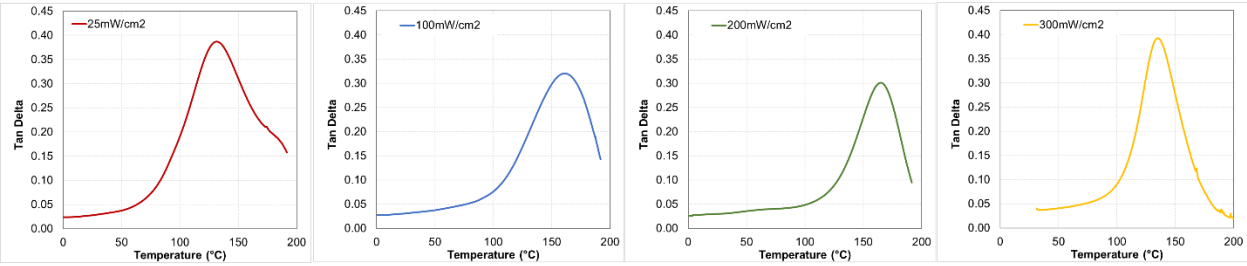

Figure 14. DMA tan delta curves for 0.75%PI as function of UV curing intensity (a) 25 (b) 100 and (c) 200 and (d) 300mW/cm^2.

To determine if the Tg reduction at 300mW/cm^2 in the 0.75%PI formulation is due to an increasingly heterogenous microstructure, the tan delta curves are generated in Figure 14a-d for 25, 100, 200, and 300mW/cm^2. As previously described, the shape and width of the tan delta curves indicate of the homogeneity of the microstructure due to the distribution of polymer mobilities. The polymer exhibits a more homogenous structure with increasing UV curing intensity. The

25mW/cm^2 coupon in Figure 14a displays a distinct, high-temperature shoulder. The shoulder is larger in magnitude than the sample in Figure 10b cured at 50mW/cm^2, but entirely disappears with increasing UV curing intensity. The reduction in a high-temperature shoulder correlates with a reduction in the FWHM of the tan delta curve; dropping from 81°C at 25mW/cm^2 to 46°C at 200mW/cm^2. Most surprisingly, though, is that the FWHM continues dropping from 200 and 300mW/cm^2 (40°C) even though the glass transition temperature decreases. Increasing UV curing intensity results in a more homogenous system, even when the cure state is reduced at ultrahigh intensities.

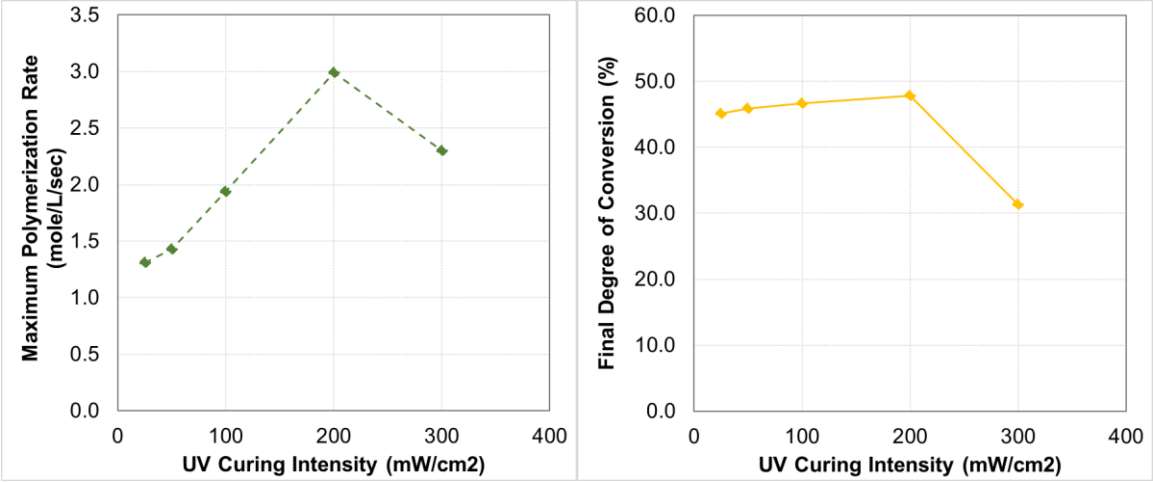

Figure 15. (a) Maximum polymerization rate and (b) degree of conversion versus UV curing intensity for 0.75%PI.

While the cure kinetics did not provide a link between polymerization kinetics and material properties as a function of PI concentration due to the formation of heterogenous microstructure, it did indicate a kinetic degradation for the 5.00%PI due to a high concentration of reactive ions. Therefore, to evaluate whether the source of degradation at high intensities is due to kinetic characteristics, the 0.75%PI formulation is monitored via RT-FTIR between 25 and 300mW/cm^2 and the results are summarized in Figure 15a-b. In Figure 15a, the maximum polymerization rate

is plotted against UV curing intensity. Initially, the polymerization rate increases linearly with intensity due to higher reactive species generated instantaneously. The polymerization rate is maximized at 200mW/cm^2 with a value of ~3.0 [M]/sec, consistent with the maximum rate value in Figure 8b. However, at 300mW/cm^2, the polymerization rate and material properties are both reduced. This may indicate the concentration of reactive ions is sufficiently high to compete for the same monomer molecules, similar to the 5.00%PI cured at 50mW/cm^2; however, the conversion as a function of intensity (Figure 15b) indicates this is not the case. Between 25 and 200mW/cm^2, the degree of conversion slightly increases, corresponding with increases in the material properties. At 300mW/cm2, the degree of conversion sharply drops off to a value of 32%. The reduction in conversion is likely due to the development of species that absorb UV radiation at the film surface, effectively reducing intensity through the thickness, and decreasing both the polymerization rate and overall conversion.

There are many parallels between increasing PI concentration and UV curing intensity; both increase the number of reactive ions formed, enhance polymerization rates, and experience material property and kinetic degradations if too high. However, the mechanisms of degradation are not the same, and furthermore, if the UV curing intensity increases the number of reactive ions generated, it begs the question of how a more heterogenous microstructure is not forming. The key lies in the spatial profile of reactive ion generation. Simply put, as the UV radiation travels through the thickness, it is absorbed by the photoinitiator to form reactive ions, and the intensity is reduced deeper in the film [82, 83, 69]. Immediately following UV exposure, the spatial profile of active centers is a function of radiation intensity at each location and the concentration of PI species [58]. The change in UV intensity as a function of distance is described by Beer's (Equation 5) and is a function of film thickness (z), initial curing intensity (I_0), as well as both the identity (molar

absorptivity (ε)) and the concentration ([PI]) of the absorbing PI species [82, 83, 69]. To model the spatial profile of active centers generated instantaneously, we first measure the molar absorptivity of the photoinitiator. Then using Beer's Law and other parameters to mimic our replication, the active site concentration versus distance into a film is modeled in Figure 16 as a function of PI concentration. At the surface exposed to UV, the active center concentration is the same as the PI concentration, though it is reduced through the thickness.

$$I(z) = I_0(10^{-\varepsilon[PI]z}) \quad 5$$

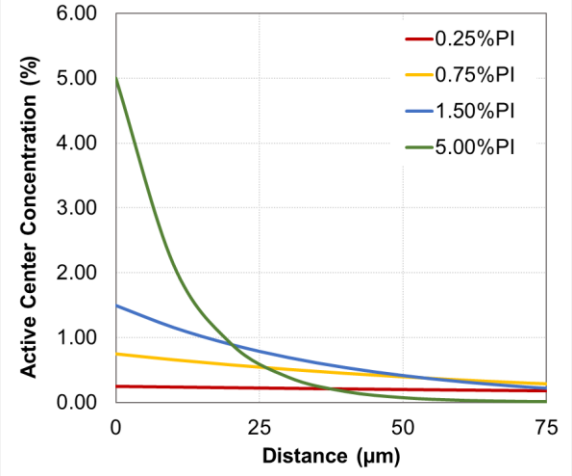

Figure 16. Active center concentration with distance immediately following UV exposure as a function of PI concentration.

Due to the high attenuation of UV intensity, active species in the 5.00%PI sample are concentrated in the first 25μm and none are even generated at the back face. With lower number of absorbing species, UV penetration is deeper and active sites are generated through the entire thickness. This profile changes as a function of time because UV can travel farther into the sample after the surface sites are dissociated [58]. However, due to ultrafast polymerization, the initial behavior describes the trend in polymerization rates. Increased polymerization rates are achieved with higher PI concentrations due to higher total number of reactive sites generated, even though

these sites are highly concentrated in space and lead to a heterogenous microstructure. The increased polymerization rate with UV intensity is unrelated to microstructure. Due to increased photolysis rates with increasing intensity, a higher number of active centers are produced instantaneously and evenly distributed throughout the thickness, leading to a higher polymerization rate. Song et al. similarly observed a faster rate of conversion deeper in the polymer film with increasing intensity [84]. Furthermore, the insensitivity of the 0.25%PI to UV curing intensity can be explained by this mechanism, specifically, that all the PI molecules are dissociated throughout the entire thickness prior to reaching the maximum polymerization rate, even at low curing intensities, due to minimal immediate UV attenuation through the thickness.

4.5. Effect of Thermal Post-Cure

Replication optical quality and stability evaluations later in this dissertation will be compared to conventional thermally cured systems in terms of performance. In order to make these comparisons, we must characterize the material properties of the systems as a function of thermal post-cure temperature. Thermal exposures were performed on all PI concentrations cured at 50mW/cm^2 and post-cured to 50, 80, and 100°C. The impact of the thermal exposure on glass transition temperature is summarized in Figure 17a. Each PI concentration exhibits a different response to the exposures. The 0.75% PI concentration already exhibited a high Tg prior to temperature, therefore the Tg does not shift more than a few degrees. The 0.25% samples increase in a linear manner, though with a small magnitude (20°C after 100°C exposure). The higher PI concentrations (1.50% and 5.00%) are characterized by significantly larger increases in Tg, 40°C increases by both formulations.

The relative behaviors of each formulation appear random, especially since the Tg of the 5.00% initially decreases with a 50°C cure. Therefore, the change in Tg from a RT, UV-cure to a 50°C post-cure is plotted as a function of PI concentration in Figure 17b. At PI concentrations between 0.25% and 1.50%, the rate of increase in Tg appears to be relatively linearly, regardless of initial Tg. Thermal curing is a diffusion-controlled phenomenon where unreacted monomer must diffuse to reactive sites, however it appears to be unrelated to residual monomer content. The relative Tg increase does trend with reduced elastic modulus; if the structure is extremely stiff, chain mobility might inhibit diffusion. However, the behavior changes entirely at 2.50% and 5.00% PI. Both systems are characterized by a decrease in the Tg with a 50°C thermal cure, though the Tg of both formulations does eventually increase with higher temperature cures.

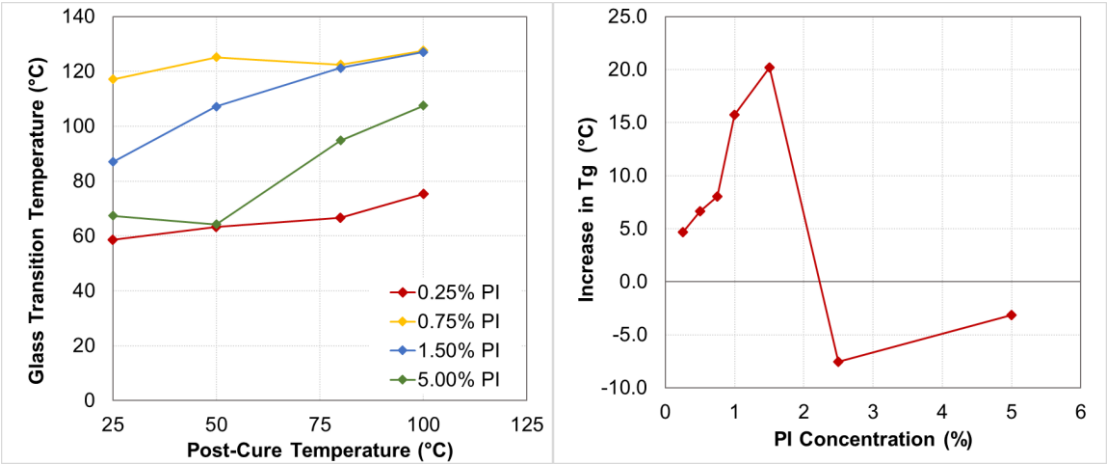

Figure 17. (a) Impact of thermal post-cure on Tg of several PI concentrations. (b) Change in Tg between RT and a 50°C post-cure as a function of PI concentration.

In order to evaluate the relative difference in behavior of the systems, the DMA tan delta curves are displayed for the two extreme concentrations (0.25% and 5.00%) as a function of post-cure temperature in Figure 18. The relative differences in behavior are immediately apparent with these plots. Starting with the 0.25%PI; the peak temperature shifts higher and peak height shifts

lower, and peak width broadens. From these trends in behavior, we can say the Tg is increasing, elastic modulus is increasing, and homogeneity is decreasing, respectively. These behaviors are characteristic of a conventional diffusion-controlled thermal cure. The 5.00% PI behavior, on the other hand, exhibits unusual behavior. With RT curing, the polymer produced was severely heterogenous; the relative peak intensity of the lightly crosslinked matrix thermal transition to the intensity of the highly crosslinked nodules is equal. However, after 50°C, the relative concentration of the microgels appears to be decreasing and the matrix increasing. This phenomenon continues with increasing thermal exposure; the two regions merge and form a single peak at 80°C, which continues narrowing with 100°C. With increasing thermal exposure, the peak temperature shifts higher and the FWHM is reduced from 105°C to 25°C. The driving force, in addition to thermally induced monomer mobility, appears to be the crosslink gradient because of the dissolution of the highly crosslinked regions into the matrix. With increasing PI concentration, the concentration gradient increases, which would explain the increasing magnitude of Tg change apparent in Figure 17b, except for the extreme PI concentrations (2.50% and 5.00%).

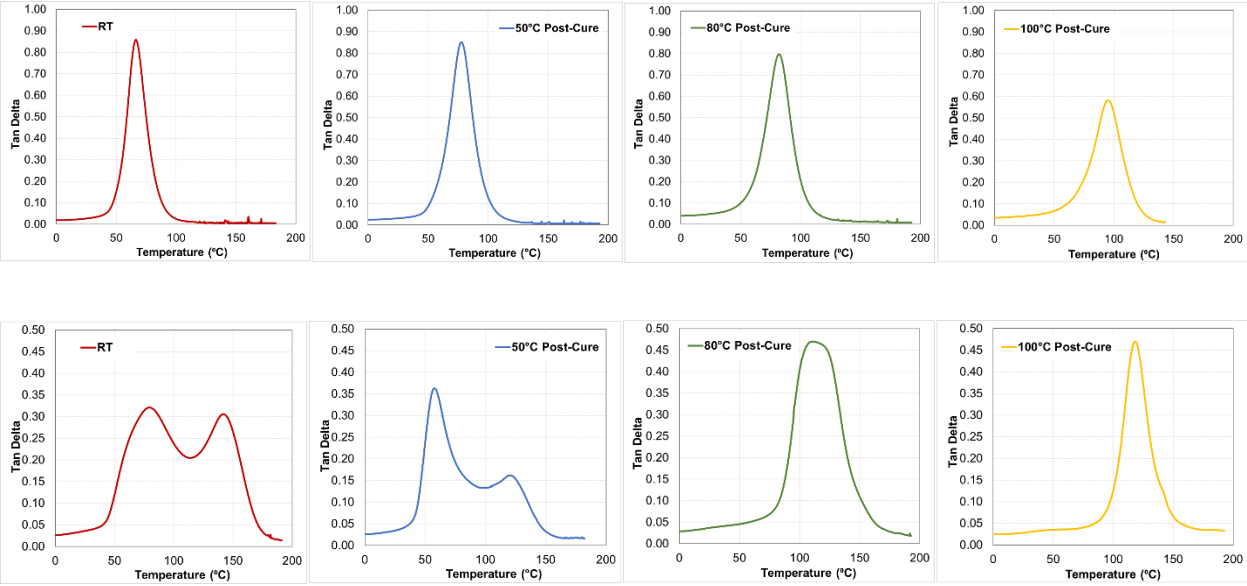

Figure 18. Tan delta curves for 0.25%PI as a function of post-cure temp at (a) RT (b) 50°C (c) 80°C and (d) 100°C. Tan delta curves for 5.00%PI as a function of post-cure temp at (e) RT (f) 50°C (g) 80°C and (h) 100°C.

Thermal exposures enhance the cure state and material properties of all PI formulations, though the effectiveness is highly related to crosslinking gradients preexisting in the microstructure. This is further demonstrated by the differential increase in elastic modulus of 0.25% and 5.00% PI formulations as a function of post-cure temperature in Figure 19. Both formulations exhibit a linear increase in modulus with post-cure temperature, though with different rates. The elastic modulus was previously attributed to the crosslink density in the matrix. The 0.25%PI formulation was already relatively homogenous and additional crosslinking with thermal exposure only modestly enhances its stiffness by 10% to a 550ksi value after 100°C. The 5.00%PI formulation reaches the same stiffness value after 100°C, but the increase from its modulus value at RT is 100% in comparison. The rate of change in the elastic modulus of the 5.00%PI is substantially higher than its change in other material properties, further reinforcing the idea that homogenization act as an additional driving force on top of thermal diffusion and that the elastic modulus is directly related to the crosslink density of the matrix material.

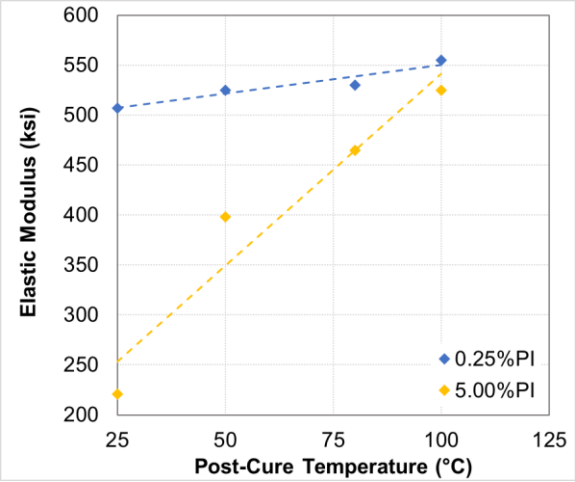

Figure 19. Elastic modulus versus post-cure temperature for 0.25%PI and 5.00%PI concentrations.

While the as-manufactured material properties of high PI concentration formulations are undesirable due to the microstructure, they can be modified with post-thermal exposures to achieve material properties more conventionally related to dimensional stability. However, this is generally undesirable for replication applications due to potential increases in residual stress. Additionally, if a thermal post-cure is necessary, very high temperatures are necessary to fully homogenize the microstructure. Otherwise, the system may experience unknown changes as a function of time and temperature, complicating analyses. For that reason, when thermal post-cures are required for comparison, a fully characterized and well-behaved 0.25%PI concentration system will be utilized.

4.6. Conclusions

The goal of this chapter was to fully characterize the effect of varying formulation and processing on material properties and generate processing-structure-property relationships. These were performed by varying PI concentration, UV curing intensity, and a thermal post-cure of a single epoxy formulation and identifying parameters necessary to tailor specific material properties for parametric replication stability studies in subsequent chapters. By varying the PI concentration, the appearance of a heterogenous microstructure was observed and its critical degrading impact on material properties characterized. Then, by studying the impact of varying UV curing intensity, the spatial uniformity of the microstructure was modified. And finally, by performing a thermal post-cure, it was observed that the microstructure is not permanent and homogenization occurred in addition to a conventional increase in the cure state.

Deviations in kinetic and material property behavior were observed at ultrahigh intensities and PI concentrations due to the generation of too many reactive species that caused out-of-family behavior. In general, though, a higher degree of conversion achieved with a single-phase

microstructure appeared to be the most critical factor in enhancing material property formation. By only varying one parameter (PI concentration or UV curing intensity), the material properties in all environments cannot be maximized and optimization of both is necessary. While undesirable properties could be mitigated with a thermal post-cure, that is undesirable for replication applications due to the tradeoff with optical quality.

At low PI concentrations, the concentration of initiation sites is very low, leading to a highly homogenous system characterized by a high elastic modulus. However, also as a result of the low concentrations of reactive sites, complete consumption of the PI occurred instantaneously regardless of the UV curing intensity, preventing the low hygrothermal stability from being modified by UV radiation. On the other hand, at high PI concentrations, many reactive sites are generated under UV radiation. Due to the proximity of these sites to each other, a heterogenous microstructure was observed that degraded all the material properties. These formulations are also not readily modified with UV intensity due to the ultrahigh concentration of reactive sites, though small improvements are achieved with reductions in intensity. Intermediate PI concentrations, specifically 0.75%PI, exist at the intersection of a beneficial and degrading number of reactive species. Due to the PI concentration, a mostly homogenous microstructure is produced with material properties that can be greatly altered by UV curing intensity. By characterizing the material properties as a function of formulation and processing, replications can now be manufactured, and their stability studied parametrically.

Chapter 5. Impact of Replicating Resin Residual Stress on Optical Quality

5.1. Introduction

Manufacturing surfaces with SFE < λ/20 optical quality is critical to utilizing replicated composite optics in future, large-aperture UVOIR mirrors. A key breakthrough in this regard was achieved by using a molecularly uniform and defect-free mold release layer and optimizing its processing [39]. Therefore, in theory, subsequent replications should be an exact and inverse copy of the glass mandrel on the nanometer-scale. This behavior is observed in Figure 20a-b, where topographic maps of the inverse glass mandrel and its instantaneous replication are shown. This replication was cured at room temperature and characteristic features from the glass mandrel are reflected in the replicated surface. However, the optical surface profile did not appear locked in, and the replication optical quality degrades substantially (150%) from its initial SFE value over time. The change in SFE over the course of three weeks is shown in Figure 20c, where optical quality degrades more rapidly in the first few days and plateauing after about a week.

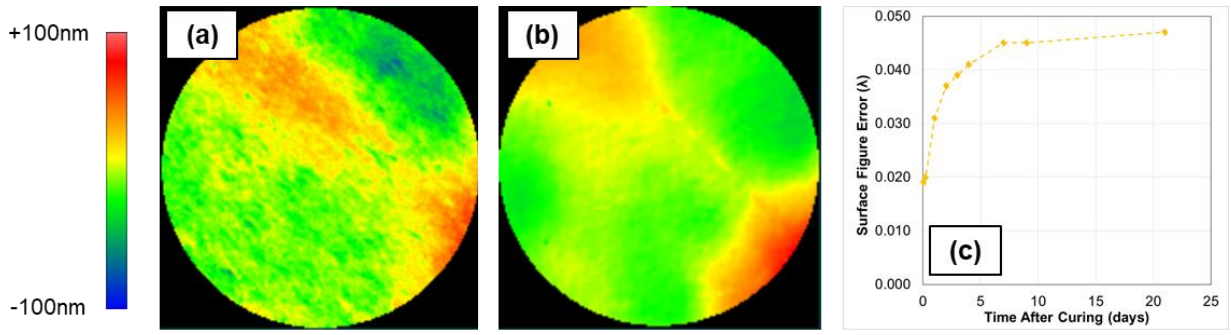

Figure 20. Laser interferometry image of the (a) inverse glass mandrel and (b) instantaneous replication with 1.50%PI and (c) SFE change of replication over time.

Any deviation of the replication optical quality from that of the mandrel degrades optical performance. Typically, the deviations or distortions are apparent at the time of mandrel release

and are attributed to various processing issues such as thermal cure or demolding anomaly. However, a relatively slow drift of the surface profile observed for the first time in Figure 20c and the reason for such behavior in replicated mirrors has not been reported in the literature. In general, there are several conventional mechanisms that can explain polymeric dimensional distortion with time, and moisture absorption is most obvious. However, this replication was stored under a nitrogen environment to avoid the moisture effect, indicating the observed optical degradation is likely due to an intrinsic material change rather than induced by an external environmental change. Since replications are bonded structures, any inherent polymeric dimensional change that occurs after manufacture, such as cure shrinkage, will result in a non-zero residual stress to form. Therefore, understanding the formation of residual stress over time as a function of formulation and processing is critical to maximizing stability. Furthermore, understanding potential quality-stability tradeoffs characteristic of UV cured replications as well as the influence of the resin formulation and processing will provide a more fundamental understanding of the reason behind the optical drift observed in Figure 20c.

In this chapter, we investigate how material and processing modifications impact residual stress formation and replication optical quality in order to produce mandrel-limited surfaces. I will vary both resin formulation and UV curing intensity to relate degradation over time to an inherent resin property; thermal post-processing to relate CTE mismatch magnitude to SFE change; and CFRP material and laminate thickness to evaluate the efficacy of minimizing distortions with increasing composite stiffness. In order to quantitatively evaluate the impact of these material and processing variations on optical quality, a data analysis technique is used to isolate distortions in the replication from the original inverse-mandrel shape. The data is then used to generate a model

predicting degradation in replication optical quality as a function of any resin material and processing history, CFRP material, or CFRP laminate thickness.

5.2. Measuring Optical Change in Terms of Residual Stress

To evaluate optical changes, laser interferometer measurements of the replication are taken as a function of time, as shown in Figure 21a. It is clear in the raw images in Figure 21a that dimensional distortion is occurring over time, though detail of how the changes are manifesting is not immediately clear. This is because the changes to the optical surface are compounded on top of the initial, inverse-mandrel shape of the replication. To isolate the changes to the surface, the raw images can be processed to exclude the dependence on the initial shape by subtracting the initial surface from each subsequent image. By processing the data using this method, a pixel-by-pixel topographic map of the changes only is produced, as shown in Figure 21b. The visual appearance of the subtracted surfaces as a function of time are more systematic than the raw images and it is now apparent that the replication surface is swelling as a function of time.

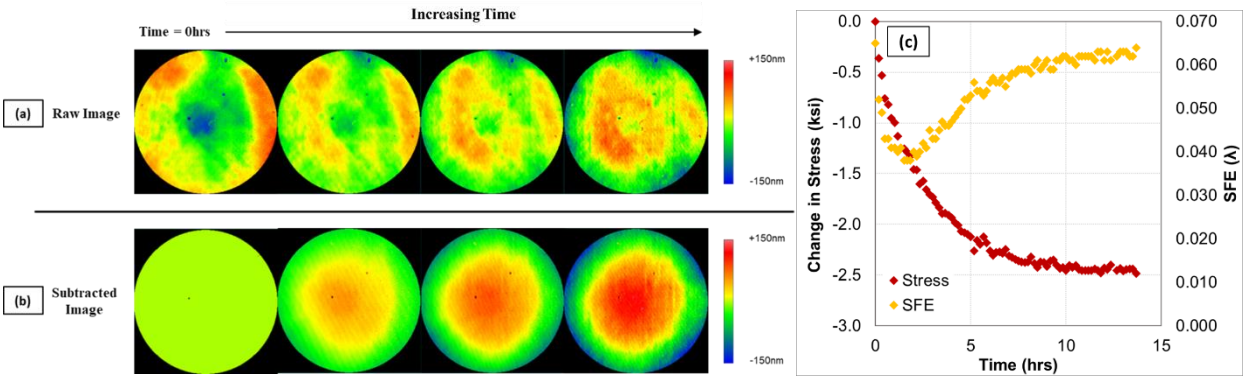

Figure 21. Laser interferometry of (a) raw and (b) processed images as a function of time. (c) Plot of SFE and stress values as function of time.

In addition to qualitative images, the quantitative results of the subtraction technique are significantly more useful then the raw SFE values. By monitoring SFE over time, Figure 21c, the

behavior is complicated. Initially the SFE improves before worsening again. We know from the subtracted images that the surface changes are only moving in one direction (swelling). As the replication swells, the initial concave shape of the raw image is being filled in, flattening the surface and reducing SFE. However, continued swelling pushes the raw image surface into a convex, higher SFE shape. Therefore, the SFE is not a good metric to monitor changes as a function of time due to the dependence of the value on the initial replicated surface shape.

$$\sigma = \frac{E_s t_s^2}{6Rt_f} \qquad 6$$

More methodical quantitative changes can be extracted from the subtracted surfaces than the raw images. As the replication swells (or in some cases shrinks), a spherically-uniform, out-of-plane deformation forms with increasing magnitude over time. This is because as the polymer film changes dimension, it is constrained laterally by its interfacial bond to the substrate, and all deformation must occur out of plane. Since the optical change in the subtracted images are characterized by a uniform radius of curvature, the deformation can be converted to a residual stress value via Stoney's equation. Stoney's equation (Equation 6) calculates the residual stress in the replicating resin film (σ) as a function of the CFRP substrate biaxial modulus (E_s) and thickness (t_s), the film thickness (t_f), and the radius of curvature (R) of the subtracted image [85]. Furthermore, when the residual stress is plotted as a function of time, Figure 21c, the stress values only change in one direction, which is consistent with the observed behavior. Utilizing this subtraction technique removes the impact of initial surface shape from evaluation and will be used to quantitatively compare residual stress magnitude with resin formulation and processing in order to understand root-cause of stress formation. Furthermore, it can be linked to material property differences via residual stress values.

5.3. Residual Stress Formation as Function of Resin Formulation and Processing

5.3.1. Effect of Photoinitiator Concentration

An optical change over time was observed in Figure 20 for a room temperature UV cured replication. We are interested in the understanding the root-cause as well as developing a correlation between some inherent material property and the magnitude of degradation. Therefore, replications are fabricated with a PI concentration ranging from 0.25% to 5.00% and the residual stress of these replications is monitored as a function of time until they stop changing. An example of the replication stress behavior over time for one sample (5.00% PI) is shown in Figure 22a. Immediately following the curing process, the residual stress is zero, however a negative, compressive residual stress forms over the course of ~7days. Similar to the time-scale in Figure 20c where SFE changes were observed, the surface exhibits little-to-no dimensional change following the 7 days. Therefore, we define replication optical degradation as the magnitude of stress that forms over 1 week. The residual stress formation is plotted versus PI concentration in Figure 22b, which spans linearly from tensile (low PI) to compressive (high PI) stresses.

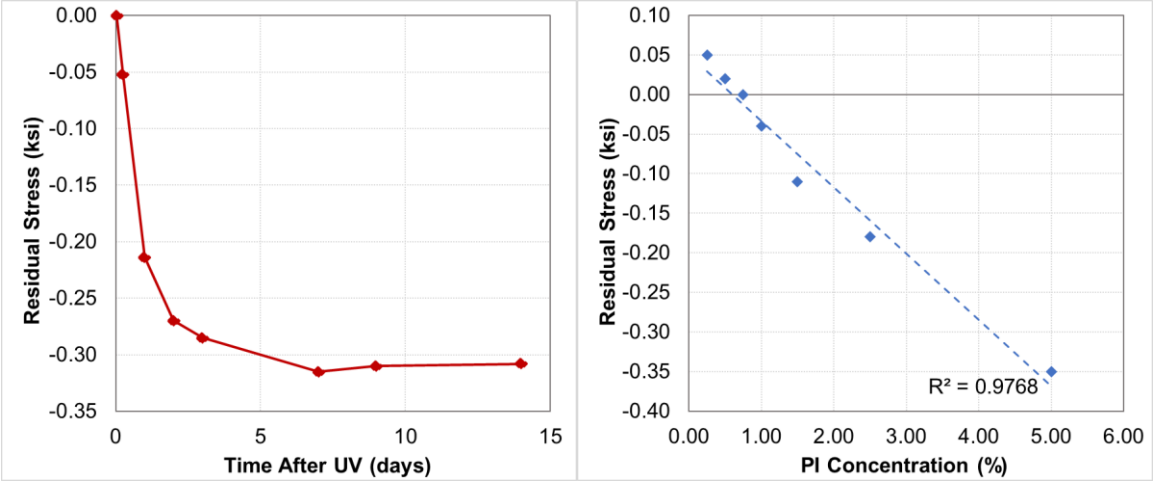

Figure 22. Replication residual stress (a) as function of time for 5.00% PI replication and (b) as function of PI concentration after 7 days.

Tensile residual stresses are consistent with cure shrinkage, which is a byproduct of chemical crosslinking [73]. Since this is unavoidable, the cure shrinkage is evaluated as a function of PI concentration in Figure 23a, with increasing shrinkage as a function of increasing PI concentration. This result is consistent with the degree of conversion measurements in Figure 7 because higher PI concentrations experienced more conversion (covalent bond formation), and consequently a larger cure shrinkage. Interestingly, the shrinkage is linearly related to degree of conversion, even though the microstructures produced are wildly different. However, when the cure shrinkage as a function of time is evaluated in detail, Figure 23b, it is apparent the dimensional changes due to cure shrinkage are only occurring over a time-span of several hours as opposed to the 7 days over which the replicated surface quality degrades. Conventional cure shrinkage is not the primary source of optical distortion over time. In addition to a different timescale over which changes occur, the stress direction is also inconsistent. Most of the replications (PI > 0.75%) exhibit a compressive stress formation over time as opposed to a tensile stress consistent with cure shrinkage. Therefore, to understand the mechanism of optical change, we must understand the formation of compressive residual stresses.

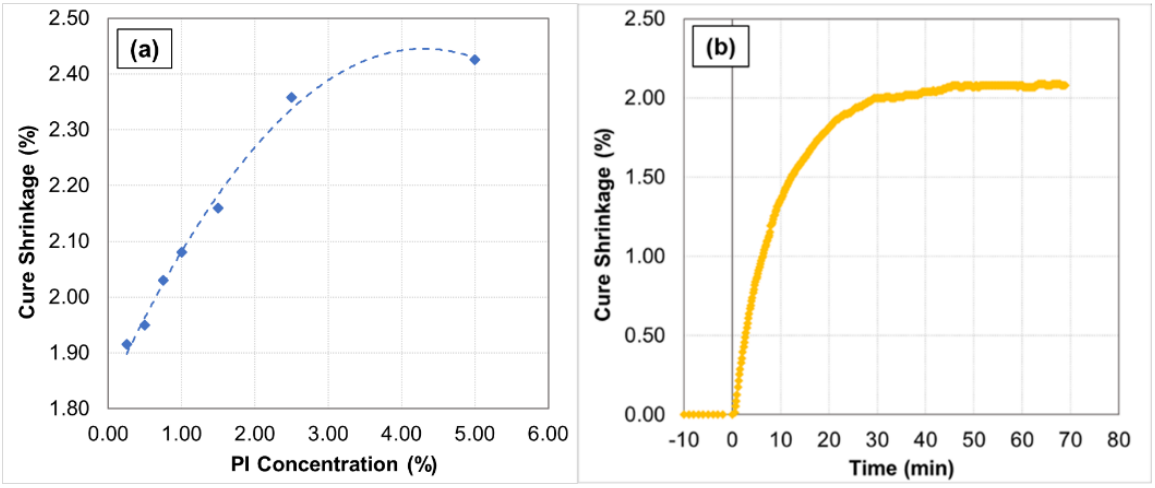

Figure 23. Cure shrinkage versus (a) PI concentration and (b) time for 1.00% PI.

Unlike tensile residual stresses, compressive stresses do not commonly occur in polymer films, and until radiation-cured coatings became popular in the late 1990's the mechanism of formation was unknown. Many studies were performed to understand and control the film stress because failures often occurred due to the formation of large compressive stresses and unwanted wrinkle formation [82, 83, 69, 86]. The mechanism of compressive stress formation was hypothesized to be a result of the cure gradient through the thickness causing a chemical potential to exist between the highly crosslinked solid surface and the less highly crosslinked base. The chemical potential is the driving force for diffusion of the less-cured material into the solid skin over time, swelling the skin [82, 83, 69, 86]. Evidence of this theory as the mechanism of compressive stress formation has been supported by many experiments; confirming the presence of a solid skin [82], monitoring the depth-wise rheological gradient profile as a function of time [69], and correlating the magnitude of solid film swelling to different oligomer bath concentrations [82].

The existence of an intensity gradient in UV cured films is well documented and related to the attenuation of radiation as it travels through the film. Due to reductions in UV intensity deeper in the film, the extent of crosslinking is also reduced, leading to a cure gradient. As previously discussed, the intensity gradient can be modeled using Beer's Law (Equation 5) and is a function of film thickness, PI identity, and PI concentration. The film thickness and PI identity are a constant for the replications manufactured in Figure 22b. Therefore, the only variable impacting stress formation (Figure 22b) that modifies the cure gradient according to Beer's Law is the PI concentration. In order to model the gradient in our systems, the molar absorptivity and film thickness are input into Equation 5, generating intensity profiles as a function of PI concentration

in Figure 24a. It is apparent that the intensity drops as it penetrates deeper into the sample, and that drop occurs more quickly with a higher concentration of the radiation-absorbing PI sites.

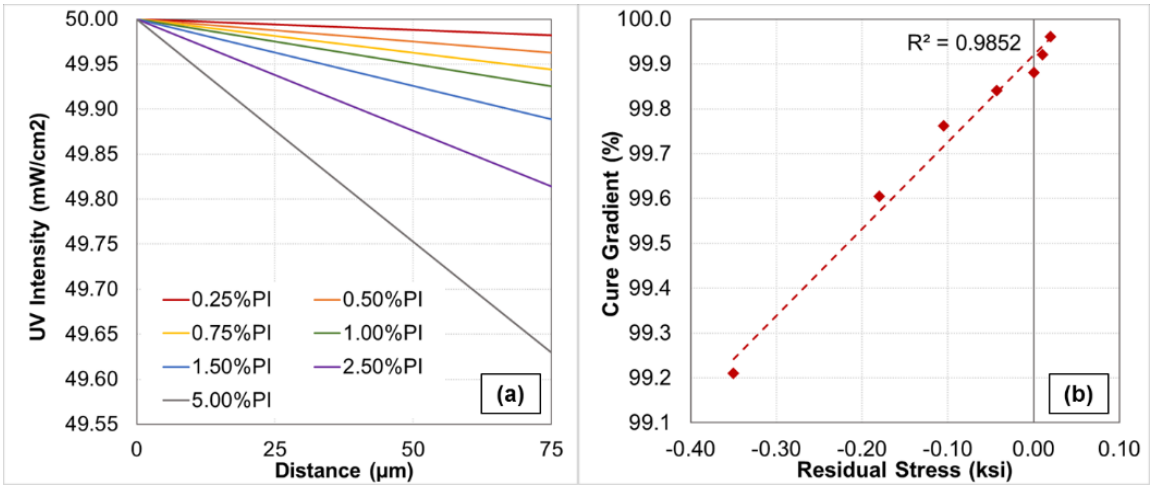

Figure 24. (a) UV intensity versus distance and (b) cure gradient versus residual stress for several PI concentrations.

UV intensity gradients through the polymer film are not disputed, however, to definitively say it is root-cause for optical distortion over time, we need to connect the cure gradient to the formation of compressive residual stresses. The cure gradient is defined as the ratio of intensity at the back face to the incident intensity ($I_{75\mu m}/I_0$ x 100%). A linear relationship is evident between the cure gradient and the compressive stress formation in Figure 24b. A higher cure gradient with increased PI concentration causes a higher driving force for monomer diffusion and corresponds with a higher compressive residual stress. These results are consistent with Payne, et al. where increased wrinkle density and amplitude were observed with PI concentration and attributed to larger intensity gradients [86]. However, at low PI concentrations, the cure gradient is small and cure shrinkage appears to counteract the compressive stress, causing a net-zero stress at 0.75% PI, and even shifting the 0.50% and 0.25% PI replications into small, but net-tensile stresses. It is interesting to note that though each film exhibits different material properties, conversion, and microstructure, the diffusion of less-crosslinked material into the solid skin was not impeded. This

behavior is further reinforced by the degree of conversion plot, Figure 7, where all PI concentrations undergo a very similar amount of diffusion-controlled conversion following the removal of UV radiation.

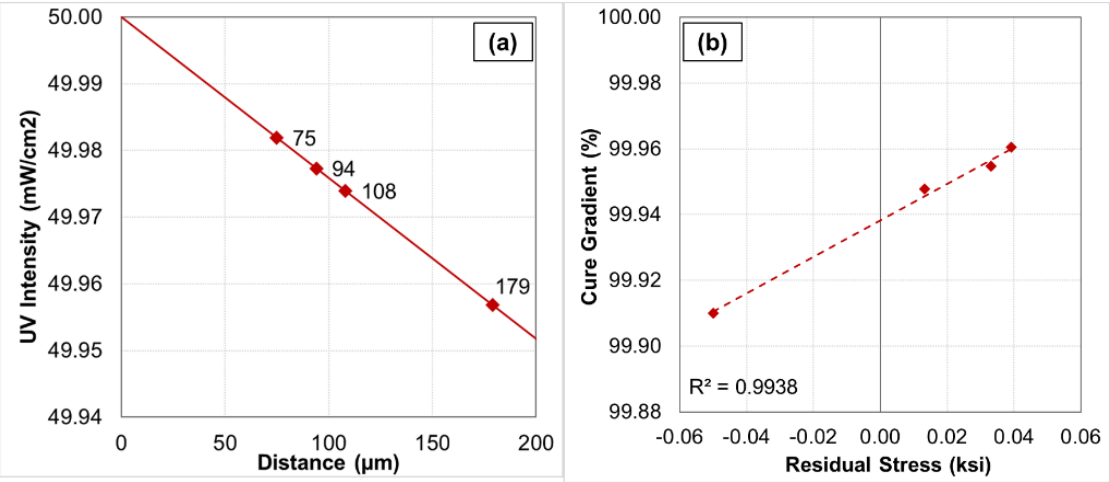

Figure 25. (a) UV intensity versus distance and (b) cure gradient versus residual stress for 0.25% PI concentration replications fabricated as a function of thickness.

While there exists a linear relationship between cure gradient and residual stress as a function of PI concentration, the tensile stresses formed at low gradients do not strongly reinforce this mechanism. Additionally, the 0.25%PI cure state was observed to be indifferent to UV curing intensity in Figure 12a specifically because the radiation was not absorbed highly during photoinitiator dissociation. Therefore, replications with 0.25%PI concentration were manufactured as a function of increasing thicknesses to evaluate whether a small concentration of the absorbing PI species results in a compressive stress if the film is sufficiently thick. The UV attenuation (Figure 25a) was modeled using Beer's Law (Equation 5) and residual stress monitored over time for replications manufactured with different film thicknesses. A linear relationship exists between cure gradient and residual stress (Figure 25b), spanning from tensile at thin layers to compressive with thicker layers. This observation reinforces the mechanism of cure gradient driving compressive residual stress formation in radiation cured films and is consistent with literature

studies; Stolov et al. for example, observed a reduction in tensile stress with increasing film thickness [83]. Furthermore, the cure gradient at which the zero-stress state exists is roughly 99.94%, like the value for zero stress in Figure 24b as a function of PI concentration.

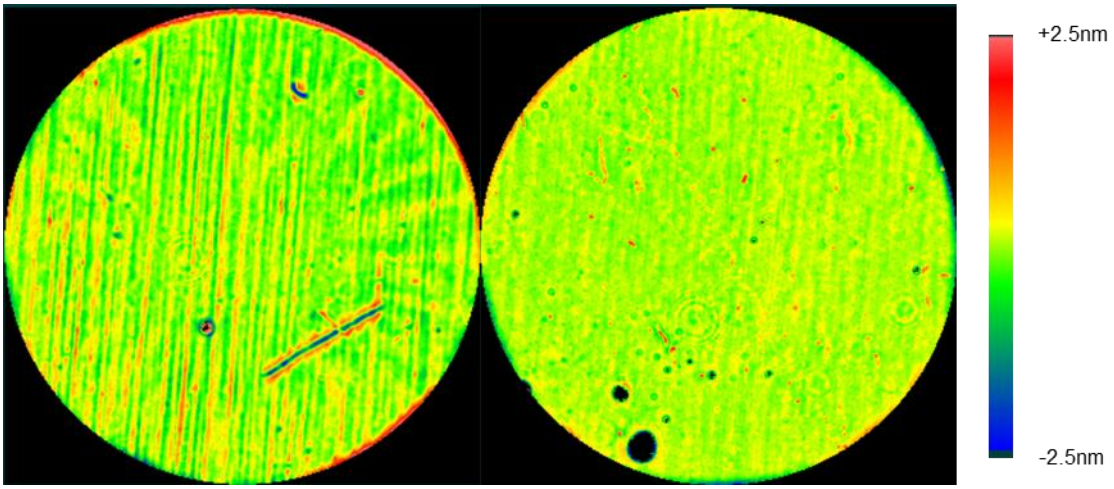

Figure 26. Interferometer images with a band pass filter (100-1500μm) to highlight fiber print-through on replications with (a) 25μm and (b) 75μm thick resin layers.

Since the cure gradient value corresponding with zero stress in this specific resin formulation is known, film thickness can be tailored to engineer zero-stress replications as a function PI concentration. However, as replication thicknesses must become very thin to achieve zero stress with high PI concentration samples, another optical quality issue becomes more prevalent: fiber print-through. Carbon tows in the CFRP composite can transpose their geometry to the surface of the replicating epoxy, causing roughness in the mid-range spatial frequency and degrading resolution. The impact of resin thickness on the magnitude of print-through is shown in Figure 26 for replications manufactured with 25μm and 75μm resin layers. The surfaces have been filtered to highlight the features and measure roughness in the mid-frequency domain. In Figure 26a where the film is 25μm thick, the fiber features are distinct with high intensities, leading to a 6.3nm SFE error. By increasing the film to 75μm in Figure 26b, the fiber print-through features

are diffuse, lower intensity, and not continuous across the face of the replication, corresponding with a reduction in SFE error to 2.5nm. High errors in this regime are not tolerated for space based UVOIR mirrors; future missions require <5nm in this region [3]. The film thickness necessary to achieve a zero stress with 5.00%PI is 5μm, substantially thinner than the films in Figure 26. The roughness on the 25μm thick film is already too high for precision space missions, let alone 5μm thick films; therefore, tailoring film stress with thickness is impractical.

All the PI concentrations except one was characterized by a non-zero residual stress that degrades the replication from mandrel-limited optical quality. It should be noted, though, that these stresses are very small in comparison to thermally induced CTE mismatch stresses; the largest value is -0.35ksi for the 5.00%PI concentration. These small stresses are undesirable but will induce substantially less optical distortion than a conventional two-part epoxy resin cured at an elevated temperature. The 0.75%PI concentration replication is characterized by zero residual stress due to the balance of cure shrinkage and cure gradient-induced compressive stress.

5.3.2. Effect of UV Curing Intensity

The impact of modifying material properties with UV cure intensity was previously investigated in Section 4.4. The benefit of increasing the curing intensity was demonstrated for several PI concentrations where higher radiation resulted in polymers with enhanced material properties. This was specifically demonstrated in Figure 12a for the 0.75%PI formulation where the Tg was shifted up 40°C by increasing the cure intensity from 25-200mW/cm^2. Coincidentally, this also happens to be the PI concentration associated with a zero-residual stress (Figure 24b). If the material properties could be modified without inducing any residual stress, that would be extremely beneficial to replication stability studies. While in theory, the residual stress formation

should not be impacted by the UV curing intensity because the cure gradient is a ratio across the film thickness; in reality, several studies have reported changes in stress formation when the curing intensity was modified. Whether UV intensity impacts stress formation appears to be highly dependent on material, curing, and thickness of the system [86, 83, 87, 88]. For example, Luciani et. al observed a reduction in compressive wrinkle formation due higher crosslinking deeper in the film [87] while Schmidt et al. attributed a higher tensile stress to increased conversion and cure shrinkage [88].

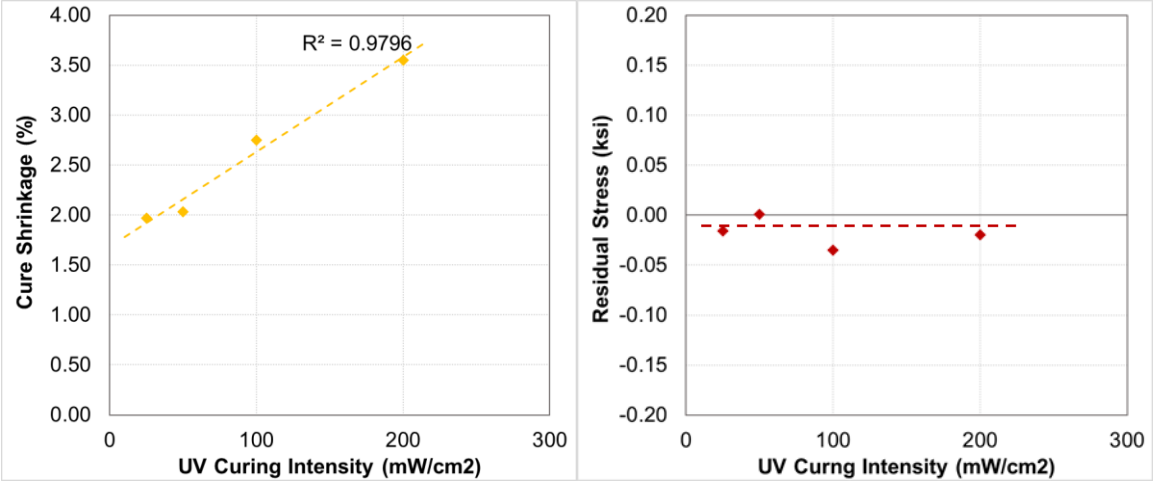

Figure 27. UV curing intensity vs. (a) cure shrinkage and (b) residual stress.

We previously observed the importance of cure shrinkage in stress formation for low PI concentration replications in Figure 24b. Since polymeric conversion increased with UV intensity in Figure 15b, the cure shrinkage also is likely to change with intensity. To evaluate cure shrinkage, a UV coupled-rheometer was used to monitor the dimensional change from monomer to polymer as a function of UV curing intensity, which is shown in Figure 27a. The shrinkage increases with intensity due to increased conversion values which may impact residual stress formation, though the only way to know is monitor stress formation. Therefore, replications are manufactured with 0.75% PI between 25-200mW/cm^2 and residual stress formation plotted versus intensity in Figure

27b. Surprisingly, the residual stress is entirely independent of the UV curing intensity, though there are slight variations due to noise between the samples. This behavior follows the theoretical prediction according to Beer's Law and is optimal for our applications.

Some of the studies in literature where stress was modified by UV curing intensity might be due to a change in the cure gradient. For example, in wrinkle coatings, the gradient is so severe that the UV radiation is fully absorbed before reaching the back-face and liquid resin was still present. For our system where cure gradient is not impacted by increasing the cure intensity, stress insensitivity would make sense. However, the cure shrinkage increases with UV intensity, but that behavior is not reflected in residual stress formation. While shrinkage increases, not all shrinkage results in tensile stress formation; only after the liquid monomer undergoes adequate conversion and gelation to adhere to the substrate [86]. Furthermore, as found by Schmidt et. al [88] and Stolov et.al [83] higher UV curing intensity retards onset of tensile stress because it delays the gelation of the film, negating the increased net shrinkage from impacting stress formation. Due to observed indifference of the residual stress formation to UV intensity, the delay in resin gelation with higher intensity offsets the increased cure shrinkage, resulting films with a residual stress formation insensitive to curing intensity. This is specifically beneficial for the 0.75%PI concentration because of its zero-stress state, leading to mandrel-limited optical quality for several cure states.

5.3.3. Effect of Thermal Post-Cure Temperature

Thermal post-curing is the most common and conventional technique to increase resin cure state, however, it is known to induce optical distortion (Figure 3). Since we now understand the source and magnitude of stress formation in UV cured replications, we are interested in comparing the stress incurred by thermal post-treatments, specifically as a function of post-cure temperature.

These comparisons will continue throughout the dissertation to evaluate if equivalent performance during stability testing can be achieved with RT curing. Replications will be manufactured with 0.25%PI concentration, post-treated for 16hrs at 50, 80, and 100°C, and the residual stress evaluated. The formulation was selected due to its homogenous microstructure that does not change with thermal post-cure, its insensitivity to cure state modification without thermal, and the material properties.

Table 4. Properties of 0.25%PI replication post heat-treated to 50, 80, and 100°C.

Post-Cure Temperature (°C)	Residual Stress (ksi)	Cure Shrinkage (%)	CTE (μm/m/°C)
25	0.04	-	75.80
50	1.90	0.15	54.68
80	3.51	0.22	51.83
100	4.66	0.27	50.70

The residual stress that forms due to each post-cure exposure is shown in Table 4. Thermal post-processing induces highly tensile stresses compared to RT cured samples. Even a modest 50°C post-cure for the 0.25%PI shifts the residual stress ~2ksi in tension. This residual stress value is greater than 5x the magnitude of any replications cured at room temperature as a function of PI concentration. With RT processing of the UV cured resin, the largest stress formed was -0.35ksi, however, an equivalent stress would be formed by <10°C thermal post-cure. During a thermal exposure, tensile stresses can form as a result of cure shrinkage, stress relaxation, CTE mismatch between the substrate and resin layer, or a combination of all the above. Table 4 also summarizes the cure shrinkage during the post-cure which was measured by placing RT cured neat resin in a TMA for 16hrs at the various temperatures and monitoring the change in dimension. The shrinkage leads to a change in stress state because the dimension of the resin film shrinks while adhered to the composite substrate. Shrinkage can be converted from a percentage to a stress value using Equation 7, where E_f is the biaxial modulus of the replicating resin, and is shown as a function of post-cure temperature in Figure 28a. The stress arising from cure shrinkage is substantially smaller

than the stress forming in the real replications exposed to each temperature, indicating it is not the only mechanism of dimensional change during thermal exposure.

During the thermal hold at elevated temperatures, stress relaxation can also occur, in which the thermal energy increases polymer chain mobility, allowing movement in a manner to partially or fully relieve internal stresses. If stress is fully relieved at the elevated temperature, that is the new zero-stress state. During cool down, the stress induced is a function of the delta temperature (ΔT) and CTE mismatch of the resin and substrate components as calculated by Equation 8. The residual stress formed by CTE mismatch is shown in Figure 28a as a function of post-cure temperature. Full stress relaxation at the elevated temperature followed by CTE mismatch also results in a residual stress less than the real stress measured in the replications. Neither the cure shrinkage nor stress relaxation-CTE mismatch mechanisms can fully describe the behavior of the replications individually.

$$\sigma_{Shrink} = \%\, Shrinkage\ x\ E_f \qquad 7$$

$$\sigma_{CTE} = \left((CTE_f - CTE_s)x\ \Delta T\right)E_f \qquad 8$$

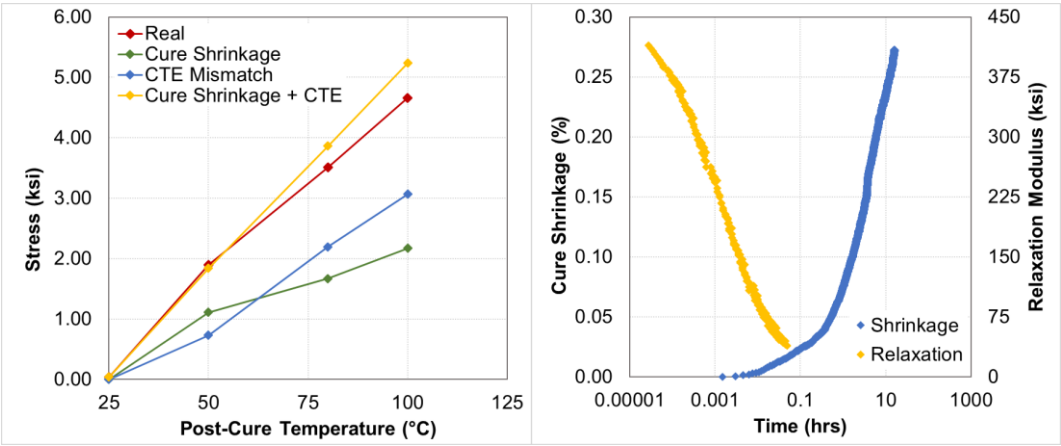

Figure 28. (a) Stress due to real 0.25%PI replication, cure shrinkage, and CTE mismatch as a function of post-cure temperature. (b) Relative rates of stress relaxation versus cure shrinkage.

If stress relaxation-CTE mismatch and cure shrinkage stress contributions are added together, as shown in Figure 28a, they account for the real stress formed in the replication as a function of post-cure. For this to be true, however, stress relaxation must occur substantially faster than the rate at which cure shrinkage occurs. Otherwise, the shrinkage will be relaxed later in time at temperature, and tensile stress formation is only due to CTE mismatch stresses. Stress relaxation rates can be predicted with time-temperature superposition (TTS) testing, which relies on the principle that viscoelastic polymers behave the same at higher temperatures and longer time (details in Section 3.4.2). Relaxation behavior for 0.25%PI neat resin at 50°C as a function of time is shown in Figure 28b. Full stress relaxation at RT occurs in ~10days, however, that time is substantially shortened at higher temperatures; occurring in <1hr at 50°C and even less time at 80°C and 100°C. Cure shrinkage of the 100°C post-cured sample is plotted on the same graph as relaxation in Figure 28b in order to visualize the relative rates of each with respect to each other. The onset of the shrinkage is delayed, with the majority occurring between 1 and 16hrs. More than 95% of the stress has relaxed at the point when cure shrinkage starts to occur. Due to the significantly faster relaxation than shrinkage, both mechanisms are necessary to describe the formation of residual stress in 0.25% PI replications as a function of post-cure temperature. The impact of thermal post-cure on stress formation would be minimized with a resin that is characterized by both a minimal cure shrinkage and a significantly slower stress relaxation.

The TTS stress relaxation behavior is plotted as a function of PI concentration in Figure 29a, which is highly related to previously characterized material behavior. In these plots, the instantaneous relaxation modulus is virtually identical to the static elastic modulus of the sample [89]; with increasing PI concentration, the value drops similarly to Figure 9b. With increasing time, the relaxation modulus slowly decreases until it reaches a “flow” region in which the

relaxation modulus sharply drops off with time. The time at which flow onsets is generally correlated with crosslink density due to long-range mobility [89, 90]; the 0.25%PI has the lowest degree of conversion (Figure 7) and earliest onset. With increasing conversion as a function of PI concentration, the onset of flow shifts later in time. Additional information can be gleaned from the slope of the flow region. Steeper slopes in this regime correlate with reduced molecular weight distributions, or a higher homogeneity in the microstructure [89]. The 0.25%PI sample is characterized by an extremely sharp slope due to its homogenous microstructure; the slope gradually decreases with increasing PI concentration as the heterogeneous microstructure (Figure 10 and Figure 11), or crosslink distribution, is increasing. Furthermore, Lee et al. [91] have shown nanoscale reinforcements in an epoxy matrix (similarly to the highly crosslinked nodules) can shift the flow region later in time and reduce its slope, which is consistent with the observed behavior in Figure 29a and might be additionally contributing to the later onset and reduced slope of the flow region. It should be noted that the master curve for any PI concentration above 1.50% was not accurately measured due to the extremely high driving force for molecular rearrangement with heterogenous microstructure. During the test, the thermal exposure was enough to induce the homogenization of the structure and change the properties.

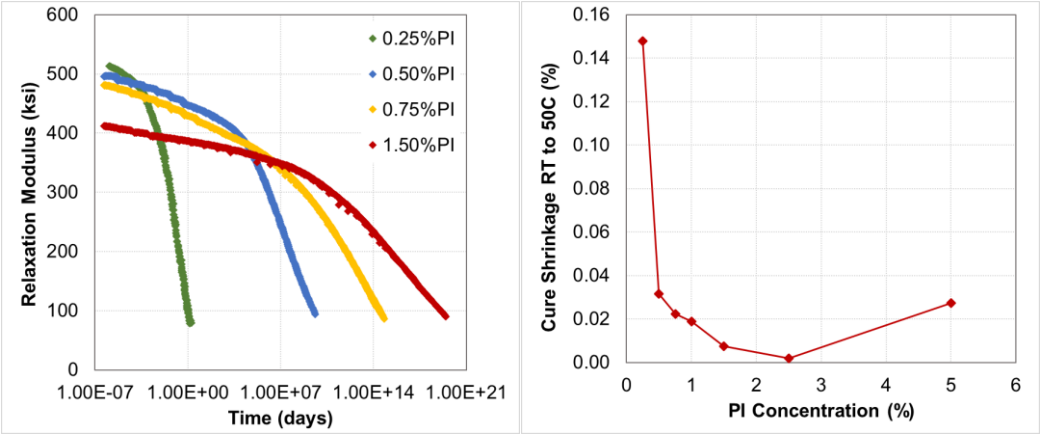

Figure 29. (a) TTS plots and (b) cure shrinkage at 50°C as a function of PI concentration.

The cure shrinkage due to a 50°C hold is also shown as a function of PI concentration in Figure 29b. Cure shrinkage is the highest for 0.25%PI and decreases with increasing photointiator, up until 5.00% PI where it increases again. While the degree of conversion is lowest for low PI concentrations, which would lend itself to being highly modified by a thermal cure, this behavior is not consistent with change in Tg due to a 50°C post-cure previously measured as a function of PI concentration. In Figure 17, Tg values increased more with higher PI concentration, which does not correlate with decreasing shrinkage values. The prior change in Tg observed is likely not a result of additional crosslinking, but due to conformational change; due to the highly homogenous microstructure, the 0.25%PI experiences the largest amount of thermally induced crosslinking, and consequently, the largest cure shrinkage. In this case, the low degree of conversion and homogenous microstructure in the 0.25%PI cause a fast stress relaxation and high cure shrinkage. By increasing the PI concentration, slower stress relaxation and reduced shrinkage are likely to contribute to a higher thermal stability and reduced tensile residual stresses.

5.4. Relating Residual Stress to Optical Quality

The formation of residual stresses in UV cured replicating resins was investigated as a function of formulation, processing, and thermal post-processing. Any change to the resin stress state drives an optical distortion. However, the impact of stress on SFE degradation has not been quantified because this value is highly dependent on the CFRP composite substrate. By increasing the stiffness of the composite, the substrate can resist deformations and reduce the SFE distortion induced by the resin residual stress. We want to understand the quantitative relationship between composite stiffness and SFE, then use the experimental data to build a general model predicting optical quality degradation.

5.4.1. Optical Quality as a Function of Resin Residual Stress

We previously fabricated replications as a function of PI concentration (Section 5.3.1) with a wide range of residual stress values spanning from tensile to compressive, so we first evaluate the optical degradation of these replications to isolate the relationship between stress and SFE degradation. All replications utilized the same composite substrate material and thickness, so the only difference is in resin stress. The optical changes to several different PI concentrations are isolated with the subtraction technique and shown in Figure 30. In Figure 30a-c, the distortions due to residual stress formation in 0.75%, 1.50%, and the 5.00%PI replications are shown. The 0.75%PI replication is characterized by a very flat surface with no global shape change. Only diffuse, local changes in features are present, likely due to angular alignment during processing or localized thickness changes. With increasing PI concentration, the residual stress becomes more compressive and the optical distortion manifests as a concave surface. The magnitude of distortion increases with stress; the residual stress of the 5.00%PI sample in Figure 30c is approximately twice as large as the 1.50%PI sample in Figure 30b. However, it is important to correlate the SFE degradation with specific values of residual stress in the film.

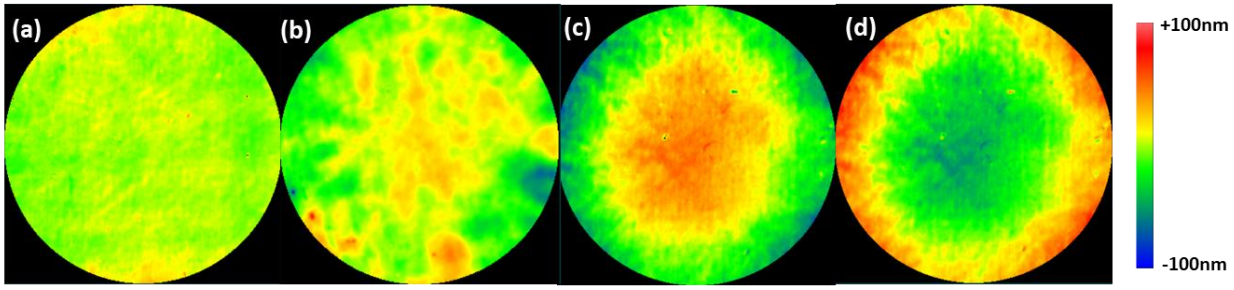

Figure 30. Optical distortion of replications due to formation of residual stresses in (a) 0.75% (b) 1.50% and (c) 5.00% PI concentrations. (d) Inverted distortion of the 5.00%PI sample.

Therefore, in Figure 31, the SFE degradation of the replications are plotted against the residual stress that formed in the film as a function of PI concentration. As anticipated, with

increasing residual stress, the SFE optical degradation is larger. This behavior is insensitive to a tensile or compressive direction and the SFE degradation is symmetric. Since the residual stress causes a spherically uniform distortion in the replicating resin layer, it is insensitive to convex (compressive) or concave (tensile) surface shape. This is demonstrated in Figure 30d where the optical degradation in the 5.00%PI replication (Figure 30c) is inverted in the software. Topography changes are of the same magnitude SFE distortion; a 0.041λ value in both instances. This behavior is only true because we are manufacturing flat mirrors on a quasi-isotropic CFRP composite substrate. If concave mirrors were manufactured, the impact of stress is not necessarily symmetric with respect to SFE distortion. For example, if a concave replication was manufactured, a tensile residual stress would degrade the optical quality less than the formation of an equivalent compressive stress. For convex mirrors, the opposite is true.

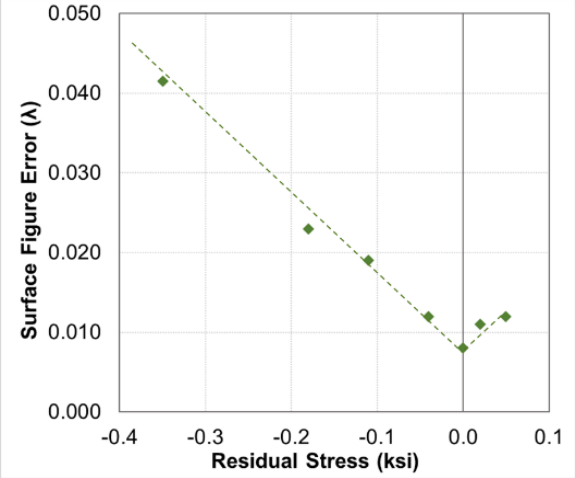

Figure 31. SFE degradation versus residual stress for all PI concentrations.

To minimize distortion, a minimal residual stress is necessary. For our system, this occurs with 0.75% PI. However, even with practically zero residual stress, the replication exhibits a small change in the SFE. These changes are ~5nm and are likely due to localized thickness variations in the replicated film, errors in manual data masking, instability in the interferometer laser over time,

or potentially different amounts of time out of the dry-box before surface imaging. Even small residual stresses can degrade the replication past λ/20. The residual stresses induced by CTE mismatch during thermal post-cures (Section 5.3.3) are substantially larger, and unless the SFE increase due to stress formation can be reduced, thermal exposures to increase cure state are not advisable for these applications.

5.4.2. Optical Quality as a Function of Composite Laminate

A method to mitigate optical distortions induced by nonzero residual stresses is to increase the stiffness of the underlying substrate. The relationship between substrate properties and deformation can be calculated mathematically in terms of radius of curvature through Stoney's Equation. However, we are interested in distortion in terms of SFE. To observe how successful increasing the composite laminate stiffness is in reducing optical distortion, several CFRP substrates are manufactured with varying fiber moduli and laminate thicknesses (details in Section 19). Replications are fabricated on the various substrates with the 1.50%PI resin, specifically because of its non-zero residual stress. The stress formed in all samples was the same because it is controlled by the resin, however its impact on SFE is plotted in Figure 32 against the flexural stiffness of the substrate. It is immediately apparent that the substrate plays a huge role in dictating optical quality by resisting stress-induced distortions. Over the stiffness range shown, the SFE varies from almost mandrel-limited to one order of magnitude higher.

$$D = \frac{E_s t_s^3}{12(1-\nu^2)} \qquad 9$$

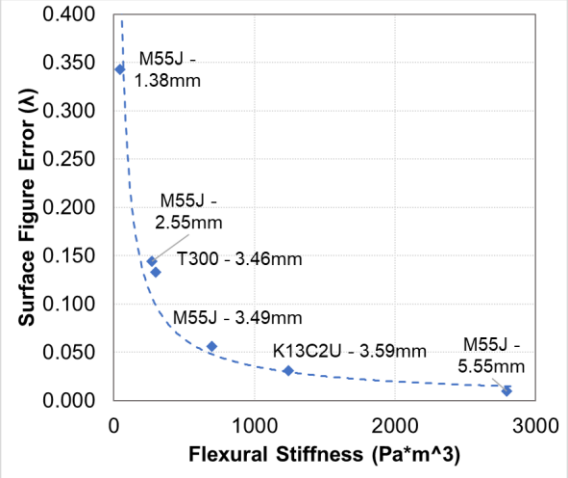

Figure 32. SFE versus CFRP flexural stiffness.

The substrate stiffnesses were calculated using Equation 9 where D is flexural stiffness and ν is Poisson's ratio. Increasing stiffness in Figure 32, regardless of how it was achieved, relates to reduced SFE errors. However, upon a closer inspection of Equation 9, the stiffness is linearly related to composite modulus (controlled by fiber modulus) and the laminate thickness cubed. Therefore, the most efficient manner to enhance structural rigidity is to make the substrate thicker. However, since mass on space telescopes is critical, increasing stiffness using low-cost, low-stiffness pan-based carbon fibers and compensating with thick laminates is not advisable. More expensive, stiff pitch-based carbon fibers should be used because they exhibit low, potentially negative CTE values, and allow maximum light-weighting. However, depending on the stiffness required for different mission requirements, increased rigidity may not be possible with a solid laminate and might have to be achieved with laminated sandwich composite core configurations. These sandwich configurations afford significant increases in stiffness and strength to the structure with a minimal weight penalty. However, the introduction of core structures can potentially cause print through of features to the replication surface, similarly to fiber print-through, and increase mid-frequency errors.

5.5. Modeling Optical Quality

While the formation of a non-zero residual stress in the replicating resin is the driving force for dimensional distortion, the impact on optical quality degradation is dependent on utilizing a sufficiently stiff substrate. We previously observed the impact of stress and composite stiffness on SFE change; however, we are interested in predicting that deformation for any resin or composite configuration. The goal is to rearrange Stoney's Equation with SFE substituted for radius of curvature because both are metrics of dimensional distortion. Developing this model relies on experimental data. First, we know SFE is linearly related to stress due to the behavior of samples as a function of PI concentration in Figure 31. Therefore, the SFE must be inversely related to radius of curvature via Stoney's Equation. In Figure 33, the SFE is plotted against the inverse radius of curvature for the 1.50% PI concentration replications manufactured on different composite substrates. A linear trend relationship exists between SFE and stress, which is mathematically described by Equation 10. Now that we know the conversion factor between SFE and radius of curvature, Stoney's Equation (Equation 6) is rearranged and substituted into Equation 10 to produce Equation 11. This equation describes the relationship between resin material, resin stress, composite modulus, composite laminate thickness, and optical SFE change due to stress formation.

$$SFE = \frac{43.826}{R} \tag{10}$$

$$SFE = (43.826)\, x \frac{6 t_f \sigma}{E_s t_s^2} \tag{11}$$

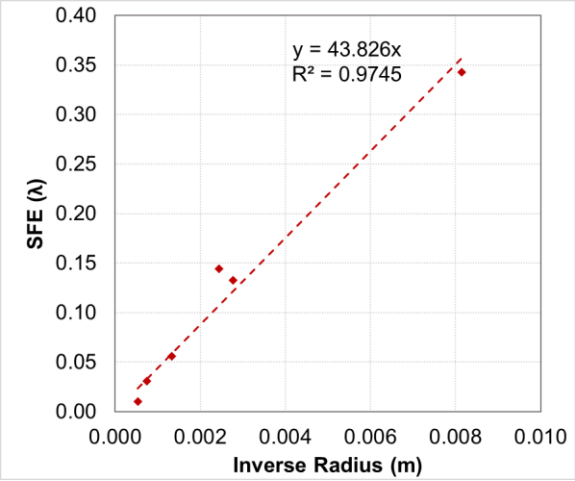

Figure 33. SFE vs. inverse of radius of curvature.

We can now use Equation 11 to simulate some theoretical situations and develop an understanding of the relative impact of each component in the replication stack to SFE degradation. In Figure 34, the SFE distortion is plotted for stress values ranging from 0 to 2.0ksi on laminates manufactured with three different carbon fibers. In Figure 34a, the laminates are 5mm thick, and in Figure 34b, the laminates are 10mm thick. In both cases, a higher stress linearly relates to an increase in SFE, which was observed in Figure 31. Also as expected, higher stiffness fibers (K13C2U > M55J > T300), and thicker laminates (10mm vs. 5mm) reduce SFE due to their impact on resisting deformations. While a zero residual stress state in the replication is desired, realistically they are not always, so being able to design the substrate based on initial resin stress is quite useful. For example, say the 0.25%PI sample with a 50°C post-cure was selected based on some specific characteristics, but it has a 1.98ksi residual stress value. According to Figure 34a, a 5mm thick laminate of K13C2U is right on the cusp of constraining the distortion to a λ/20 SFE value necessary in space based UVOIR applications. More shockingly, Figure 34b indicates this might not even be possible with an extremely thick, 10mm laminate manufactured with T300 fibers.

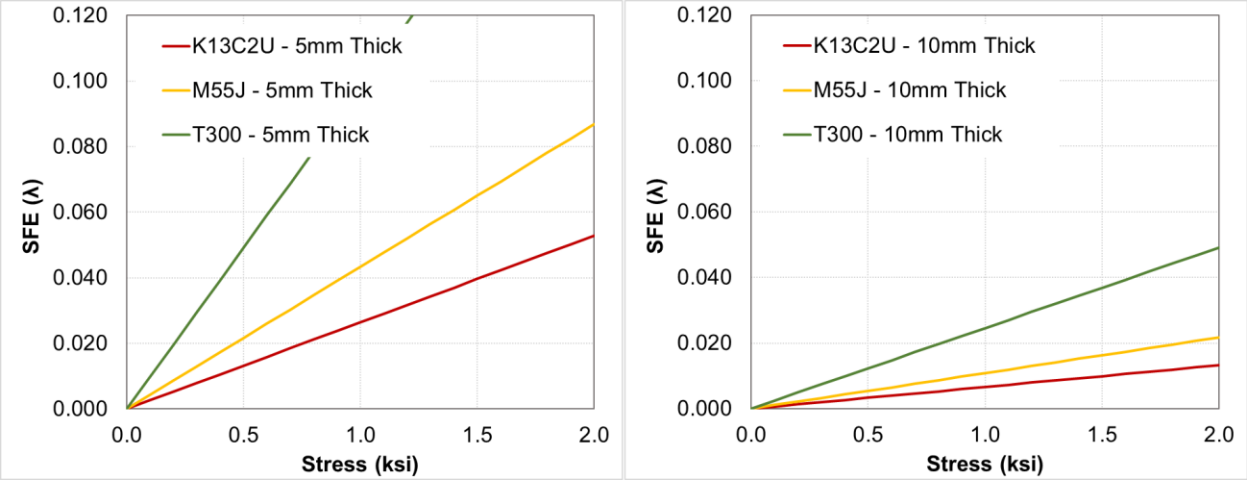

Figure 34. Impact of film stress and carbon-fiber modulus on SFE for (a) 5mm and (b) 10mm thick CFRP laminates.

While all the trends in Figure 34 are obvious, something not as immediately apparent is the non-linear relationship between SFE and composite laminate flexural stiffness. In Figure 35, for an arbitrary value of 0.63ksi resin stress, the composite flexural stiffness required to achieve specific SFE values was calculated with three different carbon fibers composites. Interestingly, the flexural stiffness required is different depending on the modulus of the carbon fiber. If a 0.032λ is required, the laminate stiffness required to achieve this is 100% higher for a T300 laminate than a K13C2U laminate. This behavior was unexpected, but can be traced to a factor of laminate thickness being dropped from the equation for flexural stiffness (Equation 9) when deriving Stoney's Equation (Equation 6). When the resin stress is bending the substrate, due to the moment arm, the thickness drops from a cubed to a squared value. Therefore, to minimize the impact of stress on SFE, it is more effective to use a higher stiffness carbon fiber.

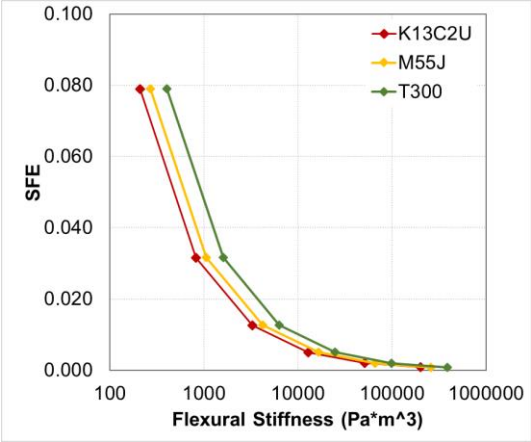

Figure 35. SFE vs. flexural stiffness of CFRP laminate for 0.63ksi residual stress.

While the trends in SFE distortion were mostly anticipated as a function of film stress, composite modulus, and composite thickness, it is important to develop a model to understand exactly how changing each parameter directly impacts the SFE value. Without performing this derivation, the relationship between SFE and flexural stiffness for different substrates would never have been noticed. Developing this model is specifically important in simulating substrates necessary to resist changes and optical distortions that will occur due to varying environmental conditions. For example, if CTE and CME values are known, the stress developed due to an environmental change can be predicted in terms of SFE.

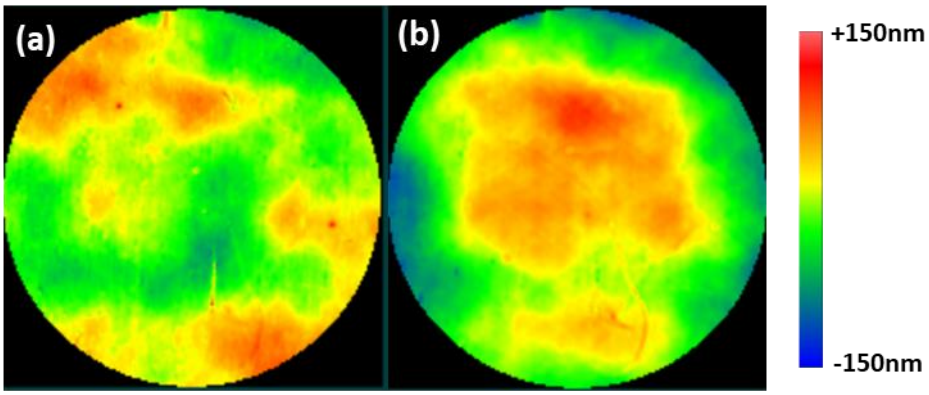

Figure 36. Laser interferometry images of a 5.00%PI (a) immediately after UV exposure and (b) after stress formation.

However, it should be noted that the optical changes predicted by the model are compounded on top of the initial surface shape. This is displayed in Figure 36 where the initial shape of the 5.00%PI replication is shown in Figure 36a and is characterized by a concave shape and 0.044λ SFE value. Over the course of time, this replication forms a -0.35ksi residual stress, which is isolated in Figure 30c and the final shape is shown in Figure 36b. Following compressive stress formation, the replicated surface is convex and characterized by a 0.058λ SFE value. The degradation in optical quality between the two state is only 0.014λ, substantially less than the 0.041λ predicted by the model and shown in Figure 31 because the convex stress is filling the concave shape and then swelling out-of-plane again. The model is only characterizing the distortion due to a specific event and to fully model the optical behavior under a changing stress state, the predicted surface must be added to the initial surface. However, monitoring changes in the residual stress provide a pathway to clearly monitor differences in replication optical stability as a function of formulation and processing in order to link optical behavior to material properties.

5.6. Conclusions

Non-zero residual stresses in the replicating resin layer were shown to degrade replication optical quality from mandrel-limited with a magnitude dependent on formulation, processing, or post-processing. Inherent changes in the stress state occur in UV cured epoxy resins over time due UV attenuation through the film forming a crosslink density gradient, causing oligomer diffusion, and resulting in compressive stress formation. The magnitude of compressive stress is directly related to the cure gradient through the thickness, with increased stresses relating to a higher concentration of absorbing PI species and thicker films. Replications with mandrel-limited optical quality are produced when the compressive stress formation is balanced with the tensile cure

shrinkage, resulting in a net zero stress state. For our system this is achieved with 0.75%PI concentration. Furthermore, UV curing intensity can be used to modify resin cure state without impacting stress formation. Thermal post-cures also utilized to increase polymeric cure state induce substantially larger residual stresses than RT processing with a magnitude related to cure shrinkage and CTE mismatch. Even low temperature exposures (50°C) induce stresses 5x that of any RT cured sample.

While stress formation in the resin layer is the driving force for optical quality degradation, the impact on SFE degradation is controlled by the CFRP composite because increasingly stiff substrates resist and minimize distortions. Lower stress, higher stiffness carbon fibers, and thicker laminates were all shown to be related to smaller SFE distortions. This data was then used to develop a model predicting SFE distortion as a function of those parameters by finding the relationship between SFE and radius of curvature changes to substitute in Stoney's equation. By doing this, interestingly, it was shown that the SFE is not directly related to substrate flexural stiffness. Laminates utilizing higher stiffness carbon fibers more efficiently resist stress-induced distortions. While this model was developed to understand optical degradation of the replication from the glass mandrel, it can be applied to environmental stability evaluations. Any change in stress due to thermal (CTE) or hygroscopic (CME) expansions and contractions will result stress and dimensional distortions. Often, avoiding any change in the stress state is not possible, and understanding the relationship between film stress, CFRP laminate, and SFE distortion can be crucial in designing a substrate necessary to perform within the mission requirements.

Chapter 6. Replication Terrestrial Stability Concerns: Humidity and Time

6.1. Introduction

The biggest challenge for the use of replicated mirrors in ultrahigh precision space applications is to ensure the replicated surface retains its optical shape with exposures to various environments, including 1. varying hygrothermal environments prior to launch and 2. space environment over long periods of time [29]. The discussion will be split into two domains; this chapter deals with stability concerns prior to launch and the next chapter will discuss the effect of space radiation on the replicated material. Between fabrication and integration before launch, telescope mirrors can experience several years on Earth; the HST primary mirror spent 11 years in these stages and the JWST, 17 years (as of 2020) [3, 2, 12]. During the intervening years, environmental fluctuations, or even dimensional relaxations with time can induce permanent optical changes, degrading performance [47, 35, 29]. Furthermore, these stability concerns are unique to replicated mirrors compared to glass or other inorganic materials. While dimensional stability is a critical barrier to entry, the studies in the literature are limited, both in number and in scope. There is a lack of parametric studies to provide a fundamental understanding in the role resin material properties play in replication dimensional stability over time in various environmental exposures.

This dissertation seeks to remedy the gap by performing comprehensive studies on replication stability as a function of resin properties and environmental conditions. In this chapter, we investigate dimensional stability concerns replicated mirrors will experience specifically on Earth: hygroscopic and long-term storage. We first perform hygroscopic stability tests as a function of PI concentration and UV curing intensity. The magnitude and hysteresis of hygroscopic

distortions are related to the resin material properties and residual stress values, respectively. Replications are then monitored over long storage times as a function of material properties and residual stress to quantify distortions due to relaxation phenomena. Finally, a process to accelerate stress relaxation is developed, enhanced stability is quantified, and the limit to its efficacy is evaluated as a function of large, thermally induced residual stresses.

6.2. Hygroscopic Stability as a Function of Photoinitiator Concentration

Hygroscopic stability in replicated composite mirrors is critical because replications experience highly varied environmental conditions during fabrication and integration, followed by a complete dry out in space. For example, during the JWST manufacturing process, each mirror segment made 11 trips across the country to 6 different facilities [12]. This is an issue for replicated mirrors because epoxy resins are commonly understood to undergo swelling, plasticization, and reduced adhesion when exposed to moisture-rich environments [66, 67]. Swelling is particularly concerning because it can induce large distortions in the replicated surface, which are potentially irreversible. Brosens et. al. have shown that the stresses formed during a humid exposure for a typical epoxy resin can be much larger than the deformation caused by thermal expansion alone [35]. Conventionally, the swelling behavior can be predicted by measuring the CME of the material.

Correlation between the measured CME values and real replication behavior is not well defined due to CME measurement on bulk-sized materials with micrometer-scale resolution. An effort to correlate predicted and measured behavior was performed by the Small-JASMINE group at JAXA. First the CME of their CFRP sandwich structure was characterized with conventional techniques; then their replicated structures were placed in several different humidity environments

to mimic conditions (such as ground to orbit), the distortion modeled, and real distortion measured with laser interferometry. Not only were the errors between the model and real observations 25%, the dimensional changes were considered unacceptably large due to the asymmetric distortions [37]. Therefore, real replications must be manufactured and monitored to correlate material properties to distortion and hysteresis. Understanding the behavior is crucial in controlling and minimizing distortions, in order to ultimately utilizing replicated composite mirrors in UVOIR space applications.

Hygroscopic stability will be characterized by two different metrics; distortion when placed in a high-humidity environment and hysteresis when returned to the initial dry environment. In real applications, replicated mirrors will experience highly fluctuating humidity environments that are impossible to predict or simulate in testing, therefore a worst-case scenario of 100%RH will be used to bound the uppermost optical degradation with moisture absorption. Upon launch, however, the replicated mirrors are returned to and maintained at a 0%RH environment. To evaluate any hysteretic optical change due to water sorption on Earth, the same replications will then be returned to the initial dry environment and optical quality monitored. These two tests will bound dimensional distortion due to moisture absorption and any potential hysteresis, as well as identify which properties are crucial to minimizing these optical changes.

The impact of PI concentration will be evaluated on dimensional distortion in 100%RH because the material properties have been fully characterized and span over a large range of values. As previously stated, conventional polymeric distortion due to moisture absorption is characterized by the CME; as polar water molecules diffuse through the polymer, interact with the hydroxyl groups on the polymer backbone, and interrupt the interchain hydrogen bonding. The intersegmental hydrogen bond distance is increased, causing swelling of the network with a

magnitude characterized by the CME [75, 67, 66]. Reduced CME values are directly correlated to higher elastic modulus and lower moisture absorption due to the concentration of species diffusing into the structure and its ability to resist distortions [75]. Previous testing of moisture absorption and modulus values (Figure 9a and Figure 9c) indicate that neither property is maximized at a single PI concentration. Instead, the 0.25% PI exhibits the maximum modulus and 0.75% PI exhibits the lowest moisture absorption. To predict the relative CME magnitude as a function of PI concentration, the saturated moisture content is divided by the elastic modulus for all PI concentrations, shown in Figure 37a. This behavior predicts relatively similar stability behavior for PI concentrations between 0.25% and 1.00% due to the tradeoff in moisture absorption and stiffness. However, above 1.00% PI, both moisture and modulus values degrade as a result of their heterogenous microstructure, leading to a sharp increase in relative CME value. In theory, the lower PI concentrations will exhibit a similar, but enhanced hygroscopic behavior compared to higher PI concentrations.

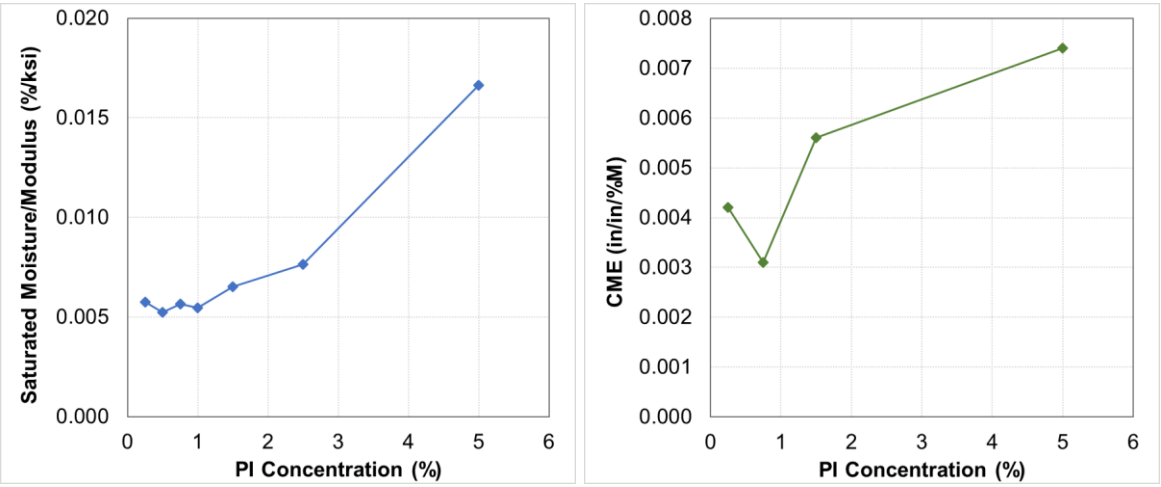

Figure 37. (a) Relative and (b) real CME values as a function of PI concentration.

Since we are concentrating on correlating a material property to maximum stability, replications are fabricated as a function of PI concentration and distortion monitored over time in

100%RH. The distortion is monitored in terms of strain, plotted against the moisture content at each moment in time (from Fickian model), and the CME measured from the slope. The CME is displayed as a function of PI concentration in Figure 37b and the trend is very similar to the predicted behavior. The 0.25%PI and the 0.75%PI are characterized by similar values to each other, with a small increase at 1.50%PI, and a substantial increase at 5.00%PI. Not only is the trend in the CME value consistent with material property trends, the actual values of CME are very similar to those measured by Ardebili et al. [92] on several unfilled epoxy resins (3-6 x 10^{-3} in/in/%moisture). The strain versus moisture content plots used to calculate CME are shown in Figure 38a for several PI concentrations; while the behavior is initially linear, at longer times, deviations start to occur in the strain-response. Due to the longer period before strain deviation occurs with increasing PI concentration, the more accurate the CME value is. Even though the 0.25% PI and 0.75% PI samples were predicted to behave similarly, the 0.25% PI is only characterized by a few data points before non-linearity occurs and measurement noise may account for the different measured values between the two formulations.

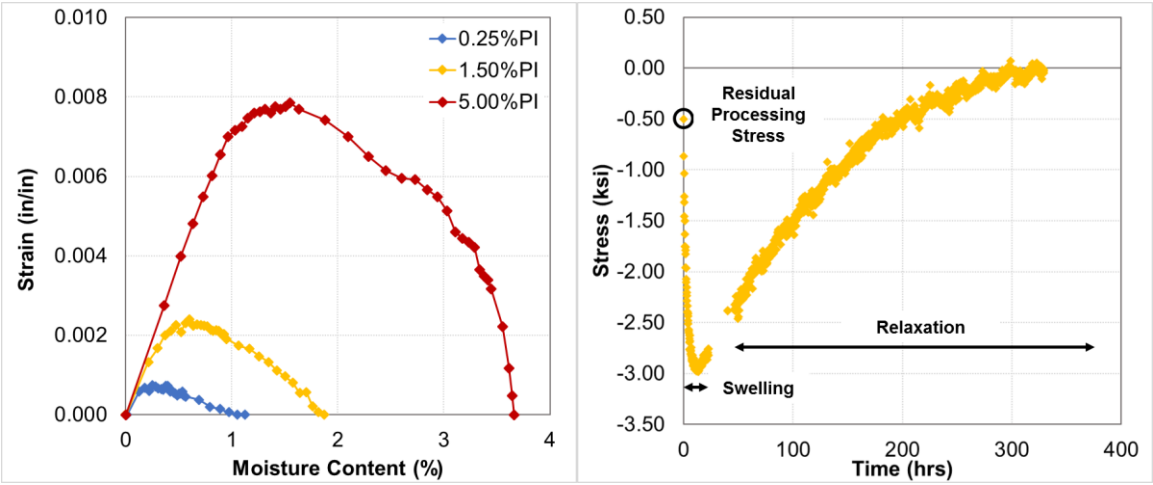

Figure 38. (a)Strain versus moisture content for 0.25%, 1.50%, and 5.00%PI concentration. (b) Stress as a function of time in 100%RH for 5.00%PI replication.

Initially, the amount of swelling in each system shown in Figure 38a was directly related to the amount of moisture in the system, however, eventually the curve starts to plateau, and ultimately the strain drops with additional moisture absorption. This behavior occurs for all PI concentrations, though the strain and moisture content at which the decrease in strain occurs is different. While lower PI concentrations are characterized by a reduced CME and appear to stop swelling at smaller moisture contents, tracking replication stability in this manner does not provide insight into the behavior. Therefore, the subtraction technique previously described in Section 5.2 will be utilized to analyze the samples in Figure 38a in terms of stress over time. An example of stress over time is shown in Figure 38b for the 5.00%PI replication as it absorbs moisture in 100%RH. There are three regimes describing the stress state as a function of time in Figure 38b; a non-zero residual processing stress, a swelling stress, and finally a stress relaxation regime. The formation of the non-zero processing residual stress was previously described Section 5.3 and is different for each PI concentration. Swelling occurs immediately after being placed in 100%RH and produces a negative compressive stress due to expansion of the network by absorbed moisture. However, swelling only occurs for a short period of time before stress relaxation begins to dominate and continues until the stress relaxes back to a net-zero state. The relaxation of stresses can account for the observed decrease in strain observed with higher moisture contents in Figure 38a.

The swelling and relaxation behavior in Figure 38b due to moisture absorption is attributed to the replicating resin only. While the CFRP composite has a non-zero residual processing stress and does absorb moisture, compared to the resin, changes in dimension due to absorption are negligible in comparison. The specific composite substrate used for these replications absorbs less than 0.1% moisture in 14 days and this moisture is concentrated in the outermost ~0.1mm of the

~4mm thick composite substrate. The moisture that does diffuse into the composite substrate only causes plasticization of the cyanate ester matrix which only accounts for 40% of the material (V_f = 40%). On the other hand, the replicating resin layer absorbs more moisture at a faster rate with reduced thickness, so the moisture-induced swelling and stress relaxation are significantly more impactful in the resin layer. At longer lifetimes in humidity, the hygroscopic behavior of the composite might need to be taken into consideration, but this discussion will focus primarily on the replicating resin.

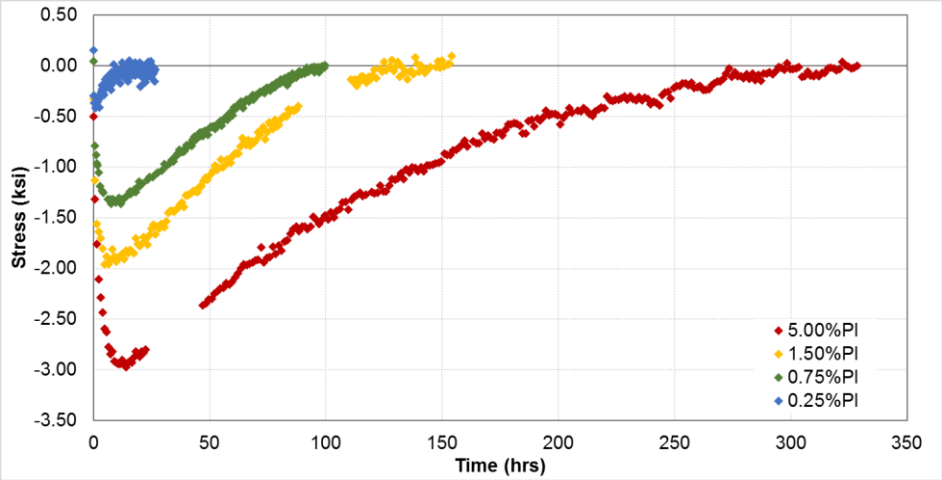

Figure 39. Stress as a function of time in 100%RH for 0.25%PI, 0.75%PI, 1.50%PI and 5.00%PI replication.

Now that we have an idea of how to monitor the hygroscopic optical changes, the stress profile as a function of time in 100%RH is plotted in Figure 39 for all PI concentrations. Each concentration exhibits the same three regimes of stress behavior observed in Figure 38b, though their magnitude and time-dependence are different. Overall, lower PI concentrations exhibit higher stability when placed in high-humidity environments due to the smaller fluctuation in residual stress values. Most interestingly though, is that the 0.25%PI and the 0.75%PI are characterized by similar CME values, but exhibit significantly different stress profiles as a function of moisture

absorption. To characterize the differences in the stress profile that may be contributing to hygroscopic stability, the moisture-induced behavior from Figure 39 is summarized in Table 5. In Table 5, it is apparent that earlier onset of stress relaxation translates to higher stability because the replication undergoes smaller dimensional distortions due to swelling stresses. For example, the 0.25% replication only swells for 3hrs before switching to relaxation. After the three hours, a total swelling stress of -560psi causes 0.028λ of distortion. On the other hand, the 5.00% replication undergoes swelling for 14hrs with a total swelling stress of -2400psi, corresponding to an eight-fold increases in dimensional distortion over the 0.25% replication (0.225λ).

Table 5. SFE deviations during moisture absorption as a function of PI concentration.

Photoinitiator Concentration (%)	Time Swelling Switches to Relaxation (hrs)	Swelling Stress (ksi)	SFE Change due to Swelling Distortion (λ)
0.25	3.0	-0.56	0.028
0.75	7.7	-1.40	0.099
1.50	8.8	-1.65	0.140
5.00	14.0	-2.39	0.225

To understand what controls an early onset of stress relaxation, it is important to note that the replications are not saturated when their behavior switches from swelling to relaxation. Using the diffusion coefficient values, the concentration gradient of moisture in the film can be modeled for using Fick's 2nd Law of diffusion for an infinite thin film, Equation 12. The concentration gradient is modeled for each PI sample at the time swelling switches to relaxation in Figure 40a and at the time of full relaxation for each replication in Figure 40b. Several things are immediately apparent; none of the samples are fully saturated when they start to relax nor when they are fully relaxed, and increased moisture in the sample does not correlate with relaxation rate. The 5.00%PI replication contains the most moisture and is the only coupon with any present at the back face when relaxation begins, though it experiences the largest optical distortion due to hygroscopic environments. Furthermore, the 0.25%PI sample has the least amount of moisture in it, which is concentrated in the outermost 25μm, yet it exhibits the fastest transition from swelling to

relaxation. Both phenomena are occurring at the same time and Brazel, et. al have shown that faster stress relaxation than swelling shifts the transition earlier in time [93]. This would mean faster stress relaxation relates to enhanced replication hygroscopic optical stability.

$$\frac{M_t}{M_\infty} = 1 - \frac{8}{\pi^2}\sum_{n=0}^{\infty}\frac{1}{(2n+1)^2}\exp\left(\frac{-D(2n+1)^2\pi^2}{4\,l^2}t\right) \qquad 12$$

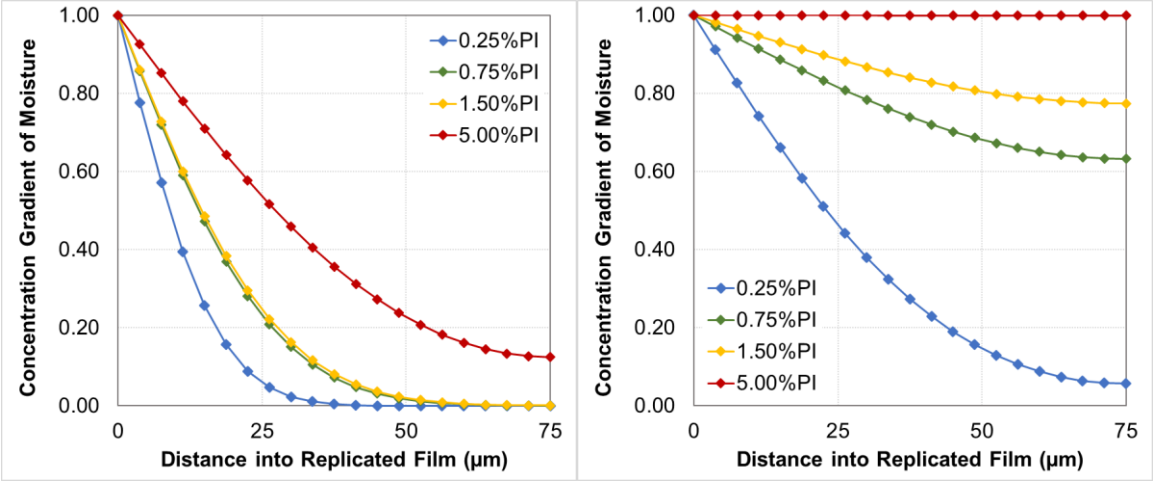

Figure 40. Concentration gradient of moisture in the replication film (a) at the time swelling switches to relaxation and (b) after full relaxation for 0.25%, 0.75%, 1.50% and 5.00% PI.

Since the relaxation behavior is critical to hygroscopic stability, understanding the relationships between relaxation rates, PI concentration, material properties, and relative humidity of the polymer are important. Stress relaxation can be predicted by generating master curves, previously plotted as a function of PI concentration in Figure 29a. With increasing PI concentration, the relaxation rate is slower due to higher crosslinking and heterogeneity in the system, which is consistent with the observed behavior in Figure 39; however, the time-scales are substantially different. This is because the relaxation behavior of polymers is highly impacted by the presence of moisture in the system due to plasticization effects. As water molecules diffuse into the polymer and interrupt the interchain hydrogen bonding, “pseudo-crosslinking” is reduced and the polymer chain mobility is increased. The amount of moisture that is dissolved in the

material, or extent of plasticization, is controlled by the relative humidity of the environment (Henry's Law) with higher absorption at higher %RH environments [75]. To model relaxation rate dependence on absorbed moisture, TTS master curves are shown in Figure 41 as a function of absorbed moisture for the 0.25%PI resin. The material was saturated at different relative humidity environments prior to testing in a humidity-controlled DMA. It is clear in Figure 41, with increasing moisture in the resin, the static elastic modulus is decreased and the relaxation rate is increased. Plasticization effects allow easier structural rearrangement and enhances polymer chain mobility due to a reduction in the pseudo-crosslinking impact of hydrogen bonding. Higher relaxation rates allow faster accommodation of swelling-induced strains. Since the amount of moisture relates to relaxation speed, the high moisture diffusion coefficient and absorption value of the 0.25%PI allow a large amount of water to quickly enter the polymer. However, these parameters do not entirely control stress relaxation rates because the 5.00%PI replication is characterized by a higher diffusion coefficient and saturated content than the 0.25%PI; the inherent chemical crosslinking of each formulation also strongly contributes.

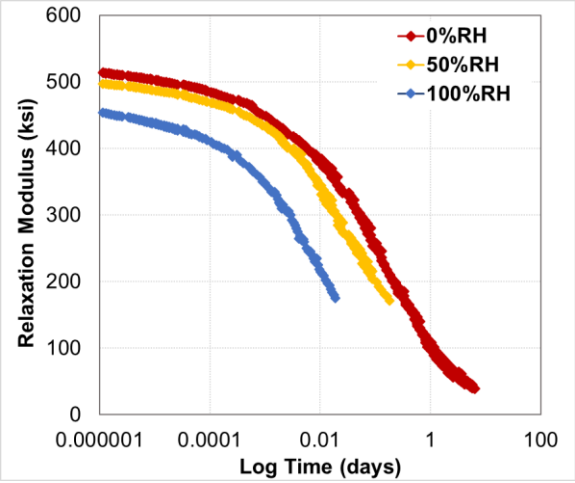

Figure 41. TTS master curves as a function of %RH for 0.25%PI.

To validate the relationship between master curve stress relaxation and the observed stress relaxation in the replications, they are correlated in Figure 42 for the 0.25%PI sample. Due to the nature of the TTS method used in this work the master curve generated displays a drop-off in the relaxation modulus but does not have fidelity to follow the relaxation modulus to zero. Therefore, the relaxation modulus behavior is extrapolated as shown in Figure 42a. This relaxation modulus is converted to stress in order to correlate the model with observed replication data in Figure 42b. When the replication data is shifted so the maximum swelling occurs at time equals zero (Figure 42c), the replication and the master curve relax in the same time frame as shown in Figure 42d, validating the correlation between the two. The characteristic shapes of the relaxation curves are not the same because the sample tested by TTS was fully saturated prior to testing and the replication is not fully saturated when it starts relaxing. Additionally, some swelling mechanisms may be simultaneously occurring.

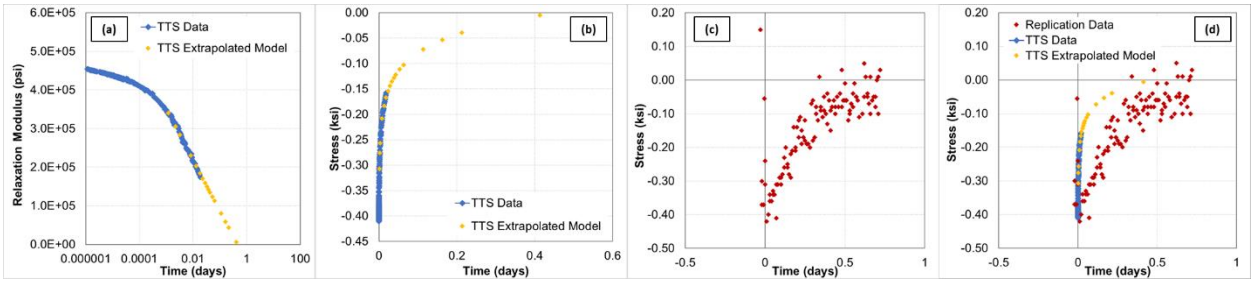

Figure 42. 0.25%PI (a) TTS master curve extrapolated to zero which is converted to (b) stress. The replication relaxation is (a) shifted to time equals zero and (d) overlaid with TTS stress data.

From these tests, we have concluded that replication hygroscopic stability is not related to the conventional CME value of the polymer, but instead how fast a material can undergo stress relaxation. The rate of relaxation controls the transition of a polymer from swelling to relaxation behavior, with earlier onset correlating to smaller swelling stresses. These smaller stresses reduce the SFE distortion and increase replication hygrosopic stability. Fast stress relaxation rates are

related to PI concentration through low crosslink density and homogenous microstructures; and further accelerated with plasticization by absorbed moisture. This description of the system explains why the 0.75%PI replication is characterized by the smallest CME of all PI concentrations yet does not exhibit the highest replication stability; the SFE distortion in 100%RH is more than 3x higher than the SFE distortion for the 0.25%PI. Since we have generated an understanding of what material properties control dimensional distortion during moisture absorption, we are interested in whether these hygroscopic-induced changes are fully reversible or induce some sort of hysteresis to the optical quality. These behaviors must be well understood when choosing a material system optimized for long-term stability in various environments because the optic must remain consistent and reproducible after cycling through humidity environments. Therefore, the replications exposed to 100%RH in Figure 39 are now returned to 0%RH and the stress is monitored as a function of time as shown in Figure 43 for the 5.00%PI.

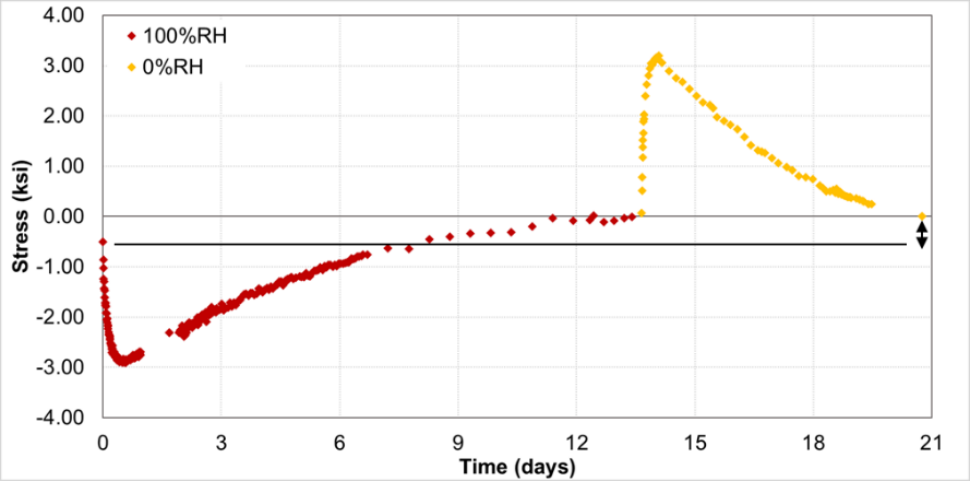

Figure 43. Sequential exposures of 100%H and 0%RH to a replication with 5.00%PI.

In Figure 43, the initial, as-manufactured dry residual stress value was non-zero. During the 100%RH exposure, swelling was followed by full stress relaxation to a net-zero state. Upon subsequent placement in a 0%RH environment, immediately the replication stress exhibits a sharp

increase in the tensile direction as the moisture is desorbed from the resin, causing shrinkage. Shrinkage continues for a short period of time before switching to stress relaxation until, once again, reaching a zero-stress state. The initial and final dry stress states have a hysteretic change in value, which we know will result in a corresponding change in optical quality. The stress and SFE change as a function of PI concentration due to humidity cycling are summarized in Table 6. As anticipated, minimal hysteresis in stress corresponds with minimal SFE change. For example, the 0.75%PI stress change was only -0.04ksi and correlates with a 0.002λ SFE change, while the 5.00%PI replication optical hysteresis is ~15x that.

Table 6. Correlation between residual stress and SFE changes after humidity cycling.

PI Concentration (%)	Change in Stress Between Initial and Final Dry States (ksi)	SFE Improvement Between Initial and Final Dry States (λ)
0.25%PI	-0.15	0.004
0.75%PI	-0.04	0.002
1.50%PI	0.33	0.009
5.00%PI	0.50	0.032

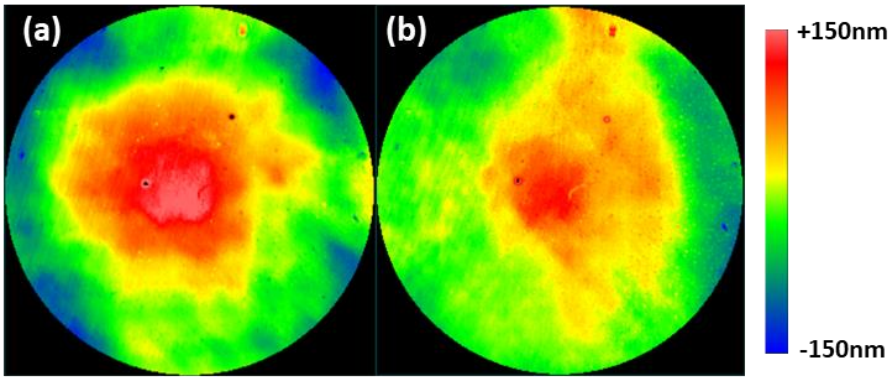

Figure 44. Interferometer images of 5.00%PI (a) before and (b) after humidity cycling.

However, something not immediately apparent is that the hysteresis in the replication stress state is equal and opposite in magnitude to the residual processing stress. During the high-humidity exposure, any non-zero stresses due to manufacture were relieved, which persists when returning to a final dry state. This means that any optical degradation of the replication from the glass mandrel described in Chapter 5 is relieved by being exposed to a high-humidity environment due

to relaxation of built-in processing stresses. This can be visualized in Figure 44 where the surface profile of the 5.00%PI replication is displayed before and after the humidity cycling. In Figure 44a, the replication is characterized by a convex shape due to its -0.50ksi tensile stress. However, after the stress relaxation in 100%RH followed by a dry-out, the same replication exhibits a flatter shape with no stress in Figure 44b. The concave optical degradation due to processing stresses are fully relieved and the replicated mirror returns to a mandrel-limited optical surface.

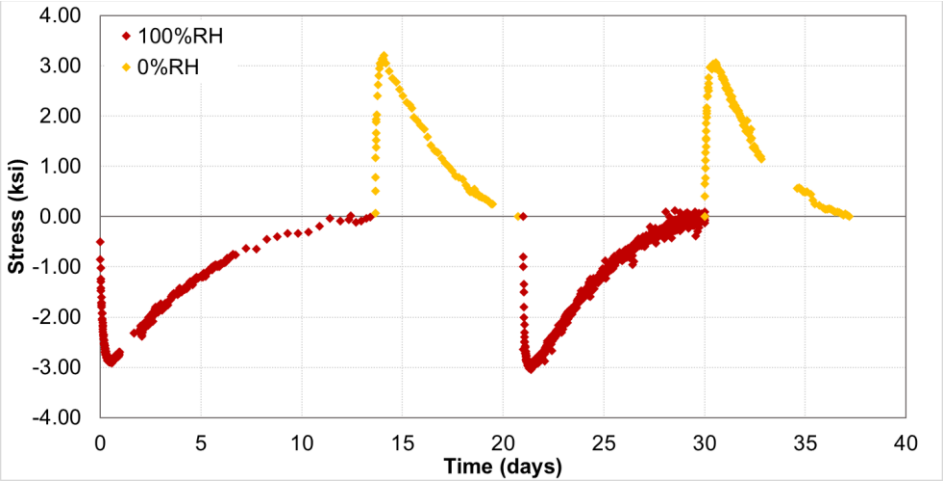

Figure 45. Two sequential exposures of 100%H and 0%RH to a replication with 5.00%PI.

Once the processing stresses are relieved during the first high-humidity cycle, we are still concerned that hysteresis may occur upon subsequent humidity fluctuations. The 5.00%PI replication from Figure 43 is cycled through 100%RH and 0%RH for a second time while the stress is monitored in Figure 45. In each step of the humidity cycles, the residual stress of the replication returns to a zero-stress state once again without hysteresis. These tests indicate that once the processing residual stress has been relieved with an initial high humidity, the replication will continue returning to a net-zero stress throughout other environmental exposures. By performing a high-humidity exposure on a replication, residual processing stresses can be relieved fully and quickly. As described in Figure 41, the level of humidity must be maintained as closely

to 100%RH as possible to fully maximize this relaxation behavior. The use of this methodology is even better suited for thermally cured systems. UV cured materials are processed at room temperature and are typically characterized by small residual stress

6.3. Long-Term Storage Stability

In Chapter 5, the critical importance of a net-zero residual stress in maximizing optical quality was established because any non-zero stress value relates to an optical degradation of the replication from the glass mandrel. It was assumed that once that stress formed, if the replication remained in a dry environment, the surface would be stable since no indication of any relaxation phenomena was observed over the course of several weeks. However, the hygroscopic stability testing in Section 6.2 highlighted the relaxation of built-in processing stresses. While these changes occurred due to increased chain mobility from absorbed moisture, we are still concerned that stress relaxation phenomena may occur under dry storage conditions. This is particularly critical because once a mirror is manufactured, it may remain in storage for several years before integration in the satellite system. Since other satellite optical components are designed around the shape of the primary mirror, if changes occur over that time, that would be catastrophic. We investigate whether relaxation occurs, and the extent of this process on optical quality degradation in terms of material properties and stress.

6.3.1. Room-Temperature Cured Replications

Stress relaxation is a known process in polymeric materials because they are viscoelastic, and the chains can flow under an internal stress. Stress relaxation between fabrication and integration manifests as a global shape change, impacting the optical prescription and causing deviation from

the optical design of the satellite. Furthermore, these dimensional distortions are not constrained to storage on Earth, which can potentially be accounted for, they will continue occurring throughout the satellite's lifetime; the HST has been in operation for ~30 years [3]. Even though these changes may translate on the order of nanometers in scale, they will affect the drift or stability.

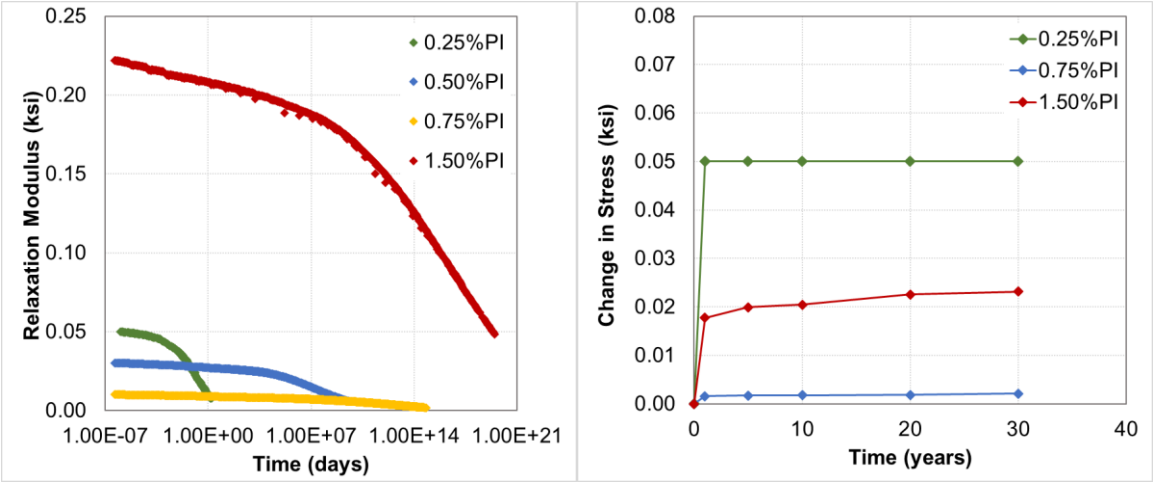

Figure 46. (a) Stress relaxation modeled as a function of PI concentration. (b) Change in stress modeled at certain time intervals for several PI concentrations.

To predict the stress relaxation behavior for each individual replications, the neat resin master curves generated in Figure 29 are combined with the measured residual stress in Figure 24 to produce master curves in Figure 46a relating residual stress change over time as a function of PI concentration. The impact of a nonzero stress state is clear. Samples that incurred higher stresses during manufacture (1.50%PI) will eventually relieve the distortions and return to the mandrel-limited optical quality. While this process may be very slow depending on the material, any drift is bad. For our system, the replications with the highest processing stress also is characterized by the slowest relaxation rate. The 0.25%PI replication on the other hand has a smaller stress, but all of it is relieved in a matter of weeks. Therefore, to characterize the tradeoff in these two properties,

the change in stress is extrapolated from Figure 46a at varying time intervals through 30 years, then plotted for several PI concentrations in Figure 46b.

It is apparent in Figure 46b that all the formulations experience the largest change in residual stress during the first year, though it continues to drift over time. Starting with the 1.50%PI, even though this formulation is characterized by a high residual stress, the surface will only experience a 10.5% relaxation of built-in stresses over 30 years due to its extremely high crosslinking and slow relaxation. On the other hand, the 0.25%PI replication is characterized by a reduced residual stress value but undergoes 100% stress relaxation almost instantaneously. Due to its low conversion value and fast structural relaxation, the 0.25%PI coupon will experience 2x larger optical distortions than the 1.50%PI replication. While the 0.25%PI replication experiences a larger total change, the optical drift occurring in the 1.50%PI replication due to its high initial stress state is undesirable. From the observed replication relaxation behavior in Figure 46b, both the residual stress value and the inherent material relaxation rate are critical to the optical distortion over time.

Distortions in each sample are not necessarily damaging to satellite performance because most of the optical change will occur immediately following fabrication before integration or use, however, they will cause deviations between the designed shape and real shape unless accounted for. Samples that are characterized by a moderate relaxation rate (fully in < 30 years) and large residual processing stresses are the most at risk to undergoing substantial optical distortion as a result of this process; both of which are commonly observed in conventional thermally cured epoxy resins. Furthermore, these behaviors indicate that both a zero-stress state and slow relaxation process are critical to maximizing optical stability over time because of the lack of driving force or polymer chain mobility; the 0.75%PI replication is characterized by both. This formulation is

predicted to exhibit <0.001λ SFE distortion over its entire lifetime. It is important to note that the resin relaxes faster than the 1.50%PI but is characterized by a smaller optical change due to its zero-stress state. In order to observe this phenomenon, replications are manufactured, stored under nitrogen for 443days, and intermittently imaged.

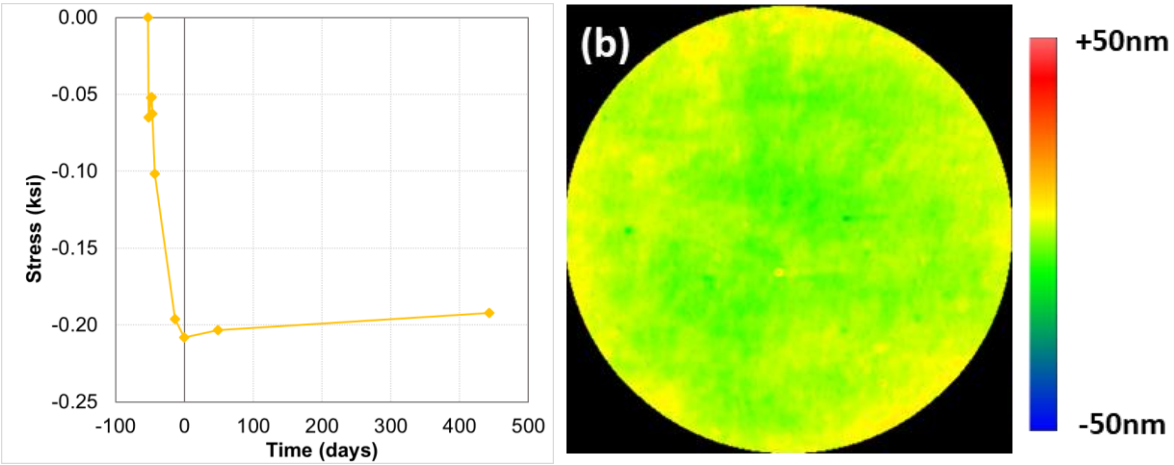

Figure 47. (a) Replication residual stress versus time for 1.50%PI replication stored under nitrogen purge. (b) 0.75%PI distortion over 1 year.

The residual stress profile of a replication with 1.50%PI as a function of time under nitrogen storage is shown in Figure 47a. This formulation was selected due to its non-zero stress and relaxation rate. The 0.75%PI sample is not expected to change at all, and the relaxation of the 0.25%PI might become convoluted with its residual stress formation. The stress is plotted in a manner where the formation of the residual stress due to the cure gradient (described in Section 5.3.1) is shifted and the maximum stress formed is located at zero days. After the maximum stress forms, a relaxation process occurs, though the relative amount of stress relieved is very small. Over ~300 days of relaxation, the stress is only relieved ~0.02ksi, which is the result of the extremely long relaxation times for this material. This behavior can be correlated to the modeled relaxation in Figure 46b; after approximately 1 year, this replication is expected to undergo a 0.018ksi relaxation and in reality, experiences a 0.016ksi relaxation. The negligible difference can be

attributed to measurement error. While the sample will continue relaxing, due to its high crosslinking (slow relaxation rate), very little additional relaxation will occur until significantly longer timeframes (decades). To further validate the critical importance of a zero-stress state, the optical distortion incurred by the 0.75%PI replication from manufacture to 443 days later is shown in Figure 47b. An extremely small vertical range was necessary to view distortions. In this case, the replication undergoes ~0.003λ SFE change from the glass master over the course of time and is mostly likely due to localized thickness differences or alignment issues due to the extremely small optical change. Without utilizing the subtraction technique, the SFE values before and after 1 year were only 0.001λ SFE different, which could also be due to measurement errors and in general would be characterized by not changing over time. In the case of the replications cured at RT as a function of PI concentration; they exhibit both small stresses and long relaxation times, making relaxation phenomena very small.

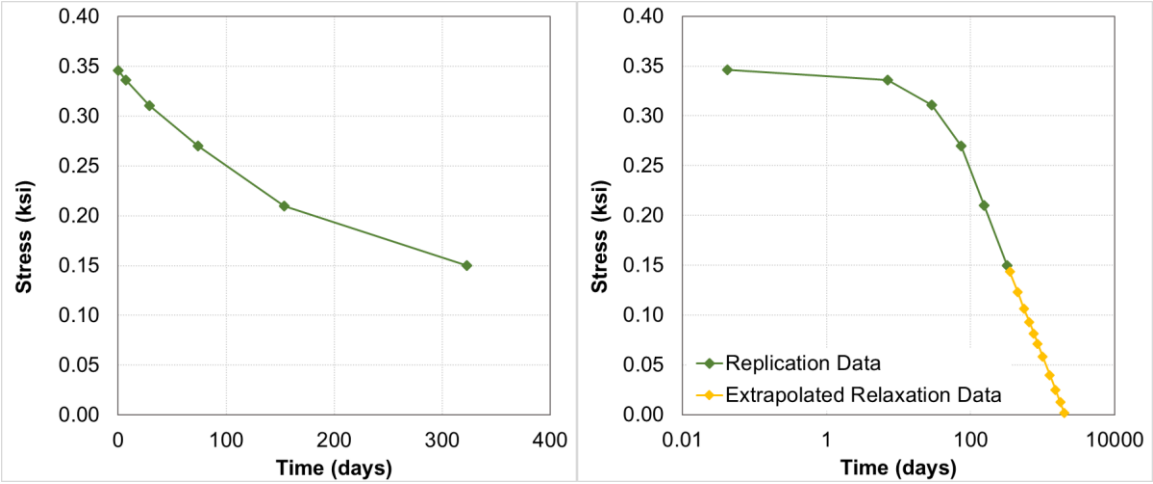

Figure 48. RT cured conventional 2-part epoxy resin (a) real replication stress relaxation and (b) extrapolated relaxation over time under nitrogen purge.

Just because stress relaxation is barely detectable in UV cured replications due to their inherently low residual processing stresses and high degree of conversion for a RT curing

processing does not mean that any resin can be utilized and expect the same results. Therefore, a conventional, two-part epoxy resin was cured at RT and the stress profile measured over time is shown in Figure 48a. Due to cure shrinkage, a small tensile stress initially forms; however the stress almost immediately starts changing. Over the course of ~350 days, more than 50% of the entire stress is relieved. Since the replication stress has already entered the "flow" regime of stress relaxation (drop-off in stress with respect to logarithm of time), the entire relaxation process is extrapolated in Figure 48b. Full relaxation of the stress built-into this replication occurs within 5 years. Due to the composite substrate it is replicated on, the relaxation in stress corresponds with a 0.021λ SFE change. This magnitude of optical change is unacceptable for UVOIR space mirrors, especially since it is occurring throughout the fabrication and integration stages. While the HST and JWST mirrors spent longer on Earth than 5 years, by switching to a high-fidelity replication process, the time between fabrication and launch should be reduced. Therefore, with the faster fabrication timelines, the optical distortions may continue occurring after reaching space, degrading performance over time. While UV cured epoxies are characterized by high crosslinking values at RT, the majority of RT cured epoxies are characterized by small crosslinking values and require an elevated temperature to enhance its conversion and material properties. Therefore, stress relaxation can be a significant problem in conventional, two-part epoxy resins.

6.3.2. Thermal Post-Cured Replications

Since stress relaxation is controlled by the crosslink density in the polymer system, polymer chain mobility can be reduced with the utilization of a thermal post-cure. However, this process induces a larger processing stress, which is the driving force for dimensional drift. Due to this tradeoff, thermal post-curing may not necessarily degrade optical stability over long periods of time. In order to characterize which parameter has a larger impact on optical distortion, master

stress relaxation curves were generated for 0.25%PI replications as a function of post-cure temperature and plotted in Figure 49a. With increasing thermal exposure, the stress relaxation is shifted later in time, however, the amount of stress relieved is substantially higher; the residual processing stress is more than 100x greater after a 100°C post-cure than just room temperature processing. To characterize the trade-off, the change in SFE due to the change in stress is plotted for various points in time over the course of 30 years in Figure 49b. In the first year, both the 50°C and 100°C coupon experience ~0.090λ SFE change due to the relief of ~1.65ksi. In this timeframe, 87% of the 50°C sample's total residual processing stress is relieved due to the extremely fast relaxation rate, even with its additional crosslinking. Even though only 35% of the initial stress is relieved in the 100°C replication over the same time, its extremely high residual stress value drives the same magnitude of optical distortion. However, the behavior between the two coupons deviates later in time. While the 50°C post-cure undergoes complete relaxation in less than 2 years, the 100°C post-cure continues to drift at a relatively linear rate of ~0.0013λ SFE degradation per year. Furthermore, if drift in stress is applied to a replicated composite mirror with the prescription of the HST [3], according to Equation 10, this would incur an additional 0.03% error every year between year number 5 and 30. Over 30 years, the total optical change in prescription would be more than 3.3%, which is unacceptable for space based UVOIR telescopes.

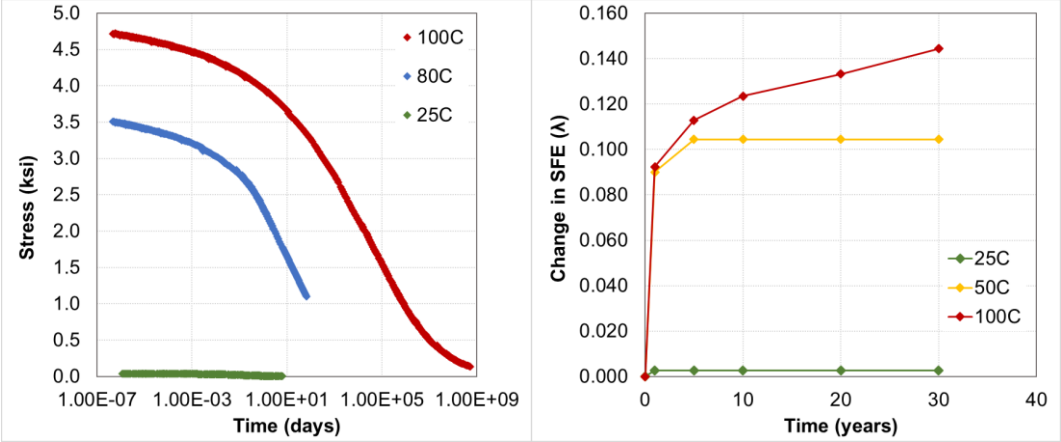

Figure 49. (a) Stress relaxation master curve and (b) SFE distortion over time for 0.25%PI replications as a function of post-cure temperature.

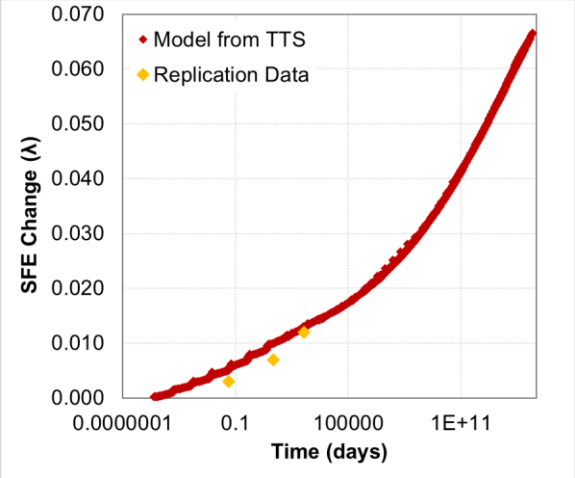

Figure 50. Real replication and master curve predicted SFE change in 1.50%PI + 50°C over time.

Though the 0.25%PI data in Figure 49 indicates thermal curing should be avoided for optical drift considerations, this formulation incurs particularly high thermal stresses compared to other PI concentrations due to its extremely fast relaxation rate and high elastic modulus. However, other formulations are characterized by reduced values of each which lead to a smaller thermally induced residual stress. We wish to evaluate whether any thermal post-treatment can be used without the higher residual stress state driving a larger optical distortion. Therefore, a 1.50%PI replication with a slow material relaxation rate is manufactured, post-cured to 50°C, and monitored

over 443days stored under nitrogen. This process is highly desirable to enhance material properties as the Tg increases by 20°C, elastic modulus by 10%, and CTE decreases by 20%. After thermal exposure, the replication is characterized by a 1.15ksi tensile stress value. The change in SFE is monitored over the course of ~1.5 years and the change in the optical quality is plotted against the master curve predicted value in Figure 50. Over the course of time monitored, this replication exhibited a 0.012λ SFE distortion, which matches with the predicted values from the master curve. Furthermore, this value will continue changing over time as predicted by Figure 50, indicating that the magnitude of residual stress in the system plays a larger role in SFE drift than relaxation rate.

This data seems to indicate that no matter how slow the stress relaxation rate of the replicating resin, a non-zero residual stress value will always cause optical drift over time. Because relaxation occurs as a fractional amount as a function of time, optical distortions will always be magnified by a larger stress value. However, manufacturing a film with zero stress is extremely difficult, especially with the material properties desired to maximize optical stability. This was achieved in one sample with UV curing due to the balance of tensile cure shrinkage and compressive gradient-driven diffusion, though, this is not generally achieved in polymeric films. A post-process is required to shift the stress state to zero and ideally would be globally applicable to any replication regardless of formulation or processing.

6.4. Enhancing Long-Term Storage Stability with Accelerated Stress Relaxation

We have demonstrated that an inherent optical drift occurs in replications over time due to the slow relaxation of built-in processing stresses. Not only does this process occur in the intervening time between fabrication and telescope integration, it will continue occurring throughout the lifetime of the satellite, critically degrading performance and restricting use of replicated mirrors

in precision UVOIR applications. Even with slow relaxation rates, any nonzero residual stress appeared to be a driving force in optical distortion. However, it was previously observed that high-humidity exposure relieved built-in residual stress at an extremely high rate compared to under dry conditions. If all stress is relieved, theoretically there would be no optical drift over time. Furthermore, this process can be applied globally to replications, regardless of formulation or processing. To characterize the effectiveness of this process in stabilizing the optical surface and preventing drift over time, a replication is fabricated, stress relieved with humidity cycling, and monitored over time during storage under nitrogen.

The resin formulation and processing utilized for comparison is the same as the sample in Figure 48 due to its fast relaxation rate. The replication was initially characterized by a 0.35ksi tensile residual stress that experienced ~ 0.14ksi relaxation in the first 150 days. An identical replication was manufactured, and stress relieved with a high and low humidity cycle which took 20 days. After the stress relaxation, the replication is characterized by a zero-stress state, and then monitored under dry nitrogen storage for an additional 90 days. A comparison of stress profiles for a stress-relieved versus the non-zero residual stress are overlaid in Figure 51. The measurements on the stress relieved replication are shifted 20 days in order to account for the time it took to stress-relieve the coupon.

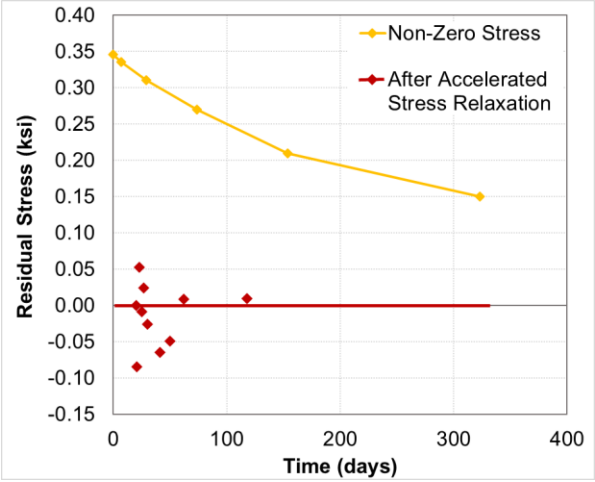

Figure 51. Residual stress profile over time in 0%RH for control versus after high-humidity stress relaxation process.

Following the relaxation process, the replication is characterized by a roughly zero residual stress value, though there is a substantial amount of noise in the data. This may be due to the density of measurements; the replication was removed often from the dry nitrogen environment which introduced a varying environment. However, upon larger time intervals between measurement (62 and 118 days), the replication was characterized by a roughly zero stress. Furthermore, the average stress over all measurements was -0.01ksi. Therefore, the scatter in the data does not indicate an instability in the replication following the stress relaxation process. In comparison to the control sample, the replication experiences no clear trend in optical drift and upon continued measurements the residual stress is expected to remain at zero. This is supported by the residual stress change between 62 and 118 days by both coupons; in the stress relieved coupon there is no change in residual stress compared to the 0.06ksi relaxation in the control sample. Relieving the residual stress enhances optical stability by removing the driving force for optical drift over time. This is particularly useful for thermally cured resins due to the high tensile stress that forms. So far, the effectiveness of this process has only been demonstrated on room temperature cured coupons that are characterized by a relatively low stress value.

6.5. Relieving Thermally Induced Distortion with Accelerated Stress Relaxation

High-humidity exposure has been shown to accelerate stress relaxation phenomena, which stabilizes replications for long-term storage by removing the driving force for optical change; the non-zero residual stress. In removing residual stress, the replicated surface is returned to the initial, inverse-mandrel shape, enhancing optical quality. This process would be particularly useful for samples that have been post-cured to high temperatures, relieving distortion induced by high tensile residual stresses and stabilizing the surface over time. However, this technique has only been demonstrated on replications with small residual stresses (<0.35ksi) and as post-cure temperature increases, so does the crosslink density of the polymer. This may decrease the efficiency of stress relaxation during the process, even with enhanced relaxation rates in high-humidity environments. To understand the effectiveness and any potential limits in utilizing this technique to enhance optical quality and temporal stability in post-cured coupons, 0.25%PI replications are fabricated, thermally post-cured at 50, 80, and 100°C, and then humidity cycled through 100%RH and 0%RH.

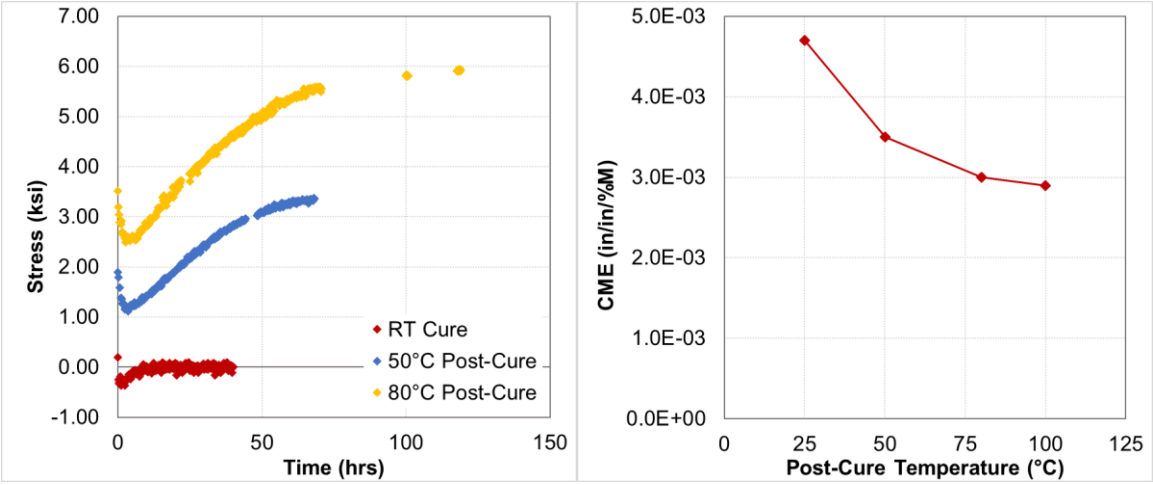

Figure 52. (a) Several real-time stress profiles under 100%RH and (b) CME values for 0.25%PI replications as a function of post-cure temperature.

The stress profile is monitored as a function of time in 100%RH, similarly to Figure 39, and is shown as a function of post-cure temperature in Figure 52a. It is apparent that each of the replications initially undergo swelling, followed by stress relaxation. Swelling behaviors can be described by the CME, which is summarized in Figure 52b as a function of cure temperature. Due to the increasing elastic modulus (Table 4) and reduced moisture absorption with higher temperatures, the moisture expansion is significantly decreased with increasing thermal exposure. By post-curing to 100°C, the CME value is decreased by 40% compared to RT. However, CME was previously unrelated to hygrosopic stability, and material changes with post-cure that cause a reduction in moisture expansion can impact other aspects of hygroscopic behavior; specifically, the onset of relaxation and the relaxation rate. With increased crosslinking as a function of post-cure temperature, the stress relaxation rate was observed to substantially decrease (Figure 49a), which should correlate to a later transition from swelling to relaxation behavior. This holds true in Figure 52a where the 80°C replication swells for twice as long (5.5 vs. 3hrs), with double the magnitude of the replication cured only at RT (-1.02 vs. -0.56ksi). Furthermore, after the onset of relaxation, it takes longer for the stress value to stabilize and relaxation to reach completion. Relaxation occurs in approximately 15, 70, and 120hrs for the 25, 50, and 80°C post-cured replications, respectively.

While the trends in swelling and relaxation behavior are all anticipated, the actual the relaxation behavior is unusual. Previously, regardless of initial residual stress, replications swelled into a net compressive mode and relaxed back to a net-zero value. In this case, though, the post-cured replications are still in a tensile state when relaxation begins and relaxation results in a replication with a higher tensile residual stress than the initial as-cured state. This phenomenon is likely due to the moisture concentration gradient through the film as swelling and relaxation occur

simultaneously with different rates as a function of thickness. While this behavior was entirely unexpected, the replication behavior during dry-out is more critical than the mechanism causing a higher tensile stress to form during moisture absorption. The stress relieved during dry-out will answer questions regarding whether this process can relieve large-magnitude residual stresses and if there are any inherent limits in utilizing this technique in terms of material relaxation or inherent stress values. Upon dry-out, the RT cured sample was previously observed (Table 6) to undergo full stress relaxation of its +0.15ksi residual stress. The 50°C post-cured replication similarly experienced full relaxation of its 1.90ksi tensile residual stress and returned to its pre-thermal exposure optical surface. However, higher tensile stresses associated with increased temperature exposures (80 and 100°C) did not experience full relaxation. During the first humidity cycle (100%RH and 0%RH), the 80°C and 100°C replications experienced a 2.5 and 2.33ksi residual stress relaxation, respectively. Since these stress relaxation values are relatively similar, whether the process is limited by a specific stress value or an inherent material property is still unknown. Therefore, a closer look is taken at the stress profile during cycling.

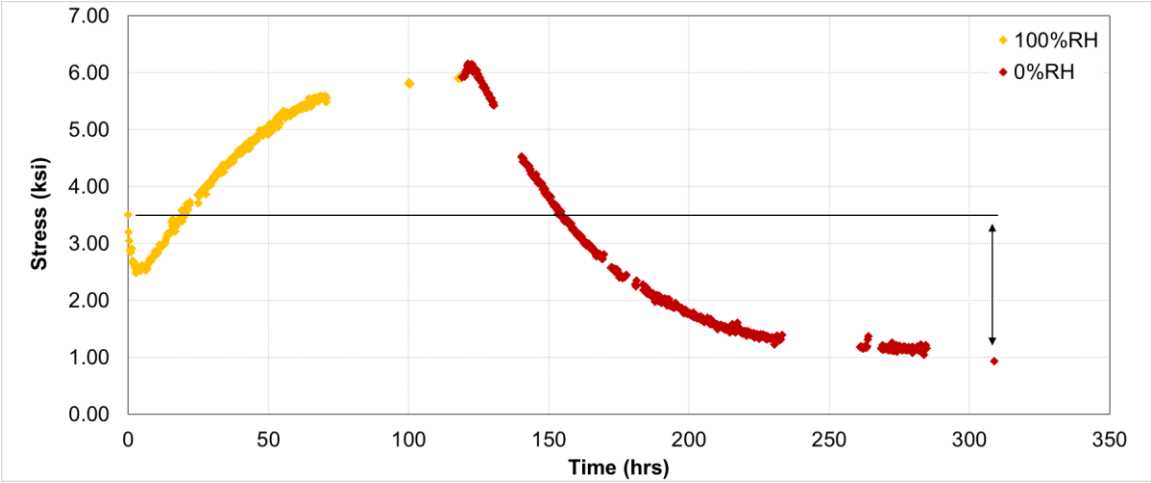

Figure 53. Sequential exposures of 100%H and 0%RH to a 0.25%PI replication post-cured to 80°C.

The sample 80°C post-cured replication from Figure 52 is monitored as a function of time in 0%RH following the initial 100%RH exposure and a summary of its stress profile is shown in Figure 53. It is initially characterized by an as manufactured 3.5ksi tensile stress that is increased to 5.9ksi during exposure to 100%RH. When the replication was placed in 0%RH, it initially becomes slightly more tensile due to moisture desorption and shrinkage before relaxation dominates. While the stress state trends towards zero, it never reaches zero and plateaus at ~1ksi, relieving 2.5ksi tensile residual stress due to a single humidity cycle. It is immediately apparent that the rate of relaxation is faster in the desorption step than the absorption step; in the same amount of time, approximately 1.5ksi more was relieved during dry-out compared to hydration. This behavior makes sense since the polymer is saturated and characterized by a higher mobility during the time moisture diffuses out of it, allowing faster accommodation of built-in stresses. However, the reason for a lack of full relaxation is still unknown and replication dry-out data is overlaid with 100%RH master curves of replications as a function of post-cure temperature.

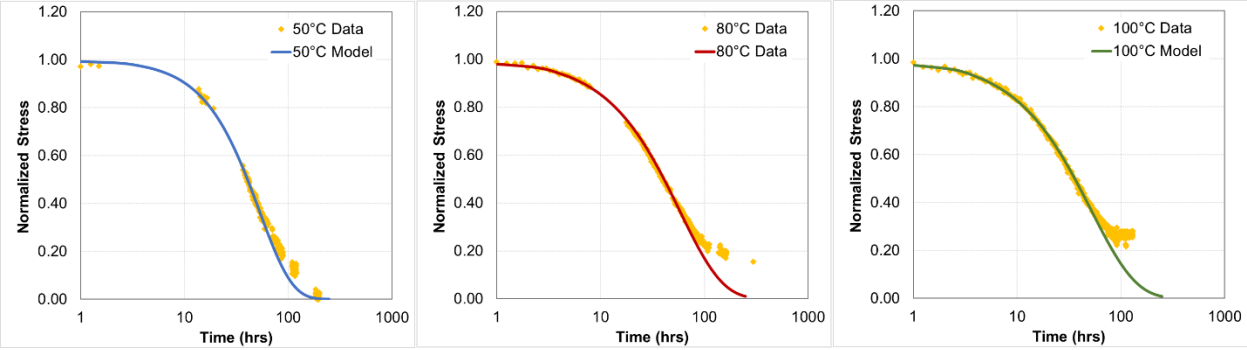

Figure 54. Normalized master curve versus real replication data of 0.25%PI formulations post-cured to (a) 50°C (b) 80°C and (c) 100°C in 100%RH environments.

In Figure 54, the master curves and real replication stress data for 50, 80, and 100°C post-cured replications are normalized to a value of 1.0 at 0.25hrs to directly compare different behaviors as a function of post-cure temperature. In all cases, the replication desorption data

initially follows the model very closely, though a deviation starts to occur later in time that modifies the total amount of stress relieved. It is clear with increasing temperature a smaller percentage of stress is relieved per humidity cycle. Only the 50°C post-cure sample exhibits 100% relaxation compared to the 72% and 46% for the 80 and 100°C samples, respectively. Even though these samples experience different amounts of relaxation, they all exhibit deviations at approximately the same time, 55hrs, even though the replications absorbed moisture longer than that. Since not all the moisture has been removed from the polymer, an effective amount must have desorbed, and the relaxation rate is slowed due to the loss of polymer chain mobility as hydrogen bonding reforms. Following the onset of deviation, relaxation is controlled by the dry relaxation rate, which describes the differences in stress relieved by each post-cure. For example, the dry relaxation rate of 50°C post-cure sample is five orders of magnitude faster than the 100°C post-cured coupon and continues to relax to zero while the 100°C plateaus almost instantaneously after deviating from the 100%RH master curve. This data indicates that while relaxation rates are substantially enhanced by plasticization, there is an inherent amount of stress that can be relieved by each system due to a tradeoff between desorption rate and relaxation rate. This is supported by similar diffusion rates in each system and wildly dry different stress relaxation rates.

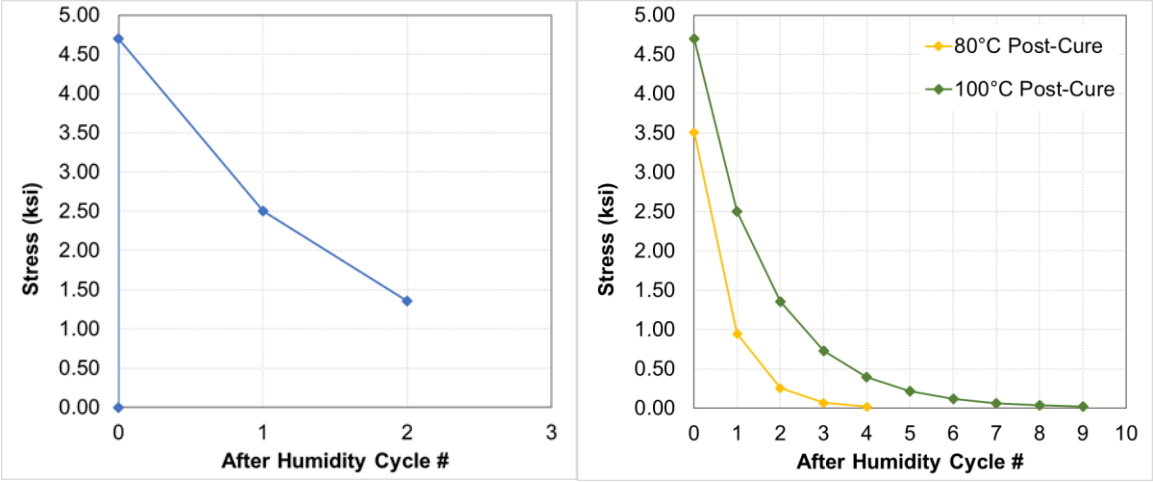

Figure 55. (a) Real stress profile of 0.25%PI replication with 100°C post-cure and (b) modeled stress relaxation profile (80°C and 100°C) as a function of humidity cycles (100%RH + 0%RH).

To further substantiate the idea that desorption time can limit the amount of stress relieved, a 100°C post-cured coupon is monitored as a function of two humidity cycles (100%RH and 0%RH). The residual stress value after plateauing in 0%RH following each humidity cycle is summarized in Figure 55a. Initially characterized with a 4.70ksi residual stress due to the post-cure process induced a significant degradation in optical quality (0.259λ SFE), which is shown in Figure 56b. However, after a single humidity cycle, approximately half (46%) of its residual stress was relieved, reducing the value to 2.50ksi. The optical distortion following this cycle is shown in Figure 56c. Compared to the thermally-cured surface (Figure 56b), a significant amount of distortion was relieved (0.131λ SFE). While this is beneficial, the behavior upon a 2nd humidity cycle is of significant interest. As shown in Figure 55a, again, only 46% of the residual stress is relieved by the humidity cycle. The total residual stress is reduced to 1.3ksi. It is obvious when looking at the optical distortion in Figure 56d, that the surface did not benefit as much as during the first cycle and only relieved an additional 0.054λ SFE.

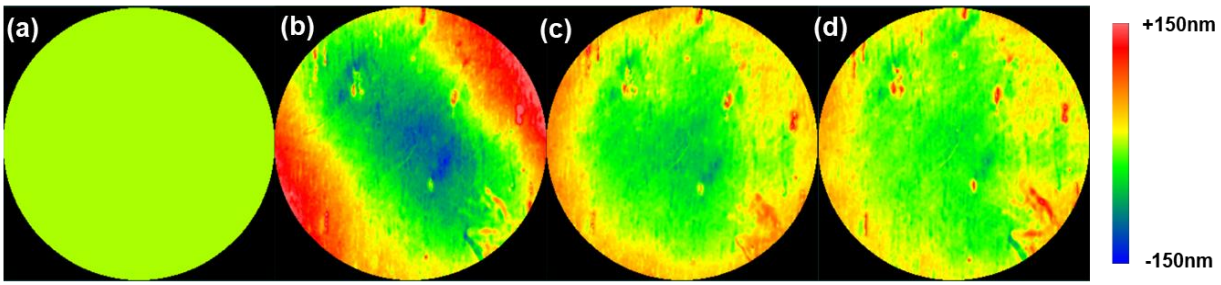

Figure 56. Laser interferometer images of 0.25%PI replication distortion isolated by subtracting the surface before 100°C exposure from each image. (b) Before 100°C (c) after 100°C (f) after 1st humidity cycle and (h) after 2nd humidity cycle.

The behavior of the 100°C post-cured replication in Figure 55a indicate there is a diminishing benefit to residual stress state with more humidity cycles since only a certain percentage of stress can be relieved with each cycle. In the 100°C post-cured replication, since only 46% of the initial stress is relieved, 7+ cycles are required to relieve the 4.70ksi residual stress. This behavior is modeled in Figure 55b. However, if the crosslink density of the material, or stress relaxation rate, are decreased, this process can become more efficient. The 80°C post-cured material relieves 73% of its residual stress during each humidity cycle and only requires 3 cycles to fully remove the thermally induced tensile stress. This is value is decreased further with the 50°C post-cure; 100% of the residual stress can be relieved during each humidity cycle. While this process can mitigate some of the optical distortion due to curing and enhance long-term storage stability, as crosslink density becomes increasingly large with post-cure temperature, the effectiveness of utilizing this technique to relieve distortion is reduced due to the polymer relaxation times exceeding desorption times.

6.6. Conclusions

Non-zero residual stresses were previously observed to cause a deviation in replication optical quality; however, these stresses can cause additional problems for replicated composite optics due to their penchant for undergoing stress relaxation. Under dry storage conditions, the initial stress is driving force for optical drift and amplifies the magnitude while the degree of crosslinking in the polymer controls the rate at which it occurs. Compared to thermally cured systems, UV cured resins are characterized by lower residual stresses and relaxation rates, corresponding to higher, but not perfectly stable replicated surfaces. Even though thermal exposures enhance crosslinking to restrict chain mobility, the large increase in residual stress offsets the benefit and induces larger optical distortions over time that continue throughout the mirror's lifetime. Since any non-zero stress will cause optical degradation over time, and fabricating replications with zero stress is very difficult, if not impossible, a post-process was necessary to accelerate relaxation changes in order to stabilize the surface.

When replications are exposed to high-humidity environments, the initial distortion is controlled by the CME; however, hygroscopic stability is unrelated to CME and is instead controlled by the time at which swelling switches to stress relaxation. As moisture diffuses in, it enhances polymer mobility, allowing faster accommodation of moisture-induced swelling stresses and driving the transition from large magnitude optical distortions control by CME to a stress relaxation. Furthermore, the zero stress is maintained upon returning to the dry state, allowing a path towards accelerating the stress relaxation process over dry storage conditions. This process was demonstrated to enhance long term stability following the procedure. And while this process is particularly desirable for thermally cured replications, only a certain amount of relaxation was achieved if built-in stresses were too large and crosslink density too high. Due to the tradeoff

between polymer relaxation rate and desorption times, multiple humidity cycling is required in certain systems to achieve a fully zero-stress state.

Chapter 7. Replication Space Stability Concerns: Thermal and Radiation

7.1. Introduction

As stated in the previous chapter, replicated surfaces must retain their shape with extremely high fidelity to be applicable for space telescope UVOIR mirror applications [29]. The previous chapter dealt with understanding replication stability concerns prior to launch and developing processes to enhance the critical properties. While optical quality and stability may be optimized on Earth, upon launch, replicated mirrors will experience additional changes in environment. Furthermore, these environmental conditions are often unavoidable; thermal excursions [94] or high-ionizing space radiation causing chain scission [95]. Optical changes accumulated in space are particularly critical because without active alignment and focusing controls, they cannot be fixed. A prescription error in the HST was realized after launch [45]. While this was repaired with adaptive optics manually installed by astronauts, it was extremely expensive and a slow evolution in optical degradation due to polymeric environmental distortions cannot be similarly mitigated. Therefore, preventing any surface change is crucial to ultimate telescope performance.

In this chapter, we investigate optical stability with respect to space environment considerations. First, thermal cycling stability is evaluated as a function of resin formulation and processing to characterize optical changes occurring as a result of thermal fluctuations experienced over a satellite's lifetime. Then, the thermal stability of replications after high-humidity stress relaxation is performed to characterize whether relieved stresses are reintroduced in new elevated temperatures exposures and whether moisture diffusing to the bondline interrupted the interfacial bond with the composite. Then, the impact of high-energy gamma radiation on material properties is evaluated to understand how radiation is impacting the polymer on the molecular scale. Finally,

the optical quality and thermal cycling stability following gamma radiation are analyzed to determine if exposures to radiation damage the ultimate optical performance.

7.1. Thermal and Thermal Cycling Stability

Satellite mirrors will experience fluctuating thermal environments throughout their lifetimes, which is a critical design consideration for all optics [94, 3, 29]. Some of these are by design, satellite mirrors operate over a certain thermal range, often at low temperatures to reduce noise [29, 94]. However, thermal excursions from the designed range can occur and survivability temperatures are designed into the system. Since replications are bonded and organic structures, thermal fluctuations can potentially induce hysteresis that permanently degrades optical performance. At elevated temperatures, the replicating resin film can undergo cure shrinkage or stress relaxation phenomena [89], which would impact the stress state, and consequently the SFE, when returning to ambient temperature. If these stresses build up, failure can occur at low temperatures by microcracking or interfacial delamination from the composite substrate.

Microcracking was previously observed by Utsunomiya et. al [29] in a composite mirror when taken to cryogenic temperatures which created optical hysteresis in the system with thermal cycling and was not repeatable upon subsequent cycles. In replicated composite optics specifically, due to relatively low adhesion strengths between the composite and the replicating resin, microcracks or delamination can occur at this interface as mechanisms to relieve the high stresses concentrated there [43]. Since there are an increased number of mechanisms that can impact the thermal stability of replicated composite optics compared to conventional materials, there is a need to characterize dimensional distortion as a function of resin formulation and processing. Thermal

testing is performed to isolate sources of different mechanisms of distortion, which is critical to minimizing optical changes as a function of thermal fluctuations.

7.1.1. Thermal Cycling as a Function of Formulation and Processing

Thermal cycling was performed on replications with a variety of material properties and the stress state was monitored in order to characterize dimensional response to fluctuating thermal environments. Replications were manufactured with 0.75%PI concentration and cured at 25, 50, 100, and 200mW/cm^2 UV intensity, then cycled between 25°C and 50°C for 250x cycles. Optical characterization was performed before and after cycling; the change in surface topography was isolated and is shown in Figure 57 for 25, 100, and 200mW/cm^2. The subtracted images display an obvious trend; with increasing UV curing intensity, the optical distortion induced by thermal cycling is reduced. In all cases, the exposure induced a tensile residual stress, manifesting as a concave shape change with higher magnitude at lower curing intensities. The 200mW/cm^2 (Figure 57c) replication is characterized by the smallest optical change; only exhibits a 0.027λ SFE change compared to the 0.070λ SFE optical distortion accumulated in the 25mW/cm^2 sample as a result of thermal cycling. The 50mW/cm^2 and 100mW/cm^2 samples fall somewhere in between.

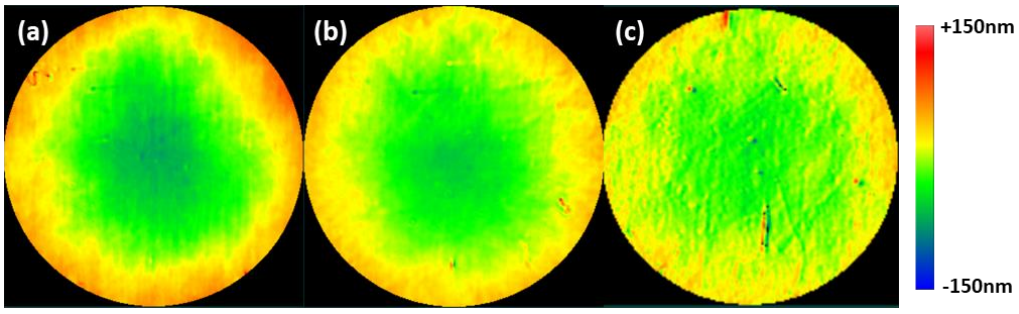

Figure 57. Laser interferometer images of the optical distortion due to thermal cycling for 0.75%PI replications cured at (a) 25 (b) 100 and (c) 200mW/cm^2.

Since all replications are characterized by a tensile stress following thermal cycling, stress relaxation at 50°C is likely the source of dimensional distortion. The real, measured change in replication stress is plotted with the modeled CTE mismatch stress (Equation 8) in Figure 58 as a function of UV curing intensity. The modeled stress is a function of CTE and elastic modulus values, therefore there is a slight reduction in predicted stress at higher curing intensities due to a large reduction in CTE value and slight increase in elastic modulus. When comparing the measured and modeled stress, the data matches well for 50 and 100mW/cm^2 replications, indicating they both underwent full relaxation during the 250x thermal cycles. However, on the low curing intensity end (25mW/cm^2), the observed change in stress is higher than can be accounted for with just CTE mismatch and is likely due to cure shrinkage phenomena simultaneously occurring. The necessity of both phenomena in describing the formation of residual stresses for 0.25%PI replications as a function of post-cure temperature was previously shown in Figure 28a. The data also deviates at high UV curing intensities, the 200mW/cm^2 sample only partially relaxed during thermal cycling. During the 250x cycles, approximately half of the CTE mismatch stress was relieved, correlating to the smaller observed SFE compared to the other samples.

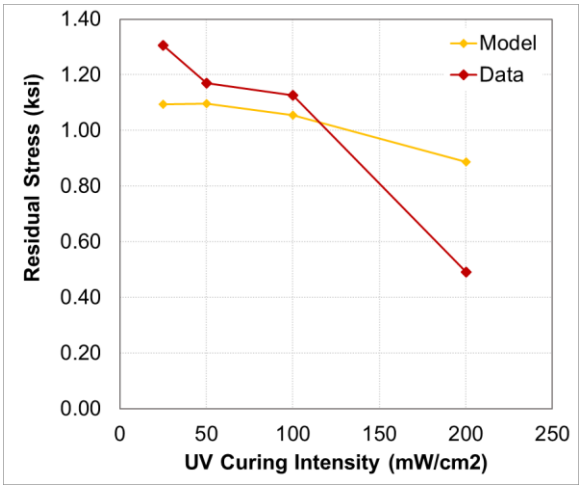

Figure 58. Real versus predicted thermally induced residual stress over 25°C range.

Since the predicted CTE mismatch stress values are not particularly different as a function of UV curing intensity and their optical response to thermal cycling does vary by quite a lot, the stress relaxation must account for the difference. While elevated temperatures provide thermal energy to the polymer that enhances chain mobility, this is mitigated with the higher number of anchored crosslink sites as a function of increasing curing intensity. The difference in full relaxation time between the 25 and 200mW/cm^2 replications is approximately 5 orders of magnitude. However, during thermal cycling, the replication is not held for long periods of time at temperature and instead, samples are repeatedly relieved of small stresses at each exposure which accumulate over cycles, leading to a build-up in tensile residual stresses at room temperature. The amount of stress relieved during each cycle can be calculated from the observed change in stress; the 200mW/cm^2 sample would experience a 0.0020ksi relaxation during each cycle. This value is 2.5x smaller than the 25mW/cm^2 sample that must relieve at least 0.0052ksi stress during each cycle to achieve full stress relaxation. While the impact of thermal cycling on optical distortion was reduced with cure intensity, it was not fully mitigated and a non-negligible ~0.50ksi residual stress and 0.027λ SFE were induced.

Thermal cycling demonstrates the high susceptibility of replicated composite optics to undergoing dimensional distortions as a result of elevated temperature exposures due to accelerated stress relaxation. This is particularly concerning during repetitive thermal excursions because a different optical hysteresis will result from each exposure, and furthermore, they will compound more quickly than a sustained exposure due to the nature of relaxation behaviors. The fastest rate of change in stress relaxation occurs instantaneously when exposed to a different stress state. However, the amount of stress relieved is dependent on both the stress relaxation rate and the CTE of the system. Both behaviors are shown as a function of temperature in Figure 59 for the

0.75%PI replication cured at 200mW/cm^2. In Figure 59a, the thermal mismatch stress value is modeled as a function of temperature with the measured CTE and modulus values. Even at low temperatures such as 35°C, the CTE induces a 0.35ksi residual stress. Furthermore, the relaxation rate is accelerated by two orders of magnitude at 35°C compared to RT. Both the driving force and polymer mobility are accelerated as the elevated temperature increases, corresponding with a larger hysteretic optical distortion. Compared to 35°C, the CTE mismatch stress at 50°C is nearly 3x higher and the relaxation rate is 3 orders of magnitude faster, meaning that not only will higher temperatures result in larger optical distortions, they will also induce them faster.

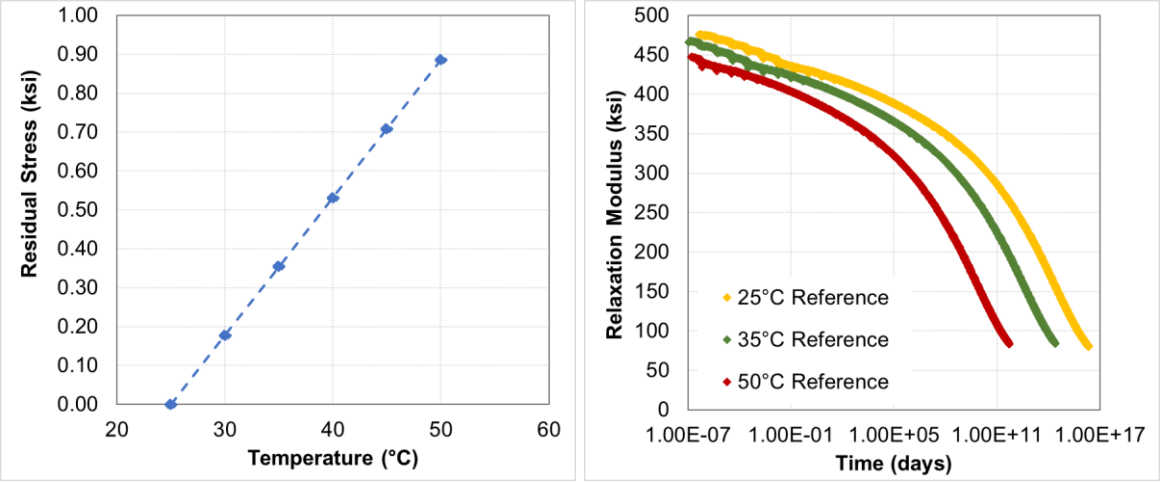

Figure 59. 0.75%PI cured with 200mW/cm^2 intensity (a) predicted residual stress and (b) master curve as a function of temperature.

The data in Figure 59 indicates that it is crucial to minimize or avoid these thermal excursions altogether due to the extremely high susceptibility of these exposures to induce optical distortions in replicated composite optics. Furthermore, to minimize damage induced by a potential high temperature exposure, the replicating resin should be characterized by a small CTE value and a high degree of crosslinking to reduce the driving force and relaxation rate, respectively. With the 0.75%PI formulation, both behaviors are enhanced with higher UV curing intensities due to an

increasing degree of conversion and crosslinking. And while formulations with higher PI concentrations are characterized by a reduced stress relaxation rate that would be beneficial to cycling stability, these formulations are not as easily modified without a thermal cure. Additionally, they are characterized by compressive residual stresses at RT that would exacerbate the stress state of the replicated films at elevated temperatures. Since the stress state is characterized by adding the CTE mismatch to residual stress, compressive residual stresses increase the driving force and tensile stresses reduce it. For maximum thermal stability, a small CTE, tensile residual stress, and zero relaxation at elevated temperatures is required. While none of the formulation and processing modifications of the UV cured resin in this dissertation have provided a relaxation rate slow enough to resist thermally induced distortions, modifications in the future can be utilized to reduce rates through the use of multifunctional monomers [56], nanoscale reinforcements [91], higher crosslinked photocurable formulations [63, 64], or hybrid systems to enhance thermomechanical performance [68, 59]. However, these formulation changes are accompanied by other material property degradations or processing disadvantages.

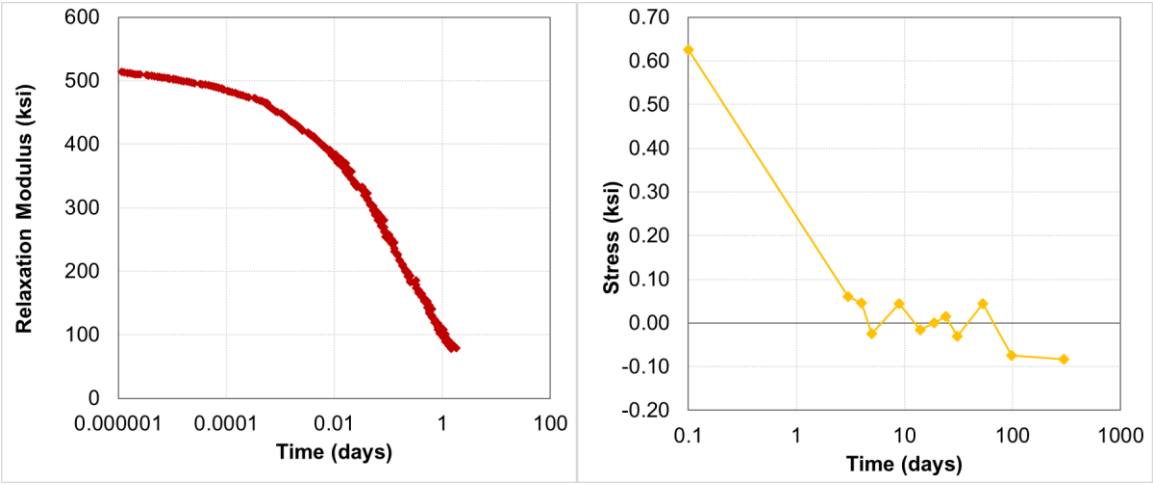

Figure 60. (a) Master curve for 0.25%PI after RT cure and (b) stress versus time for 0.25%PI after 1hr at 50°C.

Replications with slow relaxation rates can resist dimensional changes as a function of thermal environment, however, replications with extremely fast relaxation rates can fully relieve induced stresses quickly. The behavior of the 0.25%PI formulation after a short thermal exposure is of interest. The master curve for the 0.25%PI is shown in Figure 60a where 85% of stress is relieved in 1 day and 100% in less than 10 days. If the thermal exposure is short enough, the cure state will not be impacted and the relaxation rate following temperature will be fast. Therefore, a 0.25%PI replication is manufactured, post-cured to 50°C for only 1hr, and monitored as a function of time in dry storage in Figure 60b. By exposing to temperature for a very short period, a 0.65ksi residual stress value is imparted, though it relaxes in 7 days, and remains stable for 9 months following the exposure. The relaxation rate is very similar to the master curve, indicating that this short thermal excursion did not change the cure state of the resin, though this may become an issue if excursions are longer or hotter. The behavior of this replication after thermal exposure acts almost self-healing, by relieving the induced distortion almost immediately. While no optical distortion is desired, a short-term fluctuation is much more tolerable than permanent optical degradation. Besides tailoring a polymeric material that does not exhibit stress relaxation under temperature, with the resins available in this dissertation, it is currently the route to achieve the highest elevated thermal stability.

7.1.2. Thermal Stability After Accelerated Stress Relaxation

The sensitivity of replications undergoing stress relaxation in response to thermal exposures was demonstrated. However, it is generally assumed that once polymers have been cured to high temperatures, they are no longer susceptible to further thermal distortions. This behavior is particularly interesting for thermally cured replications that then undergo humidity cycling to

relieve their residual stress. By doing this, the zero-stress state temperature is returned to 25°C, and elevated temperatures can reintroduce residual stresses due to stress relaxation. This means that even though a polymer was cured to a certain temperature, it is not necessarily safe to expose it to the any temperature, even lower than the cure, without inducing further optical changes. To characterize whether thermal stresses reform for replications post-cured to high temperatures and stress relieved, samples from Section 6.5 are re-exposed to elevated temperature.

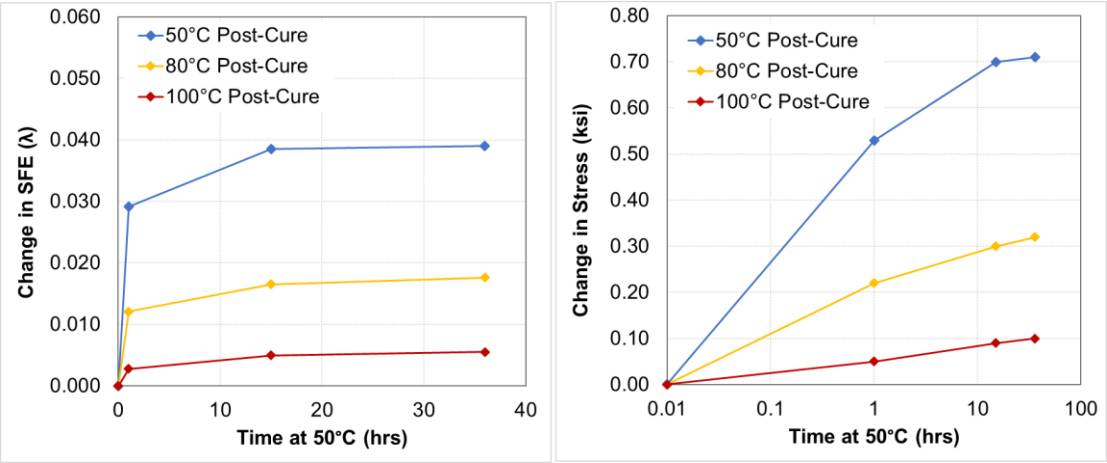

Figure 61. (a) SFE and (b) stress change over time at 50°C for 0.25%PI replications post-cured to 50°C, 80°C, and 100°C following high-humidity stress relaxation.

Replications with 0.25%PI followed by post-cures at 50°C, 80°C, and 100°C were humidity cycled to relieve some of the initial residual stress and then exposed to 50°C for incremental amounts of time. The change in SFE due to the thermal exposures are plotted as a function of time in Figure 61a. All the samples initially experience a large change in the SFE after only 1hr at 50°C, and continue to change with longer duration exposures, though at a slower rate. The magnitude of change is reduced with the higher temperature post-cured samples. The 50°C cured replication experiences SFE distortions 8x greater (0.039λ SFE) than the 100°C replication after 16hrs at 50°C. On the other hand, the 80°C and 100°C replications only experience 0.018λ and 0.005λ SFE

degradations, respectively. This behavior is not particularly surprising since with increasing post-cure temperature, the cure state is enhanced, reducing CTE values and relaxation rates. However, it demonstrates that the mechanism of thermal distortion is insensitive to the material's Tg or its initial curing temperature; it is solely a function of stress relaxation.

Since distortion is a function of relaxation, replication stress corresponding with the optical changes in Figure 61a are plotted in Figure 61b against the logarithm of time spent at 50°C. There exists an initially linear relationship for all samples, though the 50°C post-cured coupon plateaus due to full stress relaxation in the timeframe. This indicates there is a tradeoff in the humidity cycling behavior. Polymeric materials that are best suited for this treatment are characterized by high relaxation rates in order to fully relieve residual stresses during the humidity cycling. However, this behavior also reduces the subsequent thermal stability and correlates to faster and larger optical degradations. To characterize the relative increase in thermal stability at 50°C as a function of post-cure, TTS master curves are generated for each condition and shifted so the reference temperature is 50°C, shown in Figure 62a. With increasing post-cure temperature, the static elastic modulus is larger, and the "flow" regime is shifted later in time. Both features are related to the increased crosslink density and correspond with reduced polymer chain mobility. After room temperature curing, the degree of conversion is only 40.25% (Figure 7) and relaxation at 50°C is almost instantaneous. This rate is slowed with higher temperature post-cures. For example, the 100°C condition relaxes 5 orders of magnitude slower than the 25°C sample. However, even after an 80°C exposure, relaxation occurs quickly; 80% occurs in a single day.

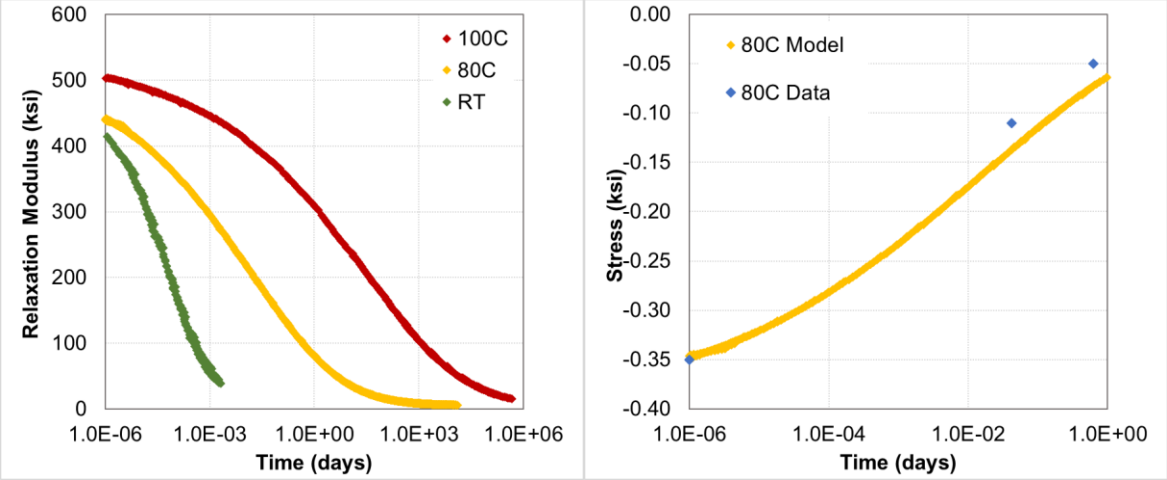

Figure 62. (a) TTS master curves for thermally cured 0.25%PI samples at 50°C reference temperature. (b) Real replication stress relaxation of 80°C sample versus TTS model.

To validate the model, the observed stress relaxation in the 80°C sample replication is compared to the master curve Figure 62b. Initially, the replication stress at 50°C is -0.35ksi and after 1hr of thermal exposure, the replication exhibits a +0.22ksi change in residual stress, matching the model. Additional time at temperature incurs another +0.08ksi in the replication, also correlating with the model. Dimensional changes will continue occurring until all the stress has relaxed at the high temperature, which it has for the 50°C post-cured sample in Figure 61b. Full relaxation for the 50°C post-cure occurred in less than 16hrs, which is why the delta stress plotted against log-time of thermal exposure switches from an initial linear relationship to a plateau in Figure 61b. In comparison, optical changes will continue occurring in the 100°C post-cured replication for decades, though with a substantially reduced SFE impact. None of the replications are insensitive to thermal hysteresis, though the enhanced material properties achieved with higher temperature cures reduce the impact of a subsequent thermal exposure on SFE degradations.

It is critical to understand any limitations in utilizing a high-humidity stress relaxation process in order to ultimately apply to process space based UVOIR replicated mirrors. Especially since it

is commonly assumed that polymeric materials are thermally stable below the glass transition temperature. The Tg of the 80°C post-cured material is 67°C; even though the material was cured 30°C higher than the exposure, and the Tg is 17°C higher, a 50°C hold for even 1hr induced a 0.012λ SFE distortion. While moisture exposures did relieve the initial optical distortion, the samples are still susceptible to incurring additional damage. Because of this, it is clear there is a tradeoff between enhanced optical quality and reduced thermal stability when performing a high-humidity stress relaxation process. Though it should be noted that even thermally cured replications that do not undergo humidity-induced relaxation are not necessarily stable at temperatures below the cure temperature. Relaxation phenomena are always driving the replicated mirror to a zero-stress state in any environment, though the impact on optical distortion is dependent on material properties and environmental conditions.

7.1.3. Cryogenic Interfacial Adhesion

While elevated temperatures should be avoided as much as possible, this is not necessarily a critical issue preventing the utilization of replicated mirrors in space based UVOIR satellites because NASA's Office of Chief Technologist Roadmap has identified operating temperatures between 0°C and 20°C [3]. However, temperatures below 20°C cannot be avoided and need to be investigated with respect to the CFRP composite and replicating resin bond. Interfacial adhesion between the composite and the replicating resin is a weak link in structural performance of replicated composite optics at low temperatures. Due to high CTE mismatch-induced strains at the weakly bonded interface, microcracking and delamination are potential failure mechanisms, which would be catastrophic. While none of the replications in Section 7.1.1 experienced delamination failures, they were all characterized by a net-zero residual stress at RT and small CTE values.

Interfacial bond failure becomes more prevalent if replications are characterized by a high tensile stress due to thermal curing, surfaces are improperly treated, or the interface is compromised by moisture interrupting bonding. The impact of surface preparation on delamination characteristics is first demonstrated in Figure 63. Replications were manufactured on CFRP substrates without plasma surface treatment to remove contaminants and modify surface chemistry. In this case, surface preparation of the CFRP composite was performed by solvent rinse only. These replications were then thermal cycled between -25°C and +50°C for 250x cycles before being removed from the chamber for optical characterization. Optical images of the replicated structures with 0.25%PI, 1.50%PI, and 5.00%PI concentrations are shown in Figure 63 following the thermal cycling. It is immediately apparent that two of the samples experienced delamination, though to different degrees. In Figure 63a, the 0.25%PI replication experienced complete delamination and fracture while the 1.50%PI replication in Figure 63b only experienced slight edge delamination at two locations. In complete contrast to those samples, the 5.00%PI replication in Figure 63c was characterized by no delamination or cracking apparent under visual inspection.

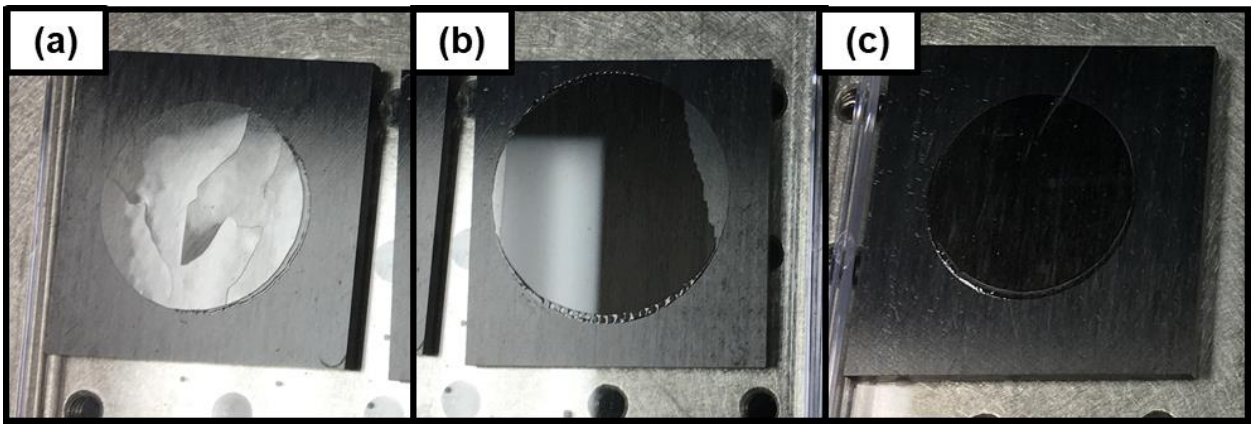

Figure 63. (a) 0.25%PI (b) 1.50%PI and (c) 5.00%PI replications after 250x thermal cycles between -25°C and 50°C.

In this case, the role stress and proper surface treatment plays in catastrophic failure is clear. The stress in films at cryogenic temperatures is a function of the polymer's material properties as described in Equation 8. The 5.00% replication is characterized by a small elastic modulus compared to the 0.25%PI. The stress imparted on each replication by a 50°C delta temperature is nearly 3x higher for the 0.25%PI formulation, 2.91ksi versus 1.16ksi. The dichotomy between the two samples is exacerbated by high stress relaxation rates in the 0.25%PI replications at 50°C compared to the 5.00%PI, which could add an additional ~1.9ksi stress at the cryogenic temperature. While it is impossible to know exactly when these coupons failed, a study performed by Barrie, et al observed a 150% increase in LSS when an appropriate surface treatment was performed on this specific K13C2U-RS3C composite structure, which could account for the observed differences in failure [43]. While the 5.00%PI replication does not exhibit any macroscopic indications of failure, a closer inspection of that sample and others with varying degrees of delamination are performed with laser interferometry.

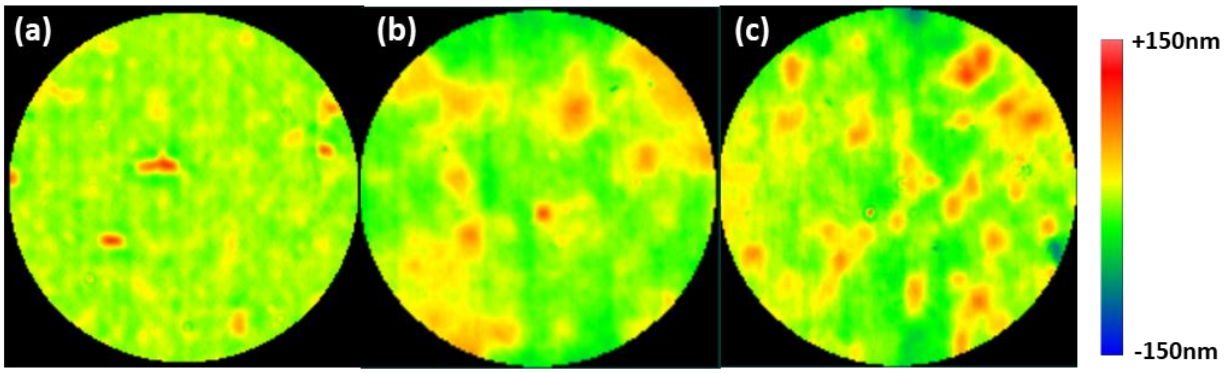

Figure 64. Laser interferometry images of optical distortion due to thermal cycling of (a) 5.00%PI (b) 1.50%PI and (c) 1.00%PI replication distortion after best-fit sphere removed.

Laser interferometry images of the optical distortion to the 5.00%PI replication due to thermal cycling is shown in Figure 64a. It is immediately apparent that there are a several localized regions of distortion. This type of optical change has not been observed in any replication as a function

residual stress change due to time, humidity, or elevated temperatures. Residual stress changes manifest as convex or concave spherically uniform distortions. Therefore, other formulations with varying degrees of macroscopic failure were examined with laser interferometry in order to determine if these features were present in other samples. The optical distortion of the 1.50%PI and the 1.00%PI replications are shown in Figure 64b and c, respectively. The regions of localized distortion also appear on these surfaces, though to a different degree. The concentration of the features in the three replications correlate with the magnitude of residual stress induced by -25°C; the stress in the 5.00%PI replication is the lowest and so are the number of features. On the other hand, the 1.00%PI replication has the highest residual stress due to its elastic modulus and consequently, the highest number of these nodules. Even though no macroscopic visual indication of failure has occurred on the 5.00%PI replication, we believe these features are indications of failure occurring at the bonded interface. They may be due to a small delamination or microcrack and are a precursor to macroscopic failure.

In order to inspect the failure features, ultrasonic testing was performed through the replicating resin, interfacial bond, and through the first ply of the CFRP composite. C-scans were generated, and the interfacial region was inspected to compare to failure features observed on the surface of the replication. These comparisons are shown in Figure 65a with observed interferometer distortion and Figure 65b-d for UT. There is an inherent gradient in epoxy resin thickness, so the UT C-scans are shown between ~68 and 80μm, which encompasses the desired thickness of 75μm. With this technique, no indication of delamination at the interface is detected and the surface distortion is most likely occurring as a result of microcracking. If the optical impact is characterized, these features are on the order of 2 to 5mm in diameter (0.5 to 0.2 1/mm spatial frequency) and only account for 0.009λ SFE distortion in this particular sample, however, the

impact on SFE would entirely depend on the number of these sites. The localized features will increase scatter, and while undesirable, this fracture mode is substantially better than delamination because it does not induce global shape distortions or cause catastrophic failure.

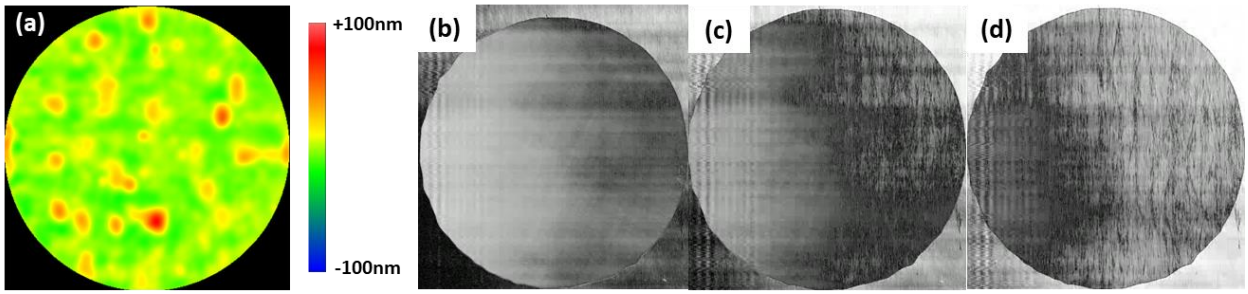

Figure 65. (a) Interferometer image of damage. UT scans of interface region at approximately (b) 68µm (c) 74µm and (d) 80µm below surface of epoxy replicating resin.

Since failure in the samples without plasma treatment was not directly observed, the limits of the structural bond are of interest in the system to bound its performance limits, specifically for composites treated with plasma surface exposures prior to replication. Therefore, replications are fabricated with 0.25%PI concentration and post-cured to different temperature: 50°C, 80°C, and 100°C. This formulation is characterized by a fast stress relaxation rate and high cure shrinkage, which was observed in Section 5.3.3 to produce samples with highly tensile residual stresses at RT after post-cure. Additionally, due to its high stiffness, the samples will experience substantially higher CTE induced stresses than other formulations during cryogenic exposure. After manufacture of the replications, the samples are cooled to -25°C, -40°C, -50°C, and -70°C (lowest temperature achieved by the chamber) and held isothermally for 1hr. After manufacture and each subsequent cryogenic exposure, the coupons are inspected for failure optically and with laser interferometry to search for the localized features observed in Figure 64. Since the CTE is known, if failure is detected, the interfacial adhesion strength can be roughly calculated. A summary of the data is shown in Table 7.

Table 7. Interfacial delamination and bond strength for 0.25%PI replications as a function of post-cure temperature.

Post-Cure Temperature (°C)	As-Manufactured Residual Stress (ksi)	Failure Temperature (°C)	Maximum Stress Before Failure (ksi)	Stress Inducing Failure (ksi)
25	0.04	-50	3.82	4.40
50	1.90	-25	3.98	4.61
80	3.51	-25	3.51	5.50
100	4.66	25	-	4.66

As the tensile stress at RT is increased by the thermal post-cure, the temperature at which failure occurs is higher. Interestingly, the replication cured to 100°C experienced failure during the cool-down and small failure features similar to Figure 64 are observed (Figure 66a). Due to the extremely fast stress relaxation rate and high cure shrinkage, the delta stress incurred between 100°C and 25°C induced some damage. The residual stress value measured was 4.66ksi. Since the method of calculating changes in residual stress tracks global distortions and the failure only induces small localized features, the measurement technique is not sensitive to how much the residual stress is counterbalanced or absorbed by the failure. In any case, we now know the adhesion strength is somewhere between 3.51ksi and 4.66ksi because the 80°C replication did not experience failure. It is important to note that during humidity cycling of thermal post-cured replications in Section 6.5, the residual stress values were shifted >6ksi in tension; however, no failure occurred at the interface. This is because the stresses measured by laser interferometry during this exposure were due to localized swelling and shrinkage distortions within the polymer film itself. The stress is exerted at the moisture diffusion front, not the bonded interface. Additionally, due to plasticization of the polymer as it absorbs moisture, the material becomes more compliant and the transfer of stress to the interface is reduced.

To more accurately calculate adhesion strength, the other post-cured samples were cooled to sub-ambient conditions. The 50°C and 80°C post-cured replication fractured during the first cryogenic exposure to -25°C due to their high inherent residual stress value; failing somewhere

between above 3.51ksi. However, the sample cured at RT was able to successfully be cooled to -40°C before failure occurred upon the next exposure to -50°C, at a residual stress value above 3.82ksi. According to the failure of the three samples, the adhesive strength is somewhere between 3.98ksi and 4.40ksi. This range is similar between all the samples and is contained in the initial prediction; between 3.51ksi and 4.66ksi. Furthermore, the interfacial adhesive strength is consistent with the 3.19ksi strength measured by Barrie et. al on this specific K13C2U-RS3C composite panel [43]. Differences in plasma processing, adhesive residual stress state, and measurement technique could account for the slight increase in strength of the replicating resin over the thermally cured Loctite 9394 utilized in the study.

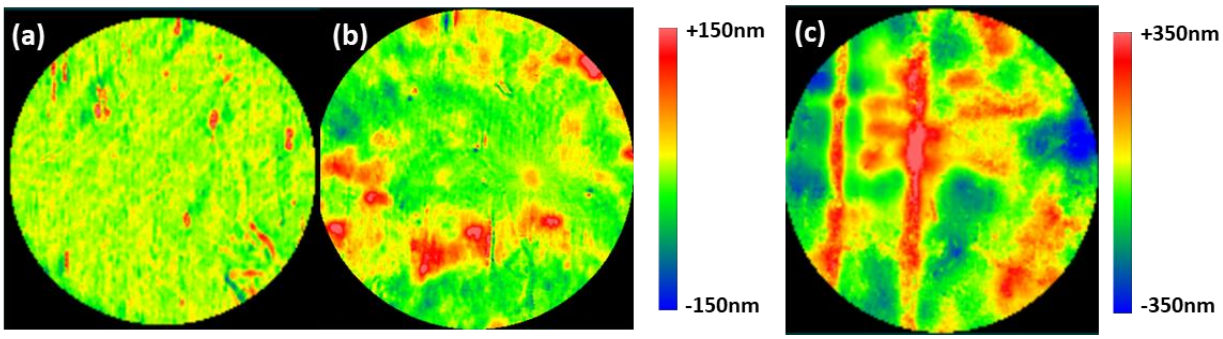

Figure 66. Evolution of the failure features in 0.25%PI + 100°C post-cure after (a) manufacture (b) -25°C and (c) -50°C.

Due to the failure of the 100°C post-cured replication during its manufacture (Figure 66a), we were interested in the progression of the failure features and how they grew or accumulated as a function of increasing stress. Initially, the 100°C sample was characterized by having ~15 small regions of high-height intensity that appear to be aligned vertically, consistent with the direction of the carbon fibers. The replication was then subjected to cryogenic temperatures and monitored with laser interferometry. As shown in in Figure 66b, after exposure to an additional 2.04ksi stress due to CTE mismatch at -25°C, the features have grown in diameter, number, and height. Optically,

there are still no indications of macroscopic delamination or cracking, and all damage must be accumulated at the bonded interface of the CFRP composite and the replicating resin. However, after inducing an additional 3.06ksi stress by cooling to -50°C, macroscopic failure is observed with the appearance of two vertical cracks running through the entire length of the replicated film. These cracks are also visible in the laser interferometer images (Figure 66c). Straight cracks such as these are generally a result of an anisotropic stress; which is consistent with the observed failure since the cracks are parallel to the carbon-fiber direction of the top ply. While the composite layup is quasi-isotropic, it is not truly isotropic, and the surface ply can exert more influence. Due to the anisotropic nature of each individual ply, thermal expansion is higher perpendicular to the carbon fibers than parallel, which would cause the observed preferential fracture direction parallel to the carbon fibers on the surface.

Table 8. Interfacial delamination and bond strength for 0.25%PI replications post-cured, then stress-relieved with high-humidity exposures.

Post-Cure Temperature (°C)	Residual Stress After Stress Relaxation (ksi)	Failure Temperature (°C)	Maximum Stress Before Failure (ksi)	Stress Inducing Failure (ksi)
25	0.00	-50	3.78	4.36
50	1.45	-50	4.16	4.57
80	0.97	-50	3.56	3.96

Now that the interfacial adhesion strength between the CFRP composite substrate and the replicating resin has been evaluated, we are interested in whether a high-humidity stress relaxation process damages the interface. It has been suggested by Ferguson [96] that water can diffuse through the face of the film and at the edge of the bond, interrupting hydrogen bonding, and ultimately impacting adhesion. Since moisture is diffusing through the entire replicating film during the accelerated relaxation process, it can reach the interface and potentially impact adhesion strength. On the other hand, due to a relaxation of built-in residual stresses, the replicated film may not delaminate over the temperature range at all. Therefore, new replications with 0.25%PI

concentration are manufactured, post-cured to 50°C and 80°C, and then undergo high-humidity stress relaxation. These coupons are then placed in a chamber and cooled to -25°C, -40°C, and -50°C. The results are summarized in Table 8 in direct comparison to samples in Table 7. The RT and 50°C post-cured replications failed at the exact same temperature as their non-relaxed counterparts. However, due to the ~2ksi reduction in the residual stress at RT, the 80°C stress-relaxed coupon failed at a lower temperature than its as-manufactured version; failure occurred at -50°C as opposed to the previous set of samples where failure occurred at -25°C. According to the failure of the three samples, the adhesive strength after high-humidity exposures is somewhere between 3.56ksi and 3.95ksi. This range may be slightly lower than extrapolated in Table 7 for the control samples, however it is not substantially different, indicating moisture ingression impacting adhesive strength is not an issue when utilizing a high-humidity stress relaxation process to stabilize the replication surface.

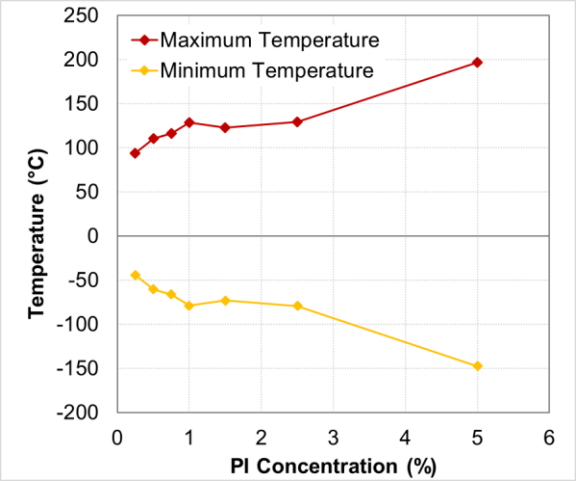

Figure 67. Safe working temperatures without failure as a function of PI concentration.

This testing further emphasizes the importance of a zero-stress state in replicated composite optics at ambient temperatures. Any nonzero tensile stress directly decreases the structural limits

of the mirror at low temperatures due to low interfacial adhesion strengths. Additionally, now safe working conditions can be calculated as a function of PI concentration. Assuming failure occurs at 4ksi, the maximum thermal limits, both hot and cold, are calculated in Figure 67. While the hot side induces a dimensional distortion due to stress relaxation, this does dictate the upper curing temperature, which is important if utilizing a thermal cure followed by accelerated humidity stress relaxation process. Higher PI concentrations can handle a larger thermal exposure without inducing damage. While a 100°C post-cure was observed to induce damage in the 0.25%PI replication, that post-cure would be acceptable for any other concentration. Additionally, the more compliant replications can achieve lower cryogenic exposures without interfacial damage. Therefore, depending on the mission requirements, a replicating resin with reduced stiffness might be necessary.

7.2. Impact of Gamma Radiation

The space environment has been shown to significantly impact various materials used for satellite applications. In the case of polymeric materials, prolonged exposure to high-ionizing radiation (gamma, x-ray, e-beam) can result in significant changes due to either chain scission, additional crosslinking, or a combination of both. The degree of these changes is based on several factors such as the dosage experienced, the atmosphere during irradiation, and the chemistry of the material being irradiated [95]. In the last few decades, high energy ionizing radiation such as gamma, x-ray and electron beam radiation has been shown to increase the cure state of epoxy resins that utilize a cationic photoinitiator [97, 65]. High-energy sources can dissociate the onium salt initiators to form reactive ions similarly to UV radiation, or directly cause epoxy-ring opening [65]. This is specifically desirable in curing epoxy-matrix composites because high-energy e-beam

and gamma radiation are less restricted by the depth limitations of lower energy UV sources [98, 99]. However, when utilizing high-energy radiation, chain scission and cross-linking reactions may occur simultaneously [100, 101].

While these studies indicate radiation is beneficial to the polymeric cure state of cationic photopolymerizations, many other instances in literature describe examples of di-functional epoxies exhibiting degradation in glass transition temperatures and reduced mechanical performance [100, 102, 101]. Changes in the polymer network structure, due to scission or crosslinking, impact the cure state as well as the mechanical and thermal behavior of the material. For the case of replicated optics where nanometer-scale variations in dimension are critical, radiation stability may impact final utilization. Therefore, the response of the system to radiation must be characterized in terms of material properties, optical quality, and optical stability. In this case, a Co^{60} gamma radiation source is used because it is a common method to simulate the material's susceptibility to space radiation environment. Additionally, this method is not restricted by the depth limitations as are other space-radiation sources, therefore radiation exposure will impact the bulk properties.

7.2.1. Material Property Changes with Gamma Radiation

The benefit of radiation has been demonstrated for epoxy resins in the presence of an onium salt photointiator. However, these studies were performed with liquid monomer where the high-energy radiation was utilized as an alternative method to dissociate the photointiator through thick coupons [97, 65]. In the case of replication, the resin is already cured and the photointiator dissociated under UV exposure. These are substantial differences which may cause the replicating resin to undergo degradation with gamma exposure. To characterize the whether chain scission or

crosslinking dominates the response of UV cured materials to gamma radiation, 1.50%PI neat polymers and replications are exposed to varying doses through 50Mrad. In general, crosslinking or scission will be indicated by changes in the material properties, however, this formulation was selected primarily for to its microstructure. Due to its heterogenous nature, specific structural information can be learned by observing the changes in each region as a function of increasing gamma radiation dose. For example, chain scission might preferentially target the highly crosslinked regions because sterically hindered bonds. We first investigate how gamma radiation is interacting with the polymer by evaluating the change in bulk material properties.

Table 9. Material properties related to stability as a function of gamma radiation dose for 1.50%PI.

Gamma Dose (Mrad)	Glass Transition Temperature (°C)	Elastic Modulus (ksi)	CTE (μm/m/°C)	Saturated Moisture (%)
0	62	425	67.7	2.76
50	82	500	56.5	2.06

The change in conventional material properties are characterized pre- and post-irradiation, then summarized in Table 9 for a 50Mrad dose compared to the control. It appears that radiation exposure is beneficial to polymeric material properties; the Tg increases by 20°C and the stiffness increases by 20%. Additionally, the CTE and the moisture absorption both decrease by 15%. These changes are all expected to contribute in favor of increased stability, which is extremely beneficial for replication applications. In the case of this specific UV cured epoxy resin, due to globally increasing material properties, fragmentation is not the primary result of radiation though the mechanism of further crosslinking is still unknown. Since the photoinitiator was fully dissociated under UV illumination, no new reactive sites are forming that increase conversion; though due to the lack of termination reactions, the reactive sites previously generated are still active. Under the nitrogen-purged radiation chamber, the polymerization mechanism is chain growth and for additional crosslinking to occur, the monomer must diffuse through the network to the reactive

sites. Like thermal energy, high-energy gamma radiation may induce additional crosslinking by driving monomer diffusion.

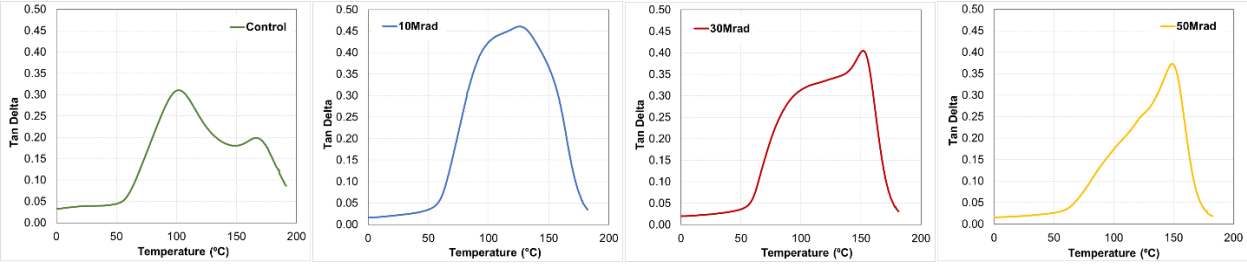

Figure 68. Tan delta curves for 1.50%PI after (a) control (b) 10Mrad (c) 30Mrad and (d) 50Mrad gamma radiation dose.

If high-energy radiation is driving monomer diffusion, it will be apparent in the DMA tan delta curves, as well as other information regarding structural changes. The tan delta curves are plotted in Figure 68 as a function of gamma radiation dose. The tan delta curve after just UV illumination is shown in Figure 68a and is characterized by two peaks. Initially, the lower temperature peak is higher in intensity than the elevated temperature peak. After exposure to 10Mrad of radiation, Figure 68b, the FWHM is reduced by 17°C due to the merging of the two individual transitions into a single peak. This behavior is like that observed as a function of thermal post-curing in Figure 18. The highly heterogenous 5.00%PI sample experienced its two peaks merging after an 80°C exposure as thermal energy drove diffusion and homogenization. However, upon additional radiation dosage in the 1.50%PI sample, it is clear the mechanism of crosslinking in thermal and radiation environments is not the same. After 30Mrad of radiation, Figure 68c, instead of maintaining the single peak, a second peak reappears. In this case, the intensity of the elevated temperature peak is higher than the lower temperature peak, which is the opposite of the non-irradiated sample. This behavior is unlike thermal curing, where once the two peaks merged, additional thermal energy only increasingly homogenized the system. In the case of radiation, it

appears that crosslinking of the low temperature material is occurring, and it is becoming more like the higher Tg, highly crosslinked nodules. As the radiation dose is increased even further to 50Mrad, Figure 68d, additional consumption of the low temperature material occurs, decreasing the FWHM by 22°C. However, the shape of the tan delta curve is still asymmetric.

Unlike thermal exposures, it appears that the high-ionizing radiation is strictly inducing crosslinking without providing energy for monomer or oligomer diffusion. Therefore, the mechanism of additional crosslinking is likely due to direct oxirane ring-opening by the radiation. This mechanism is indicated by the consumption of low-temperature material in the tan delta curves without much change to the high-temperature material except intensity. This indicates additional crosslinking is concentrated in the less highly crosslinked matrix where a higher number of unreacted monomer molecules are located. The formation of crosslinks in diglycidyl ether monomers exposed to gamma radiation without the presence of an initiator was observed by Penczek et. al [103], supporting the mechanism of direct ring-opening crosslinking in our system. Furthermore, the study measured low polymerization rates via this method, which would explain the relatively slow increase in Tg as a function of gamma radiation dose. The Tg of the 1.50%PI formulation shifted 20°C higher with a 50°C post-cure, yet to achieve the same increase in Tg with gamma requires an extremely high 50Mrad dose of radiation; a substantially higher dose of gamma radiation is necessary to completely consume the lower temperature species. Continued radiation exposure above 50Mrad was performed to 150Mrad. The tan delta curves of the two radiation exposures are overlaid in Figure 69. The consumption of low-temperature species is apparent, though the shape of the tan delta curve is still not symmetric after 150Mrad.

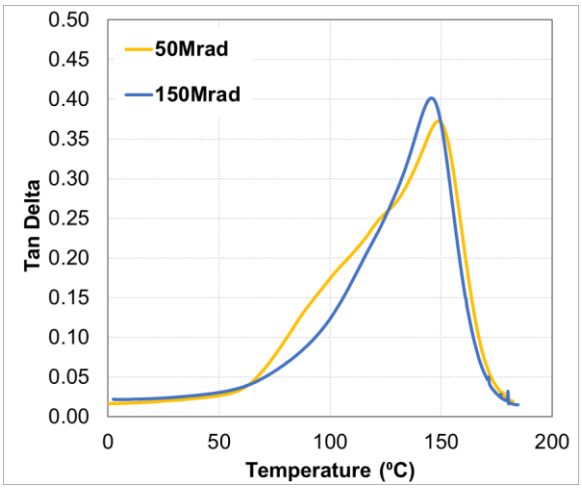

Figure 69. (a) Tan delta overlay of 1.50%PI after 50Mrad and 150Mrad gamma radiation exposure.

While the crosslinking reaction dominates the polymeric response to gamma radiation, fragmentation occurring at all cannot be ruled out, especially if we believe direct ring-opening is responsible for additional crosslinking. There is a slight, 2°C decrease in the tan delta peak temperature between 50Mrad and 150Mrad, which may be due to either testing noise or small-scale fragmentation. GC-MS can provide more detailed structural information regarding the effect of radiation on the chemical network to give an indication if small-scale fragmentation is occurring. The GC-MS scans of uncured monomer, pre-irradiation, and post-irradiation are shown in Figure 70. As shown in Figure 70a, peaks corresponding to the starting materials are indicated by #1 and #2. Peak #1 at 13.5 minutes is related to an oligomer and peak #2 at 22.2 minutes is also a reaction product due to polymerization. Figure 70b shows that even after UV exposure there remains evidence of the starting material components which is unsurprising due to the low degree of conversion values (Figure 7) However, after 50 Mrad of exposure, Figure 70c shows a complete consumption of the starting materials due to added polymerization. Furthermore, there are no additional locations of peaks appearing in the GC-MS plots after gamma radiation, indicating if chain scission is occurring, it is not fracturing the structure to form small molecular weight

molecules. Both the disappearance of starting materials and lack of evidence relating to structural breakdown corroborate the increase in modulus, Tg and reduced moisture absorption measurements previously described in for the irradiated specimens.

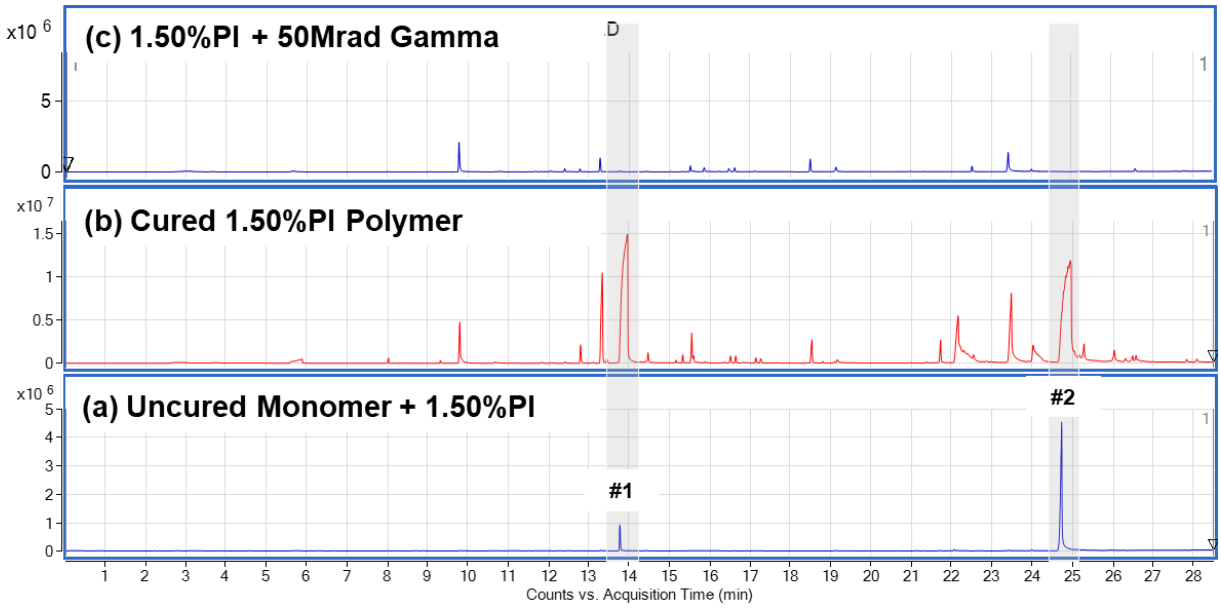

Figure 70. GC-MS scans of (a) uncured monomer + 1.50%PI (b) cured 1.50%PI polymer and (c) cured 1.50%PI polymer + 50Mrad gamma radiation dose.

The lack of detectable concentrations of chain fragmentation in this specific UV cured epoxy resin formulation is a good indication for replication optical quality and stability concerns. Penczek et. al observed higher rates of ring-opening in molecules with higher ring strain [103], therefore the higher rate of radiation-induced ring-opening compared to other bond fragmentations must be due to the lack of steric strain in other linkages. While this response to radiation is beneficial, it does deviate from behavior of other epoxy resins in the literature; for example, Laricheva et. al have shown the degradation in material properties of two-part epoxy resins due to fragmentation under gamma radiation [104]. However, his findings indicate radiation resistance is primarily a function of hardener used. While commonly utilized amine-based hardeners rank as the worst, all other hardener chemistries contain chemical bonds that are vulnerable to scission

under high energy radiation. By utilizing a UV cured formulation, no hardener is required, reducing the susceptibility to radiation-induced degradations.

7.2.2. Effect of Gamma Radiation on Optical Quality and Stability

To characterize the dimensional response of UV cured replications to gamma radiation, 1.50%PI replications are exposed to incremental doses of gamma radiation through 50Mrad. The dimensional behavior is important because the mechanisms inducing change in material properties may also manifest in terms of distortion, specifically cure shrinkage due to the crosslinking reactions. If the replicated surface is susceptible to optical changes in space as a result of gamma irradiation, they cannot be mitigated, and performance is permanently degraded. Laser interferometer images of a replicated surface before and after 50Mrad are shown in Figure 71. Visually, the surfaces appear very similar with only 0.004λ SFE change between the two states. This is especially promising data because 50Mrad is a relatively high dose of gamma radiation, and the surface is highly stable throughout the exposure range, indicating radiation is not a critical parameter preventing utilization in space based UVOIR telescopes. Upon characterization of the residual stress, though, the behavior as a function of irradiation was interesting.

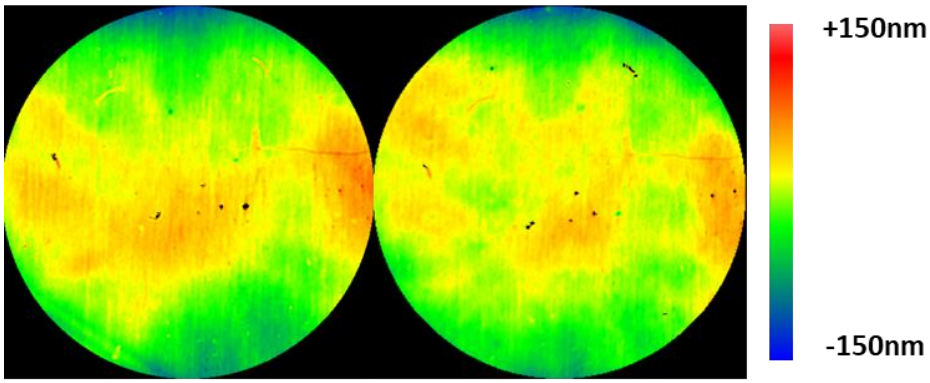

Figure 71. Laser interferometry image of a 1.50%PI replication (a) before and (b) after 50Mrad gamma radiation dose.

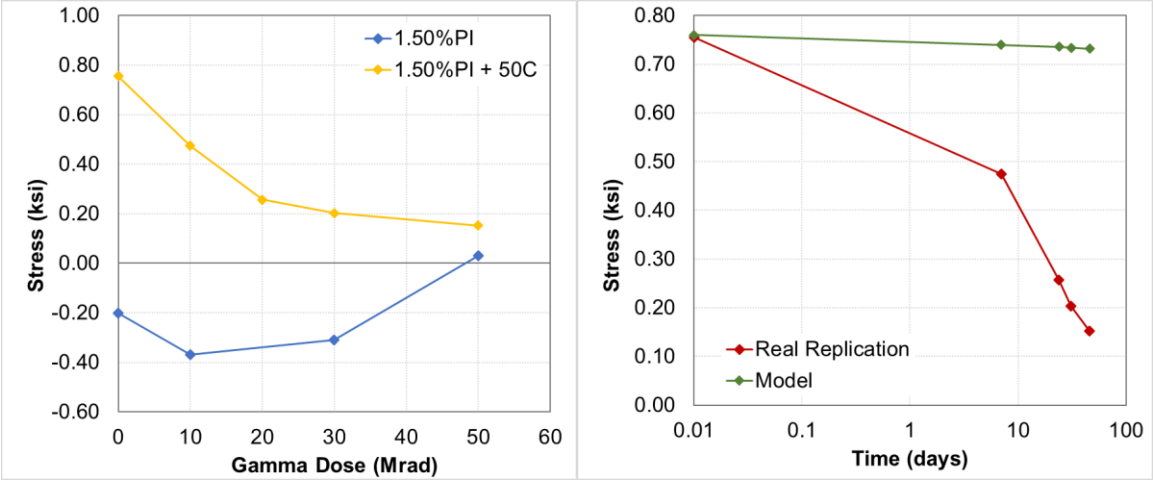

Figure 72. (a) Residual stress in 1.50%PI replications as function of gamma radiation dose for RT and 50°C post-cure. (b) Residual stress for 50°C post-cure real replication compared to resin TTS model as a function of time.

The residual stress profile of the 1.50%PI replication is shown in Figure 72a as a function of gamma radiation dose. Initially the 1.50%PI replication is characterized by a -0.20ksi compressive residual stress due to the cure gradient. With increasing radiation inducing additional crosslinks, the formation of increasingly tensile stresses as a byproduct of cure shrinkage are anticipated. In Figure 71, a lower compressive stress after 50Mrad is reflected in the shape of the replicated surface, where raised peak features appear to decrease in height after radiation. However, when stress is plotted at incremental values in Figure 72a, an increasingly compressive stress is observed after 10Mrad of radiation exposure. This behavior does turn around with additional radiation and the stress becomes more tensile at 30 and 50Mrad. Since gamma energy full penetrates through the sample, crosslinking localized to the surface cannot induce another cure gradient that would cause an increasingly compressive stress to form at 10Mrad. In order to characterize the trend in residual stress with radiation, another 1.50%PI replication was manufactured and post-cured to 50°C; the increased residual stress value will cause any changes to be magnified in comparison to the RT sample. The stress was the monitored as a function of

radiation dose through 50Mrad and is summarized in Figure 72a. Initially, the stress is characterized by a 0.76ksi tensile stress due to the thermal exposure. In this case, the residual stress only trends in one direction with increasing gamma radiation exposure; less tensile.

The direction in stress movement of the thermally post-cured sample is not consistent with cure shrinkage and appears to be operating under a relaxation mechanism. These radiation tests take several weeks (~10Mrad a week), therefore the observed decrease in stress may be an inherent and unintended side effect of the time between optical measurements. Therefore, the stress relaxation experienced by the replication is converted from radiation to time, and plotted on a log scale in Figure 72b. The stress undergoes the transition to "flow" regime in a matter of days and full relaxation is anticipated within several months. This replication stress is plotted against the stress relaxation rate predicted by the master curve for 1.50%PI. Over the same timeframe, only a 0.04ksi relaxation in stress is predicted due specifically to the time component. Additionally, the relaxation rate due to time would be expected to decrease further as radiation induces more crosslinking. Previous agreement was demonstrated between the master curves and real relaxation data, therefore the acceleration in stress relaxation must be due to the radiation exposure.

While gamma radiation yields a "net positive increase" in the degree of cure for the UV systems, fragmentation could be responsible for the reduction in film stress. The links most susceptible to fragmentation are highly strained; crosslinking reactions were previously ascribed to direct ring-opening of sterically reactive oxirane rings by gamma radiation. Fine-scale fragmentation of other highly strained linkages would explain the accelerated stress relaxation, because when they break, the molecular strain and film stress are reduced. These changes to the polymer were not detectable in any conventional material property or chemical analysis technique, indicating the occurrence of scission is extremely low or that the bonds immediately reform in a

different conformation at a lower stress state. While this relaxation behavior is not driven by chain mobility like the behavior is over time, temperature, and humidity, the observation of stress relaxation due to radiation only further drives home the idea that residual stresses should be zero, or as close to zero as possible, in replications prior to launch to prevent optical changes over time.

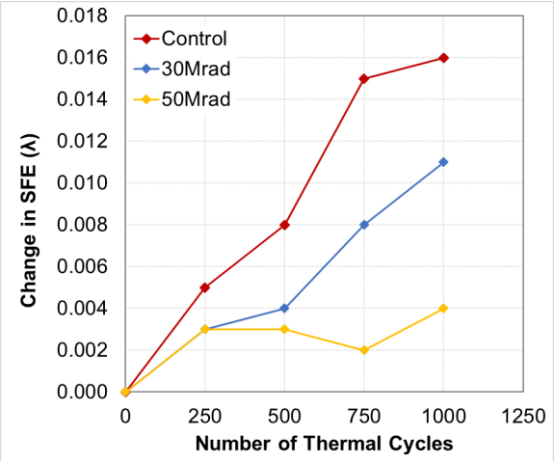

Figure 73. Change in SFE as a function of the number of thermal cycles for 1.50%PI control, 30Mrad, and 50Mrad gamma radiation dose.

The change in stress state and material properties of the replicating resin due to radiation exposure can also impact a replication's thermal behavior. While the increase in the elastic modulus can magnify the stress due to thermal changes, the reduction in CTE offsets the modulus change; the residual stress induced by a 25°C temperature is 1.03ksi for the control and 1.01ksi after 50Mrad, virtually identical. However, the higher crosslinking following radiation is likely to correlate with reduced thermally induced stress relaxation rates. Therefore, 1000x thermal cycles between -25°C and 50°C were performed on 1.50%PI replications with varying doses of radiation. The samples were monitored every 250x cycles and the change in SFE as a function of thermal cycling is summarized in Figure 73. The change in SFE increases for all replications with increasing number of cycles, however, the magnitude of the distortion is larger for the coupons exposed to less radiation prior to cycling. At each elevated temperature exposure, less stress

relaxation is occurring in the highly crosslinked irradiated materials, which correlates to smaller SFE distortions. The 50Mrad sample only experienced a 0.004λ SFE change in its surface due to 1000x thermal cycles, which is 25% smaller than the changes induced in the control sample. Enhanced thermal cycling stability is demonstrated compared to its non-irradiated counterpart.

Following 1000x thermal cycles between -25°C and 50°C, the replications then underwent an additional 1000x cycles between -50°C and 50°C. After this exposure, there is a pronounced difference in stability between the irradiated and non-irradiated samples. During the initial 1000x cycles, SFE changes were minimal and dependent on the difference in rates of stress relaxation at 50°C. However, upon the second 1000x cycles with expanded thermal limits, the irradiated replication remains stable while the control coupon undergoes complete failure. Laser interferometry images of the change in optical quality between the first and second round are shown in Figure 74. The SFE change between the first and second set of thermal cycles for the 50Mrad replication, shown in Figure 74a, is negligible and occurs as a spherically symmetric tensile stress change (small features are an artifact of angular misalignment). In comparison, the non-irradiated sample in Figure 74b, the surface entirely changes shape due to failure mechanisms at the interface. We can calculate the stress range over which failure occurred and compare it to the previous section for fidelity. Assuming full stress relaxation and a zero-stress state at 50°C, the delta temperature that induced failure is 100°C, causing a 4.12ksi tensile stress to be applied at the interface. However, the replication did not experience failure in thermal cycling when exposed to a 75°C thermal range, or 3.08ksi residual stress. Therefore, adhesive failure occurred between ~3-4ksi, consistent with previously measured values. Since the irradiated replication did not experience failure due to the -50°C exposure, we can assume that due to slower stress relaxation rates, a zero-stress state was not achieved at 50°C and a 4.12ksi residual stress was not applied to

the interface. The behavior is notably different than the non-irradiated mirrors and the benefit of gamma radiation on replication thermal cycling stability is clear.

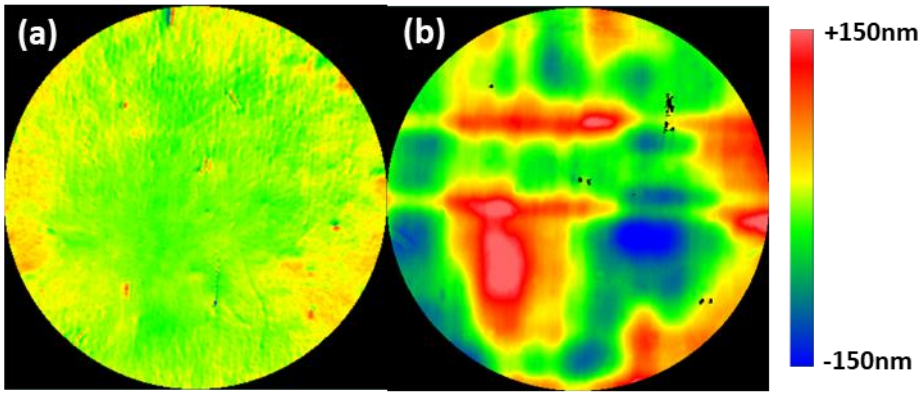

Figure 74. Optical distortion in 1.50%PI replications (a) with 50Mrad versus (b) control between the 1st 1000x TC (-25°C to 50°C) and 2nd 1000x TC (-50°C to 50°C).

Gamma radiation was shown to induce crosslinking in this specific UV cured resin chemistry. These changes as a result of gamma radiation exposure, both in terms of material properties and stress state, are beneficial to thermal stability concerns. While gamma exposure does decrease residual stresses in the replicated film, it is an extremely slow process compared to high-humidity exposures. However, due to the material property benefits of high-energy radiation exposure, gamma radiation can be utilized on Earth as a post-processing method to induce additional crosslinking, and consequently improve stability behavior. This methodology is particularly useful for low PI concentrations where the cure state cannot be modified without a thermal post-cure or high PI concentrations where low crosslinking in the matrix degrades thermomechanical performance. Gamma radiation offers an alternative method to modify the properties of a replicated mirror without unsuitable thermal exposures.

7.3. Conclusions

Replication environmental stability is particularly critical with respect to space environmental effects because any optical distortion induced in orbit cannot be mitigated or repaired. Therefore, knowing the limits of the system are crucial to not accidentally exposing the system to an environment that will cause damage. This is particularly critical to understand with respect to temperature because replicated mirrors can undergo optical hysteresis at elevated temperatures and interfacial failure at low temperatures. It was clear in this testing that any length of time spent above 25°C can induce some degree of stress relaxation, and consequently optical hysteresis when returned to ambient temperatures due to stress relaxation. While the impact is minimized with shorter exposure times, smaller CTE stresses (small CTE, modulus, and ΔT), and slower relaxation rates (high degree of crosslinking), some degree of hysteretic stress was always introduced. This is equally true for samples that have been previously cured to elevated temperatures and stress relieved. Since the zero-stress state is no longer at the high temperature, if exposed to the same temperature again, the stress relaxation phenomena can reintroduce tensile stresses.

While high temperatures should be avoided, that is not a problem since UVOIR space telescopes are not generally subject to elevated thermal exposures. However, low temperature exposures of the mirror are often utilized to reduce thermal noise, which can cause damage due to the inherently weak bond at the interface of the replicating resin to the CFRP composite. We measured the adhesion strength to be ~4ksi when proper surface preparation methods were performed, and failure manifested on the replicated mirror surface as small nodules of high height-intensity features prior to macroscopic failure. Failure was more easily induced at low temperatures in samples with a high tensile residual stress (thermal post-cure), elastic modulus, and CTE. While failure is more crucial to cryogenic exposures, it was also observed when a

conventional thermal cure was performed to increase the cure state; dictating the uppermost temperature that can be applied to enhance material properties prior to accelerated stress relaxation with high humidity. Furthermore, the adhesion strength was not impacted by humidity exposure and increased the cryogenic performance by allowing lower temperatures to be reached prior to failure.

While the thermal environment of a satellite is highly controlled, space mirrors cannot avoid exposure to space radiation. This is generally assumed to be an issue for polymeric materials due to chain scission and network fragmentation, however, the UV cured epoxy resins undergo additional curing and enhanced thermal stability after irradiation. Due to direct ring-opening reactions, the crosslink density was increased, slowing the rate of stress relaxation at elevated temperatures over non-irradiated parts. Furthermore, due to a small concentration of ring-opening and chain scission reactions, stress relaxation occurred at ambient conditions. The rate of relaxation was highly accelerated over RT due to the chemical fracture of highly strained bonds, and not limited by polymer mobility to a more equilibrium conformation. Due to the benefits of gamma radiation exposure, specifically the ability to change the cure state of formulations otherwise only modified by undesirable thermal treatments, irradiation can be utilized on Earth as a post-processing method to enhance dimensional stability.

Chapter 8. Conclusions

This work investigated the fundamental properties governing dimensional distortion in replicated composite optics, specifically by modifying the formulation and processing of a UV cured epoxy resin followed by parametric stability studies. It was found that a nonzero residual stress, and changes to the residual stress state under different environmental conditions highly control replication optical quality and stability. Photopolymerization was utilized to circumvent conventional optical quality-stability tradeoffs that occur with thermal curing, resulting in a replicated film characterized by a low residual stress without sacrificing high material properties. Variations in PI concentration, UV curing intensity, thermal post-cure, and high-humidity exposures were found to further impact both the formation and relaxation of stress, modifying optical stability.

Optical changes were monitored in terms of resin residual stress change by subtracting the initial replication surface shape from subsequent surfaces and converting the spherically symmetric distortion to a stress via Stoney's Equation. Using this technique to monitor distortion served twofold interest; isolating optical changes due to a change in environment and quantitatively linking the observed changes to conventional polymer material properties. Even though the CFRP composite substrates are 50x thicker and 100x stiffer than the replicating resin, small residual stresses, such as those due to cure shrinkage, cause nanometer-scale optical deviations. The impact of resin residual stress on degradations in optical quality can be minimized by utilizing a higher stiffness carbon fiber, or thicker composite substrate. A model was developed to describe the relationships between resin and composite material, stress, and thickness values.

Cure shrinkage and other cure-induced stresses are particularly crucial to maximizing optical quality. The formation of a nonzero processing stresses was shown to degrade replication

optical quality from the glass mandrel. In conventional two-part epoxy resins, thermal stresses induce stress values 10x higher than in photopolymerization. Furthermore, even when cured at RT, shrinkages are unavoidable and net tensile stresses are formed. With photopolymerization, cure gradient driven diffusion can offset the formation of tensile stresses, even shifting stress values into a net-compression. In this photoinitiator-monomer system, zero stress films can be manufactured by varying the PI concentration and film thickness. Furthermore, the UV curing intensity can be varied to modify the resin material properties without impacting the zero-stress coating.

While the replicating resin's material properties bear no impact on the formation of processing stresses, they relate to replication stability. Conventional metrics such as CTE, CME, and elastic modulus control the magnitude of distortion due to a hygrothermal environmental change. However, it was observed that stress relaxations during environmental exposure induced optical hysteresis when returned to the initial environment. Polymer network crosslink density controls the rate of stress relaxation, with increased PI concentrations, UV curing intensities, and thermal exposures corresponding with slower relaxation rates. Furthermore, these dimensional distortions can occur under no change in environment if a nonzero stress is present, however, relaxation rates are accelerated in the presence of elevated stress, temperature, and humidity conditions.

Elevated thermal curing of conventional two-part epoxies was avoided as a process to enhance the polymeric cure state for optical quality considerations and a photopolymerization technique was selected due to its high cure state and material properties with RT curing. Since the Tg is substantially higher than RT, as high as 140°C in some instances, it was expected if a polymer was heated to a value substantially below its Tg, it would not incur any distortion except that which

is described by CTE mismatch values. However, all materials in this study were characterized by some relaxation at elevated temperatures, though the magnitude and speed were controlled by the driving force and crosslink density. Formulations characterized by larger CTE and modulus values as well as reduced relaxation rates were most susceptible. Additionally, the formation of thermally induced residual stresses was also particularly bad during thermal cycling due to the accumulation of an equivalent stress upon each subsequent cycle compared to longer exposure times where a diminished amount of stress is relaxed with time. For one formulation (0.75%PI), the same amount of stress relaxation occurred after 250x thermal cycles between -25°C and 50°C that would otherwise occur in 25 million years of sustained exposure to 50°C.

Once non-zero residual stresses are induced, they are not stable over time and can damage the cryogenic performance. The inherent viscoelastic nature of the replicating resin allows stress relaxation to occur under dry storage conditions, though only when driven by a non-zero stress. A replication with zero processing stress was characterized by a 0.001λ SFE change between initial fabrication and after over 1 year of storage. While other RT UV cured replications exhibit a net-stress value, they are small (<0.003λ SFE) and most of the optical distortion occurs during the first year. However, when large tensile stresses form as a result of thermal exposure, the distortion over time is larger (>0.100λ SFE) and continue to occur with a critical magnitude after launch and throughout a lifetime of 30 years. Furthermore, any tensile stress directly reduces the cryogenic performance due to the relatively weak adhesive strength at the replicating resin-composite interface (~4ksi). For example, a replication exposed to +50°C was shown to experience microcracking at the interface at a temperature 25°C higher than its RT cured counterpart. Depending on the value of tensile stress, failure may occur between 0 and 20°C, the desired operation range for UVOIR optics necessary to reduce thermal noise during imaging.

Since non-zero residual stresses are so detrimental to replication stability and manufacturing a zero-stress film is virtually impossible, a post-process was required to accelerate relaxation of stresses. When replications were exposed to high-humidity environments, distortion was initially characterized by conventional swelling, though after a short period of time, the relaxation of built-in processing stresses was observed at a very fast rate due to moisture-induced plasticization. Normally hysteresis in the stress state has been shown to degrade optical quality, though in this case, the zero-stress state was maintained upon returning to the initial dry environment and the replication to its initial mandrel-limited optical quality. This technique to accelerate the built-in stresses of a thermally cured system are particularly desirable, though there is an inherent limit to the amount of stress that can be relieved which is dictated by the rate of desorption compared to stress relaxation. However, multiple cycles can fully relieve stresses. For example, one replication post-cured to 80°C only requires 3 humidity cycles to fully remove 3.91ksi of residual stress distortion.

Once optical quality and stability have been tailored on Earth and launched into space, high-fidelity dimensional control is still required, even under unavoidable ionizing space radiation. Due to the onium salt photoinitiation of the epoxy compared to a conventional hardener chemical class, chain scission is not the primary response of the system to high-energy gamma radiation. Instead, due to ring-opening reactions, the cure state and material properties are enhanced. These reactions minimally impact optical quality by accelerating stress relaxation rates through fine-scale fragmentation. However, the net reaction is crosslinking, which results in enhanced thermal stability by reducing relaxation rates. Compared to an irradiated coupon, the control replication experienced interfacial failure during thermal cycling. Not only are high-energy radiative space

environments not damaging the replication, they enhance its stability and can be utilized as a post-cure process to modify the properties of a replicated composite optic.

In this dissertation we have generated an understanding of which properties are crucial to maximizing replication quality and stability. An as-manufactured net-zero residual stress, slow stress relaxation rate, and minimal CTE and CME values are desired. With photopolymerization, zero stress films have been manufactured that are characterized by small environmental expansions. If no elevated temperature exposures are required for a mission, the 0.75%PI formulation has demonstrated high technology readiness with respect to space based UVOIR satellites. However, with formulation and processing utilized in this dissertation, a thermal stability can still be improved upon.

When trying to enhance thermal stability, several processes have been suggested; the first being a high thermal cure to minimize relaxations and post-polish to the desired optical quality. In addition to this process being extremely time and labor-intensive, the system is characterized by a high tensile stress value which was shown to directly limit cryogenic performance. The same thermal cure followed by humidity cycling to relax residual stresses is much more promising as a technique to simultaneously maximize optical quality and stability. Careful resin material selection is required that is amenable to the process and exhibits thermal stability following residual stress removal. Several humidity cycles may be necessary, and while they do take time, require substantially less labor and if they can be performed in several months, are also timesaving compared to polishing.

While post-processing techniques provide a path to further enhance replication stability, so do modifications to the replicating resin chemistry. A resin with an extremely fast stress relaxation would exhibit “self-healing” properties as a function of different environments. This was

demonstrated with the 0.25%PI formulation upon a short thermal exposure that did not shift the cure state, full relaxation occurred in 7 days. While the removal of stress and return to initial optical surface are promising, a substantially faster rate is required, on the order of minutes, without the fear that many cycles may eventually increase the cure state and lose the "self-healing" behavior. Additionally, inorganic additives, such as those used in the dental industry, can be incorporated into a UV cured formulation to resist polymer mobility, though their presence may increase high-frequency scatter. The last technique to enhance replication stability is by modifying the chemistry of a UV cured epoxy to reduce residual stress rates even further. Due to substantially higher conversion values and shorter distances between crosslinks, potentially switching to a cycloaliphatic epoxy would reduce relaxation rates. Additionally, interpenetrating networks of acrylate-epoxy systems can reduce polymer chain mobility due to restriction by the other network, enhancing resistance to relaxation events. However, in all these cases, the impact on residual stress and conventional material properties must be characterized.

A critical finding of this work is the integral role stress plays on every aspect of replication stability; all distortion on the nanometer-scale can be described by its influence. This work moves replicated mirror technology closer towards utilization in space based UVOIR telescope applications. Now that controlling factors of dimensional stability have been identified, further modifications to resin chemistry can be performed to additionally enhance the replication environmental stability.

References

[1] B. Agrawal, J. Kim and M. Allen, "Cost-effective Large Apertures for Future Imaging Satellites," in *AIAA Space Forum*, Pasadena, 2015.

[2] H. Stahl, "Optics needs for future space telescopes," in *Optical Science and Technology*, San Diego, 2003.

[3] I. Trunper, P. Hallibert, J. W. Arenberg, H. Kunieda, O. Guyon, H. P. Stahl and D. W. Kim, "Optics technology for large-aperture space telescopes: from fabrication to final acceptance tests," *Advances in Optics adn Photonics,* vol. 19, no. 3, pp. 646-685, 2018.

[4] W. Wetherell, "The Calculation of Image Quality," in *APPLIED OPTICS AND OPTICAL ENGINEERING*, Academic Press, 1980, pp. 171-315.

[5] J. Harvey, S. Schroder, N. Choi and A. Duparre, "Total integrated scatter from surfaces with arbitrary roughness, correlation widths, and incidident angles," *Optical Engineering*, vol. 51, no. 1, pp. 1-11, 2012.

[6] J. Harvey and A. Kotha , "Scattering effects from residual fabrication errors," in *International Conference on Optical Fabrication and Testing*, Tokyo, 1995.

[7] R. Parks, "Overview Of Optical Manufacturing Methods," in *25th Annual Technical Symposium*, San Diego, 1982.

[8] K. Brown, "Lightweight Substrates for Mirrors," *NASA Tech Brief,* p. 19, January 1991.

[9] L. Matson and D. Mollenhauer, "Advanced Materials and Processes for Large, Lightweight, Space-Based Mirrors," in *IEEE Aerospace Conference*, 2003.

[10] P. Chen, C. Bowers, D. Content, M. Mrzouk and Romeo R.C., "Advances in very lightweight composite mirror," *Optical Engineering,* vol. 39, no. 9, pp. 2320-2329, 2000.

[11] P. Chen, A. Smith, T. Saha and R. Romeo, "Progress in very lightweight optics using graphite fiber composite materials," *Optical Engineering,* vol. 37, no. 2, pp. 666-676, 1998.

[12] B. Gallagher, M. Bergeland, B. Brown, D. Chaney and Tracy, "JWST mirror production status," in *SPIE Optical Engineering and Applications*, San Diego, CA, 2011.

[13] L. Peebles, Carbon Fibers: Formation, Structure, and Properties, Boca Raton, FL: CRC Press, 1995.

[14] W. Asher, "Epoxy Replication - Advantages And Limitations," in *SPIE Replication and Molding of Optical Components*, Los Angeles, 1988.

[15] H. Weissman, "Epoxy Replication of Optics," *Optical Engineering*, vol. 15, no. 5, pp. 436-441, 1976.

[16] T. Gajjar, D. Shah, S. Joshi and K. Patel, "Prediction of Spring-back Deformation for CFRP Reflectors Manufactured using Various Processes," *International Journal of Applied Engineering Research,* vol. 13, no. 6, pp. 144-148, 2018.

[17] J. Hwang, C. Jin, H. Seo and C. Kang, "Effect of the number of CFRP prepregs and roughness at the bonding area on the spring-back and flexural strength of hybrid composites of cfrp combined with CR980," *Metals,* vol. 9, pp. 1054-1066, 2019.

[18] J. Hochhalter, Replicated Mirrors using Carbon Fiber Reinforced Polymers, University of New Mexico, 2005.

[19] J. Hochhalter, J. Massarello, A. Maji and P. Fuierer, "The origins of fiber print-through in lightweight composite optics," in *SPIE Optics and Photonics*, San Diego, CA, 2006.

[20] J. Massarello, J. Welsh, J. Hochhalter, A. Maji and P. Fuierer, "Fiber print-through mitigation technique for composite mirror replication," *Optical Engineering,* vol. 45, no. 12, p. 123401, 2006.

[21] J. Koyanagi, Y. Arao, S. Utsunomiya, S. Takeda and H. Kawada, "Time and Temperature Dependence of Surface Accuracy of High-Precision CFRP Mirrors," in *18th International Conference on Composite Materials*, Jeju Island, Korea, 2011.

[22] E. Kasl, M. Mehle, J. Dyer, H. Clark, S. Connell and D. Sheikh, "Recent developments in composite-based optics," in *Space Telescopes and Instruments V*, 1998.

[23] A. Abusafieh, D. Federico and S. Connell, "Dimensional Stability of CFRP Composites for Space Based Reflectors," in *Optomechanical Design and Engineering*, San Diego, CA, 2001.

[24] J. Sultana and S. Forman, "Dimensional Stability Concerns in the Manufacture of Graphite/Epoxy Beam Steering Mirrors," in *34th Annual International Technical Symposium on Optical and Optoelectronic Applied Science and Engineering*, San Diego, CA, 1990.

[25] P. Chen and R. Romeo, "Ultra Lightweight Precision Optics Technology," in *Optical Deisng, Materials, Fabrication, and Maintenance*, Munich, Germany, 2000.

[26] P. Chen, C. Bower, D. Content, M. Marzouk and R. Romeo, "Advances in lightweight composite mirror technology," *Optical Engineering*, vol. 39, no. 9, pp. 2320-2329, 2000.

[27] J. Andrews, T. Martinez, S. Restaino, F. Santiago, C. Wilcox, S. Teare, R. Romero and R. Martin, "Carbon Fiber Reinforced Polymer (CFRP) Optics Quality Assessment for Lightweight Deployable Optics," in *Proceedings of the Advanced Maui Optical and Space Surveillance Technologies Conference*, Wailea, Hawaii, 2010.

[28] V. Iafolla, W. Holland, E. Pascale, G. Savini, S. Vives, D. Walker and M. Jones, "Final Report on Telescope and Satellite Readiness for FIR Interferometer," European Space Agency, 2016.

[29] S. Utsunomiya, T. Kamiya and R. Shimizu, "Dimensional Stability of CFRP Mirorrs for Space Telescopes Under Low Temperature Environment," in *18th International Conference on Composite Materials*, Jeju Island, Korea, 2011.

[30] B. Coughenour, S. Ammons, M. Hart, R. Romeo, R. Martin, M. Rademacher and H. Bailey, "Demonstration of robust curved carbon fiber reinforced polymer deformable mirror with low surface error," in *Adaptive Optics Systems II*, San Diego, CA, 2010.

[31] R. Zaldivar, H. Kim and G. Ferrelli, "Hygroscopic and thermal stability of high precision replicated epoxy composite mirrors," *Optical Engineering*, vol. 56, no. 11, 2017.

[32] R. Zaldivar, H. Kim and G. Ferrelli, "Effect of gamma radiation on the stability of UV replicated composite mirrors," *Optical Engineering*, vol. 57, no. 4, 2018.

[33] G. L. Ferrelli, H. I. Kim and R. J. Zaldivar, "Effect of photoinitiator concentration on hygroscopic stability of UV cured precision replicated composite optics," *Applied Optics*, vol. 59, no. 16, pp. 1-13, 2020.

[34] H. Meyer, R. Bauer, R. Furlong and R. Frank, "Replica Optics," Electro-Optical Systems, Pasadena, 1965.

[35] P. Brosens and V. Vudler, "Stability of lightweight replicated mirrors," *Optical Engineering*, vol. 28, no. 1, pp. 61-65, 1989.

[36] T. Kamiya, S. Utsunomiya, K. Komatsu and R. Shimizu, "IMPROVEMENT OF THE CFRP COMPOSITE MIRROR SURFACE USING A REPLICA METHOD," in *18TH INTERNATIONAL CONFERENCE ON COMPOSITE MATERIALS*, 2010.

[37] S. Utsunomiya, T. Kamiya and R. Shimizu, "CFRP composite mirrors for space telescopes and their micro-dimensional stability," in *Modern Technologies in Space- and Ground-based Telescopes and Instrumentation*, San Diego, 2010.

[38] T. Kamiya, S. Utsunomiya and R. Shimizu, "Thermal Stability of CFRP Mirrors for Space Telescopes Under Thermal Cycle," in *19th International Conference on Composite Materials*, Montrel, Canada, 2013.

[39] H. Kim, G. Ferrelli and G. Zaldivar, "Evaluating the use of self-assembled monolayer (SAM) release coatings for replicated optics," *Journal of Adhesion Science and Technology*, vol. 30, no. 23, pp. 2544-2556, 2016.

[40] G. Ferrelli, *Effect of Resin Cure on the Stability of High-Quality Replicated Composite Mirror Surfaces*, University of California, Los Angeles, 2016.

[41] F. Schreiber, "Structure and growth of self-assembling monolayers," *Progress in Surface Science*, vol. 65, no. 5, pp. 151-257, 2000.

[42] J. Trigo, "Dimensional stability characterisation of carbon fiber with epoxy and cyanate ester resin laminates due to moisture absorption," in *Spacecraft Structures, Materials and Mechanical Engineering,* , Noordwijk, 1996.

[43] C. Barrie, H. Kim, D. Marques and R. Zaldivar, "Investigations on the Effect of Plasma Treatment on the Adhesive Bonding Behavior of Ultra High Modulus K13C2U/Cyanate Ester Fiber Composites," *Submitted to Journal of Adhesion Science and Technology,* 2020.

[44] M. Davis and D. Bond, "Principle and practices of adhesive bonded structural joints and repairs," *International Journal of Adhesion and Adhesives,* vol. 19, no. 2, pp. 91-105, 1999.

[45] J. Krist and J. Burrows, "Phase-retrieval analysis of pre- and post-repair Hubble Space Telescope images," *Applied Optics,* vol. 34, no. 22, pp. 4951-4964, 1995.

[46] A. Abusafieh, D. Federico, S. Connell, E. Cohen and P. Willis, "Dimensional stability of CFRP composites for space-based reflectors," in *International Symposium on Optical Science and Technology*, San Deigo, CA, 2001.

[47] M. Pryor, "Hygrothermal stability of laminated CFRP composite mirrors," in *UV, Optical, and IR Space Telescopes and Instruments*, Munic, Germany, 2000.

[48] S. Utsunomiya and R. Shimizu, "Monitoring of Dimensional Stability of CFRP Mirrors for Space Telescopes by Using Embedded FBG Sensors," in *The 17th International Conference on Composite Materials*, Scotland, 2009.

[49] C. Decker, D. Decker and F. Morel, "Light Intensity and Temperature Effect in Photoinitated Polymerization," in *Photopolymerization*, 1997, pp. 63-80.

[50] Y. Ding and A. Sokolov, "Breakdown of Time−Temperature Superposition Principle and Universality of Chain Dynamics in Polymers," *Macromolecules,* vol. 39, no. 9, pp. 3322-3326, 2006.

[51] J. Crank, The Mathematics of Diffusion, Oxford: Clarendon Press, 1975.

[52] L. Dickson and A. Singh, "RADIATION CURING OF EPOXIES," *Radiation Physics and Chemistry,* vol. 31, pp. 587-593, 1988.

[53] J. Crivello, "The discovery and development of onium salt cationic photoinitiators," *Journal of Polymer Science Part A: Polymer Chemistry,* vol. 37, no. 23, pp. 4241-4254, 2000.

[54] R. Alonso, W. Brandt, E. Souza, R. Puppin-Rontani and M. Sinhoreti, "Photoinitiator concentration and modulated photoactivation: influence on polymerization characteristics of experimental composites," *Applied Adhesion Science,* vol. 2, no. 10, 2014.

[55] D. Chattopadhyay, A. Panda and K. Raju, "Thermal and Mechanical Properties of Epoxy acrylate/methacrylates UV cured Coatings," *Progress in Organic Coatings,* vol. 2005, pp. 10-16, 2005.

[56] C. Decker, "Kinetic Study of Light-Induced Polymerization by Real-Time UV and IR Spectroscopy," *Journal of Polymer Science,* vol. 30, pp. 913-928, 1992.

[57] B. Golaz, V. Michaud, Y. Leterrier and J.-A. Manson, "UV intensity, temperature and dark-curing effects in cationic photo-polymerization of a cycloaliphatic epoxy resin," *Polymer,* vol. 53, pp. 2038-2048, 2012.

[58] B. Ficek, A. Thiesen and A. Scranton, "Cationic photopolymerizations of thick polymer systems: Active center lifetime and mobility," *European Polymer Journal,* vol. 44, pp. 98-105, 2008.

[59] C. Decker, "Photoinitiated Crosslinking Polymerization," *Progress in Polymer Science,* vol. 21, pp. 593-650, 1996.

[60] L. Macarie and G. Ilia, "The influence of temperature and photoinitiator concentration on photoinitiated polymerization of diacrylate monomer," *Central European Science Journals,* vol. 3, no. 4, pp. 721-730, 2005.

[61] J. Lee, R. Prud'homme and I. Aksay, "Cure depth in photopolymerization: experiments and theory," *Journal of Materials Research,* vol. 16, no. 12, pp. 3536-3544, 2001.

[62] M. Sangermano, I. Roppolo and A. Chiappone, "New Horizons in Cationic Photopolymerization," *Polymer,* vol. 10, no. 136, 2018.

[63] Y. Kim, L. Kostanski and J. MacGregor, "Photopolymerization of 3,4-epoxycyclohexylmethyl-3′,4′-epoxycyclohexane carboxylate and tri (ethylene glycol) methyl vinyl ether," *Polymer,* vol. 44, no. 18, pp. 5103-5109, 2003.

[64] J. Crivello and S. Liu, "Photoinitiated Cationic Polymerization of Epoxy Alcohol Monomers," *Journal of Polymer Science,* vol. 38, pp. 389-401, 2000.

[65] U. Bulut and J. Crivello, "Investigation of the Reactivity of Epoxide Monomers in Photoinitiated Cationic Polymerization," *Macromolecules,* vol. 38, pp. 3584-3595, 2005.

[66] Y. Lin, "Investigation of Moisture-Desorption Characteristics of Epoxy Resin," *Journal of Polymer Research,* vol. 13, pp. 369-374, 2006.

[67] M. Vanlandingham, J. Eduljee and J. Gillespie, "Moisture Diffusion in Epoxy Systems," *Journal of Applied Polymer Science,* vol. 71, pp. 787-797, 1999.

[68] S. Yang, S. Kwak, J. Jin, Y. Choi, K. Paik and B. Bae, "Thermally resistant UV-curable epoxy–siloxane hybrid materials for light emitting diode (LED) encapsulation," *Journal of Materials Chemistry,* vol. 22, pp. 8874-8880, 2012.

[69] J. Song, A. McCormick and L. Francis, "Depthwise Viscosity Gradients in UV-Cured Epoxy Coatings," *Macromolecular Materials Engineering,* vol. 298, pp. 145-152, 2013.

[70] K. Yoshida and E. Greener, "Effect of photoinitiator on degree of conversion of unfilled light-cured resin," *Journal of Dentistry,* vol. 22, pp. 296-299, 1994.

[71] A. Kannurpatti, J. Anseth and C. Bowman, "A study of the evolution of mechanical properties and structural heterogeneity of polymer networks formed by photopolymerizations of multifunctional (meth)acrylates," *Polymer,* vol. 39, no. 12, pp. 2507-2513, 1998.

[72] G. Miller, V. Narayanan and A. Scranton, "Modeling of photobleaching for the photoinitiation of thick polymerization systems," *Journal of Polymer Science,* vol. 40, no. 6, pp. 793-808, 2002.

[73] C. May, Epoxy Resins Chemistry and Technology, New York: Marcel Dekker, 1988.

[74] P. Jacobs and E. Jones, "Diffusion of moisture into two-phase polymers," *Journal of Materials Science,* vol. 24, pp. 2343-2347, 1989.

[75] X. Fan, "Mechanics of moisture for polymers: Fundamental concepts and model study," in *Thermal, Mechanical and Multi-Physics Simulation and Experiments in Microelectronics and Micro-Systems,* Freiburg-im-Breisgau, 2008.

[76] W. Cook, T. Scott, S. Quay-Thevenon and J. Forsythe, "Dynamic mechanical thermal analysis of thermally stable and thermally reactive network polymers," *Journal of Applied Polymer Science,* vol. 93, p. 1348–1359, 2004.

[77] S. Lustig and N. Peppas, "Solute and Penetrant Diffusion in Swellable Polymers. VII. A Free Volume -Based Model with Mechanical Relaxation," *Journal of Applied Polymer Science,* vol. 33, pp. 533-549, 1987.

[78] S. Roy, W. Xu, S. Park and K. Liechti, "Anomalous Moisture Diffusion in Viscoelastic Polymers: Modeling and Testing," *Journal of Applied Mechanics,* vol. 67, pp. 391-396, 2000.

[79] M. Krzeminski, M. Molinari, M. Troyon and X. Coqueret, "Characterization by Atomic Force Microscopy of the Nanoheterogeneities Produced by the Radiation-Induced Cross-Linking Polymerization of Aromatic Diacrylates," *Macromolecules,* vol. 43, pp. 8121-8127, 2010.

[80] M. Wen, L. Scriven and A. McCormick, "Kinetic Gelastion Modeling: Structural Inhomogeneity during Cross-Linking Polymerization," *Macromolecules,* vol. 36, pp. 4140-4150, 2003.

[81] C. Kowandy, G. Ranoux, M. Walo, B. Vissouvanadin, G. Teyssedre, C. Laurent, A. Berquand, M. Molinari and X. Coqueret, "Microstructure aspects of radiation-cured networks: Cationicallypolymerized aromatic epoxy resins," *Radiation Physics and Chemistry,* vol. 143, pp. 20-26, 2018.

[82] S. Basu, L. Scriven, L. Francis and A. McCormick, "Mechanism of wrinkle formation in curing coatings," *Progress in Organic Coatings,* vol. 53, pp. 1-16, 2005.

[83] A. Stolov, T. Xie, J. Penelle and S. Hsu, "Stress Buildup in Ultraviolet-Cured Coatings: Sample Thickness Dependence," *Macromolecules,* vol. 34, pp. 2865-2869, 2001.

[84] J. Song, A. McCormick and L. Francis, "Depthwise Viscosity Gradients in UV-Cured Epoxy Coatings," *Mocromolecular Materials and Engineering,* vol. 298, pp. 145-152, 2013.

[85] G. Janssen, A. Abdalle, F. Keulen, B. Pujada and B. Venroy, "Celebrating the 100th Anniversary of the Stoney Equation for Film Stress," *Thin Solid FIlms,* vol. 517, pp. 1858-1867, 2009.

[86] J. Payne, L. Francis and A. McCormick, "The Effects of Processing Variables on Stress Development in Ultraviolet-Cured Coatings," *Journal of Applied Polymer Science,* vol. 66, pp. 1267-1277, 1997.

[87] A. Luciani, C. J. Plummer, R. Gensler and J. Manson, "Surface Pattern Formation in UV-Curable Coatings," *Journal of Coatings Technology,* vol. 72, no. 909, pp. 191-194, 2000.

[88] L. Schmidt, D. Schmah, Y. Leterrier and J. E. Manson, "Time-Intensity Transformation and Inteernal Stress in UV-Curable Hyperbranched Acrylates," in *European Rheological Conference,* Crete, Greece, 2007.

[89] A. Tobolsky, "Stress Relaxation Studies of the Viscoelastic Properties of Polymers," *Journal of Applied Physics,* vol. 27, no. 7, pp. 673-685, 1956.

[90] S. White and A. Hartman, "Effect of Cure State on Stress Relaxation in 3501-6 Epoxy Resin," *Journal of Engineering Materials and Technology,* vol. 119, pp. 262-2665, 1997.

[91] A. Lee and J. Lichtenhan, "Viscoelastic Responses of Polyhedral Oligosilsesquioxane Reinforced Epoxy Systems," *Macromolecules,* vol. 31, no. 15, pp. 4970-4975, 1998.

[92] H. Ardebili, E. Wong and M. Pecht, "Hygroscopic swelling and sorption characteristics of epoxy molding compounds used in electronic packaging," *IEEE Transactions on Components and Packaging Technologies,* vol. 26, no. 1, pp. 206-214, 2003.

[93] C. Brazel and N. Peppas, "Modeling of Drug Release from Swellable Polymers," *European Journal of Pharmaceuticals and Biopharmaceuticals,* vol. 49, pp. 47-58, 2000.

[94] A. Meinel, "High Resolution Optical Space Telescopes," in *Space Age Astronomy,* Pasadena, CA, 1961.

[95] C. Dispenza, F. Scro and G. Spadaro, "High energy radiation cure of resin systems for structural adhesives and composite applications," *Radiaiton Physics and Chemistry,* vol. 63, no. 1, pp. 69-73, 2002.

[96] T. Ferguson, *MOISTURE AND INTERFACIAL ADHESION IN MICROELECTRONIC ASSEMBLIES,* Atlanta, GA: Gerogia Institute of Technology, 2004.

[97] J. Crivello, "Advanced curing technologies using photo- and electron-beam induced cationic polymerization," *Radiation Physics and Chemistry,* vol. 63, pp. 21-27, 2002.

[98] W. Chappas, B. Devney, R. Olding and W. McLaughlin, "EB curing of maritime composite structures," *Radiation Physics and Chemistry,* vol. 56, pp. 417-427, 1999.

[99] D. Abliz, Y. Duan, L. Steuernagel, L. Xie, D. Li and G. Ziegmann, "Curing methods for advanced polymer composites—a review," *Polymer and Polymer Composites,* vol. 21, no. 6, pp. 341-348, 2013.

[100] S. Alessi, E. Calderaro, A. Parlato, P. Fuochi, M. Lavalle, U. Corda, C. Dispenza and G. Spadaro, "Ionizing radiation induced curing of epoxy resin for advanced composites matrices," *Nuclear Instruments and Methods in Physics Research Section B: Beam Interactions with Materials and Atoms,* vol. 236, pp. 55-60, 2005.

[101] J. O'Donnell, N. Rahman, C. Smith and D. Winzor, "Chain scission and cross-linking in the radiation degradation of polymers: limitations on the utilization of theoretical expressions and experimental results in the Pregel region," *Macromolecules,* vol. 12, pp. 113-119, 1979.

[102] N. Rami, H. Meghraoui, T. El khoukhi, M. Mouhib and A. El Harfi, "Influence of gamma irradiation on the chemical and physical properties of DGEDDS / PDA and DGEDDS / MDA epoxy resins," *Journal of Materials and Environmental Science,* vol. 4, pp. 277-288, 2010.

[103] S. Penczek, J. Wieteszka and P. Kubisa, "Radiation-induced liquid state polymerization of some cyclic ethers," *Die Makromolekulare Chemie,* vol. 97, no. 1, pp. 225-231, 1966.

[104] V. Laricheva, "Effect of ionizing radiation on epoxy oligomers of different structuresand manufacture of new promising materials on their base," *Radiation Physics and Chemistry,* vol. 77, pp. 29-33, 2008.

[105] S. Utsinomiya and R. Shimizu, "Monitoring of Dimensional Stability of CFRP Mirrors for Space Telescopes by Using Embedded FBG Sensors," in *ICCM International Conference on Composite Materials*, Edinburgh, Scotland, 2009.